Final Report

Evaluation of Concrete Pile Foundations During Hurricane Michael

Submitted to:

Florida Department of Business and Professional Regulation
Mo Madani, Program Manager
Building Codes and Standards
1940 North Monroe Street
Tallahassee, Florida 32399

Prepared by:

Raphael Crowley, Ph.D., P.E.
Principal Investigator
Associate Professor (Coastal and Port Engineering)

Ryan Shamet, Ph.D., P.E.
Co-Principal Investigator
Assistant Professor (Geotechnical Engineering)

Taylor Engineering Research Institute
School of Engineering
University of North Florida
1 UNF Drive
Building 4, Room 1501
Jacksonville, FL 322224

DISCLAIMER

The material presented in this research report has been prepared in accordance with recognized engineering principles. This report should not be sued without first securing competent advice with respect to its suitability for any given application. The publication of the material contained herein does not represent or warrant on the part of the University of North Florida or any other person named herein, that this information is suitable for any general or particular use or promises freedom from infringement of any patent or patents. Anyone making use of this information assumes all liability for such use.

EXECUTIVE SUMMARY

After Hurricane Michael struck Mexico Beach in October of 2018, several concrete pile foundations were observed to have failed during the storm. This investigation was conducted to analyze some of these failures using a structure where concrete foundations were observed to fail as a case study. Environmental loads due to wave and wind were computed on the structure using methods described by the Florida Building Code and results from these computations were compared to results from several models that were prepared using computational fluid dynamics (CFD). Results showed that the Florida Building Code performed well when compared to results from CFD. Next, the structure's foundation response was computed using a relatively simple prestressed concrete analysis and a finite element analysis (FEA). Results showed that the structure withstood forces specified by the Florida Building Code but that forces during Hurricane Michael were much greater than forces specified by the Code. As such, the structure failed due to insufficient moment capacity that was mostly the result of wave and surge action. Scour and the presence of a grade-level slab likely also affected the structure, although these effects were small when compared to the high surge-level associated with the storm. One could mitigate the high surge elevation during future construction by requiring higher structural elevations or stronger piles, but it is unclear how to do this in the Florida Building Code since doing so would increase the required return period for structures like the one at 1101 FL-30/US-98 beyond the current 100-year (and likely beyond the 500-year) return period currently specified by the Florida Building Code.

TABLE OF CONTENTS

LIST OF TABLES

LIST OF FIGURES

1   INTRODUCTION AND BACKGROUND INFORMATION

After Hurricane Michael ravaged Mexico Beach and surrounding areas in October of 2018, a team from the Federal Emergency Management Agency (FEMA) documented the damage. The resultant Mitigation Assessment Team (MAT) report "Report No. FEMA P-2077" identified several places where concrete piles failed (FEMA 2020). In particular, the MAT observed several instances where scour and erosion exceeded the ability of the concrete pile/column foundations to remain vertical. Instances were also observed where lateral loads and bending moments exceeded the material properties of the concrete foundation piles/columns, causing them to crack and break. As pointed out by FEMA, concrete piles should not be failing in these manners. Further complicating matters, embedment depths for piles that failed these ways were often unknown.

1.1 Goals and Objectives

The <u>overall goal</u> of the research presented here was to determine which failure mechanism or combinations of failure mechanisms led to the concrete pile foundation failures described above and to investigate preliminary mitigation measures to help prevent these sorts of failures from occurring in the future.

1.2 Scope of Work

To accomplish these goals, a series of research tasks were proposed. These tasks were as follows:

1.2.1 Task 1 – Information Gathering and Field Visits

The objective of Task 1 was to collect necessary data for an in-depth foundation system analysis. Specifically:

- Using Google Earth® the University of North Florida (UNF) Taylor Engineering Research Institute (TERI)/School of Engineering (SoE) conducted a historical image search of Mexico Beach to better understand the structures whose concrete piles failed during Hurricane Michael in terms of their dimensions, locations relative to the waterline, and locations of other structural elements near the piles (i.e., slabs, grad beams, etc.).

- UNF TERI/SoE contacted county building officials in Bay County, Mexico Beach, and the Florida Department of Environmental Protection (FDEP) to see if any construction drawings were available on file from permits that may have been issued.

- UNF TERI/SoE consulted with data from FEMA to determine if any of the failed structures had elevation certificates and/or letters of map revision (LOMR) that may have been used to reduce flood insurance premiums.

- Because some debris was still present along Mexico Beach, several site visits were conducted so that investigators could take detailed measurements of the debris including foundation column dimensions, rebar dimensions, prestressed strand dimensions, pile spacing, and approximate scour depths.

1.2.2 Task 2 – Maximum Environmental Loading Conditions

The objective of Task 2 was to determine the maximum load conditions that likely led to the failure of some of the concrete foundations. A representative structure was selected using data from Task 1 and was used as a case study throughout this analysis. Specific subtasks included the following:

- UNF TERI/SoE performed a component-by-component analysis of lateral loading on the representative structure. This process was dubbed a "first-level analysis." The 2016 ASCE Minimum Design Loads and Associated Criteria for Buildings and Other Structures (i.e., ASCE7) was used to compute wind loads. Wave loads were computed using two mechanisms: (1) a Morison-equation style approach using linear (i.e., Airy) waves; and (2) a quasi-static integration approach using linear waves.

- UNF TERI/SoE developed a computational fluid dynamics (CFD) model of the representative structure using Siemens' Star-CCM+ Version 2021.1 (Siemens 2021). Several approximated scour depths including situations where the subgrade had been eroded were investigated. While initially, investigators had anticipated using k-epsilon Reynolds Averaged Navier Stokes modeling (k-ϵ RANS) for this procedure, during this study it became apparent that a large eddy simulation (LES) was better able to model the breaking waves as they approached the structure. As such, all results are presented using LES turbulence closure. A Eulerian volume of fluid (VOF) approach was used to segregate

air from water throughout the modeling process. A Richardson extrapolation analysis was performed to verify approximate computational convergence.

- Results from the first-level analysis were compared with results from CFD. As will be shown below, environmental loading results were relatively comparable with results from the first-level analysis. Where results differed, the first-level analysis was generally conservative. As such, no recommendations were necessary in the context of how to modify the Florida Building Code to compute environmental loading more accurately on structures like the representative structure used in this study.

1.2.3 Task 3 – Structural Response to Maximum Loading Conditions

The objective of Task 3 was to determine how concrete piles that failed during Hurricane Michael responded to environmental loading data computed in Task 2. Specifically:

- UNF TERI/SoE used the 2014 ACI 318 Building Code Requirement of Structural Concrete to compute the representative structure's pile capacities. These values were compared with results from both the first level and CFD analyses from Task 2.

- UNF TERI/SoE developed a finite element analysis (FEA) model of the representative structure used during Task 2 using ANSYS Workbench Version 2021 R1. The soil-structure interaction (SSI) was modeled using GEO5 PILE Fine software Version 2021. Lateral bearing capacity and lateral deformation (i.e., pile distortion) were estimated using Broms, Bengt. B., 1964 "Lateral Resistance of Piles in Cohesionless Soils" and Vesic, A.S., 1977 "Design of Pile Foundations" respectively.

- Task 2 and Task 3 were to be completed iteratively in the sense that if loads from Task 2 did not lead to failure in Task 3, different sets of loads would be applied to the structure in Task 3 until observed failure was achieved. As will be shown below, investigators were able to achieve failure relatively quickly during this iterative analysis.

1.2.4 Task 4 – Develop and Test Mitigation Measures

UNF TERI/SoE investigated several failure mitigation alternatives during this task. Specifically:

- Results (see below) showed that most of the force on the structure was the result of wave loading/insufficient elevation between the structure's bottom chord and the water surface.

Bracing would do little to mitigate this issue in the context of pile yielding because bracing would simply move the concentrated stress downward toward portions of the piles where scour had occurred. As such, this analysis focused upon two mechanisms – reducing loading by slightly increasing the structural elevation; and scour mitigation which was analyzed in the context of less erosion around the foundations.

- Results from the mitigation techniques was categorized in the context of their likelihood to be successful or unsuccessful. Results were further characterized in their context of applicability to new or existing structures. Results appeared to show that the Florida Building Code mostly performs as designed in the sense that concrete pile foundations like the ones studied during this project would likely withstand a 100-year storm. However, the loading conditions during Hurricane Michael were much greater than conditions that would occur during a 100-year storm. As such, it was unclear how to properly address this in the Florida Building Code.

2 TASK 1 – INFORMATION GATHERING AND FIELD VISIT

2.1 Google Maps Investigation

Google (2022) records were available from October of 2018 and appeared to have been taken very shortly after Hurricane Michael affected the area on October 7, 2018, through October 11, 2018. Significant damage as observed along FL-30/US-98. Moving from southeast toward the northwest, most major damage was observed between approximately 700 FL-30/US-98 and the intersection of FL-30/US-98 with Salt Creek (see Fig. 2-1, below). Prevatt and Roueche (2019) observed similar damage patterns along Mexico Beach in their damage survey.

Along this route, several failed structures with concrete foundations were observed. Some of the concrete foundations withstood the forces associated with Hurricane Michael, while others failed. Examples are illustrated below in Fig. 2-2 through Fig. 2-16. Unfortunately, it appears that the Google (2022) camera after Hurricane Michael only captured usable street data southeast of S 27th St. From S 27th St. northwest through S 42nd St., significant damage was observed, but it was not possible to isolate concrete foundations from other foundations using street data because the camera from Google did not appear to take data down these side streets. As such, images in these locations were only available from the beach-side where data were collected. It is possible that further inland, additional concrete foundation damage may have been present after the storm.

Figure 2-1. Approximate major damage zone post Hurricane Michael

Figure 2-2. Evidence of structure with concrete foundations that failed during Hurricane Michael located at 719 FL-30/US-98 (former site of Toucan's of Mexico Beach)

Figure 2-3. Evidence of a structure with structural failure but little to no concrete foundation failure after Hurricane Michael located at 903 FL-30/US-98

Figure 2-4. Evidence of a structure with concrete foundations that failed during Hurricane Michael located at 1101 FL-30/US-98

Figure 2-5. Evidence of a structure with concrete foundations that partially failed during Hurricane Michael located at 1207 FL-30/US-98

Figure 2-6. Opposite angle for 1207 FL-30/US-98; data were available from the beach side at this location

Figure 2-7. Evidence of a structure with structural failure and partial concrete foundation failure after Hurricane Michael located at 1603 FL-30/US-98

Figure 2-8. Evidence of a structure with concrete foundations with structural failure but no foundation failure during Hurricane Michael located at 101 S 25th Street

Figure 2-9. Evidence of concrete foundation failure located at 106 S 25th Street and 107 S 27th Street

Figure 2-10. Evidence of concrete foundation failure located at 106 S 25th Street and 107 S 27th Street (different angle)

Figure 2-11. Evidence of a structure with concrete foundations that did not fail located at 108 S 27th Street

Figure 2-12. Evidence of a structure with partial concrete foundation failure located at 108 S 29th Street

Figure 2-13. Evidence of a structure with little apparent concrete foundation structural damage located at 112 S 30th Street

Figure 2-14. Evidence of a structure with little apparent concrete foundation structural damage located at 112 S 31st Street

Figure 2-15. Evidence of a structure with little apparent concrete foundation structural damage located at 114 S 33rd Street

Figure 2-16. Evidence of two structures with apparent concrete foundations and little observable damage located at 114 S 35 Street (right structure) and 117 S 36th Street (left structure)

2.2 Site Visits

Two site visits were conducted to assess remaining debris from Hurricane Michael. The focus of these visits was to obtain data from structures where usable Google (2022) data were available. While much of the debris from Hurricane Michael had been removed since the storm, at two locations, sufficient debris remained to estimate foundation plans. These locations were 1101 FL-30/US-98 (corresponding to Fig. 2-4) and 112 S 31st St. (corresponding to Fig. 2-13).

2.2.1 Data From 1101 FL-30/US-98

Site visit data from 1101 FL-30/US-98 are presented below in Fig. 2-17 through Fig. 2-24:

Figure 2-17. Site visit data from 1101 FL-30/US-98 showing overview of remaining debris

Figure 2-18. Close-up of failed concrete pile at 1101 FL-30/US-98

Figure 2-19. Close-up of another failed concrete pile at 1101 FL-30/US-98

Figure 2-20. Close-up of second row of failed concrete piles at 1101 FL-30/US-98

Figure 2-21. Close-up of prestressing strands in far-left pile shown in Fig. 2-19

Figure 2-22. Another close-up of failed concrete piles at 1101 FL-30/US-98

Figure 2-23. Beach-side overview of failed concrete piles at 1101 FL-30/US-98

Figure 2-24. Close-up of timber pile cap that ran along the tops of the piles at 1101 FL-30/US-98. Also shown are anchor bolts that anchored the piles to the cap. Note that the anchor bolts are mostly intact

Measurements taken at this location showed the following:

- Concrete piles were 12-in. by 12-in. They piles appeared to be prestressed with four groups 7-wire prestressing strands.

- Total exposed pile height was 11.5 ft. Based upon the paint patterns that were observed, it appears that approximately 2 to 3 ft. of scour occurred at this location.

- 1-in. diameter anchor bolts were used to affix the piles to their timber pile caps.

- Pile spacing was approximately 12.5 ft. parallel to the roadway and 9 ft perpendicular to the roadway.

These measurements were used to develop a sketch of 1101 FL-30/US-98 (Fig. 2-25).
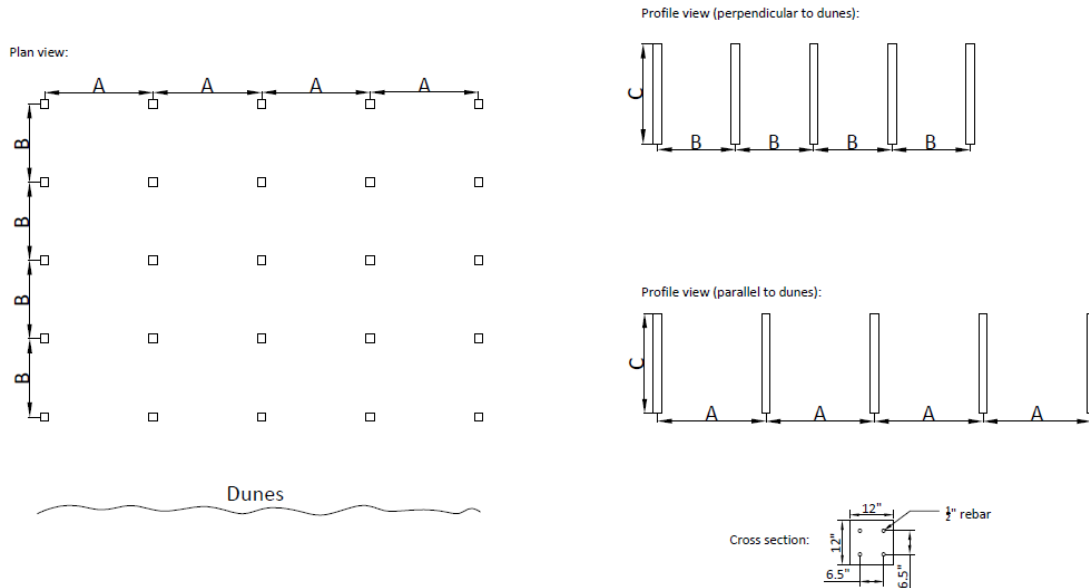
Figure 2-25. Sketch of pile layout at 1101 FL-30/US-98

2.2.2 Data from 112 S 31st St.

Since Hurricane Michael, the superstructure at 112 S 31st St. has been razed, but the concrete pile foundations remain (Fig. 2-26).

Figure 2-26. Remaining concrete pile foundations at 112 S 31st St.

Measurements were taken of the remaining structure at this location. Measurements showed the following:

- Concrete piles were 12-in. by 12-in. It was not possible to determine how these piles were reinforced since no rebar was exposed.

- Total exposed pile height was 107 in. Atop the piles were 15.5-in. beams that ran perpendicular to the dunes.

- Pile spacing varied from bent to bent along the structure. Maximum spacing was 14-ft. while minimum spacing 10.42-ft.

These measurements were used to develop a sketch associated with the structure's foundation (Fig. 2-27).

House 2 (approx. 29.94763° N, 85.41973° W)

A (parallel to dunes) = 144"
B (parallel to dunes) = 125"
C (parallel to dunes) = 168"
D (parallel to dunes) = 130"
E (perpendicular to dunes) = 130"
F (column height) = 107"
G (beam height) = 15.5"

Plan view:
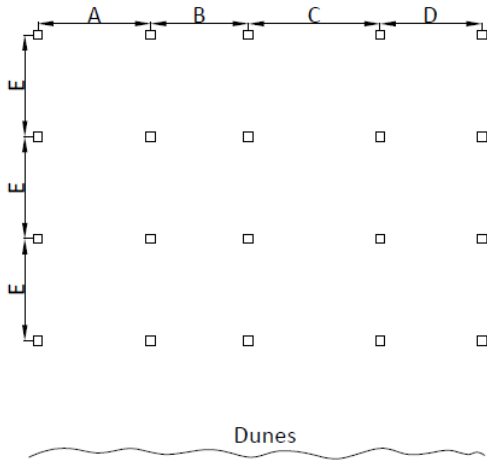
Profile view (perpendicular to dunes):
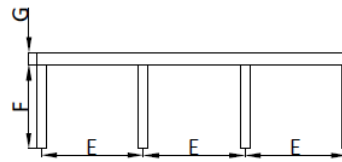
Profile view (parallel to dunes):

Cross section:

Dunes
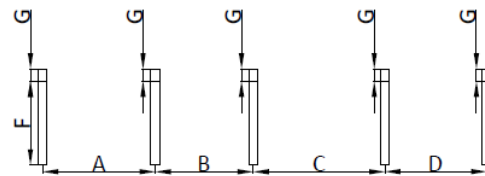
Figure 2-27. Sketch of pile layout at 31 S 31st St.

2.3 Government Records Search

At this point in the forensic investigation, investigators chose to target the locations with the most available data – 1101 FL-30/US-98 and 112 S 31st St. Government officials were contacted in unincorporated Bay County to determine if permits were ever filed for either of these two locations. Officials in Bay County referred investigators to officials in Mexico Beach because Bay County does not keep permit records associated with incorporated Mexico Beach. Mexico Beach officials confirmed that permits were filed at both locations, but that in each case, the permits were so old that only paper records were kept. Unfortunately, in both cases, these paper records were destroyed during Hurricane Michael. Data were also consulted from the FLDEP to determine if they had any permit records on file at either of these locations. However, despite the information from Mexico Beach, no FLDEP records were found at either of these locations. FEMA records were examined to determine if any LOMR were filed for either 1101 FL-30/US-98 or 112 S 31st. Unfortunately, there were no LOMR records at either location.

2.4 Selection of Representative Structure

Similar data were available at both 1101 FL-30/US-98 and at 112 S 31st St. At the 112 S 31st St. location, there was some question about what the original structure's configuration (this was not very clear from the historical image data). While the government record search did not yield any usable permit data, the search did reveal the identity of the previous homeowner, and these data were confirmed using a search on Zillow (2022) that showed that the property had been sold in 2019. The homeowner at 112 S 31st St. was located using several Google searches and contacted to see if he would assist with the investigation. The former homeowner was more than happy to confirm which structure was which, and he also confirmed that the remaining foundation was certified as "structurally competent" prior to the 2019 property sale. Interestingly then, these properties represent two datasets – one where the concrete pile foundations failed and another where the concrete pile foundations withstood the forces associated with Hurricane Michael.

While either the 1101 FL-30/US-98 or the 112 S 31st St. properties could be used for subsequent analysis, investigators reasoned that the purpose of this project was to investigate "failure." As such, subsequent investigation focused on the property located at 1101 FL-30/US-98. As shown in Fig. 2-17 through Fig. 2-24, the piles at 1101 FL-30/US-98 appeared to fail via insufficient bending moment capacities. Furthermore, analysis of the paint along the pile-lengths appeared to show that the location of these moment failures was very close to a grade-level slab that had been installed around the piles. This is particularly evident in Fig. 2-18 through Fig. 2-22 where, as shown, breakage appears to have occurred very close to the paint-line. Using Google (2022) historical image data, previous images of the structure at 1101 FL-30/US-98 were obtained (see Fig. 2-28 through Fig. 2-31). As shown in the historical images, the piles are clearly painted white above grade-level and a slab was clearly installed around the piles.

From the historical images, an approximate three-dimensional model of the structure was estimated and drawn using computer aided drawing (CAD). This model was used for subsequent analysis (Fig. 2-32 and Fig. 2-33).

Figure 2-28. 1101 FL-30/US-98 in November 2007 (Google 2022)

Figure 2-29. 1101 FL-30/US-98 in April 2009 (Google 2022)

Figure 2-30. 1101 FL-30/US-98 in May 2011 (Google 2022)

Figure 2-31. 1101 FL-30/US-98 in June 2015 (Google 2022)
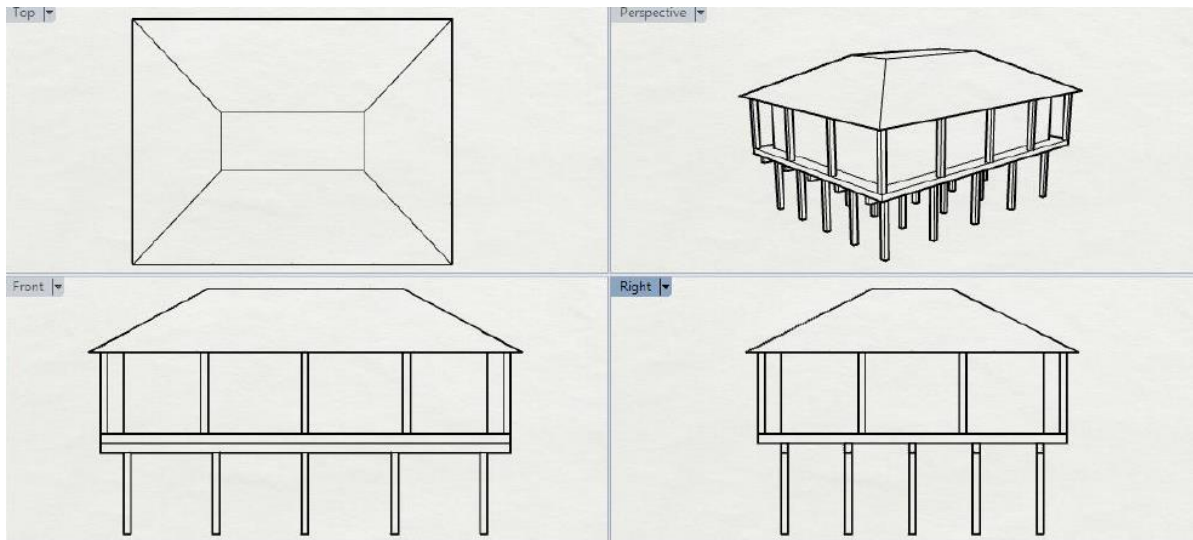
Figure 2-32. CAD approximation of 1101 FL-30/US-98 showing top-view (top-left), isometric view (top-right), front-view (bottom-left) and right-side view (bottom-right)
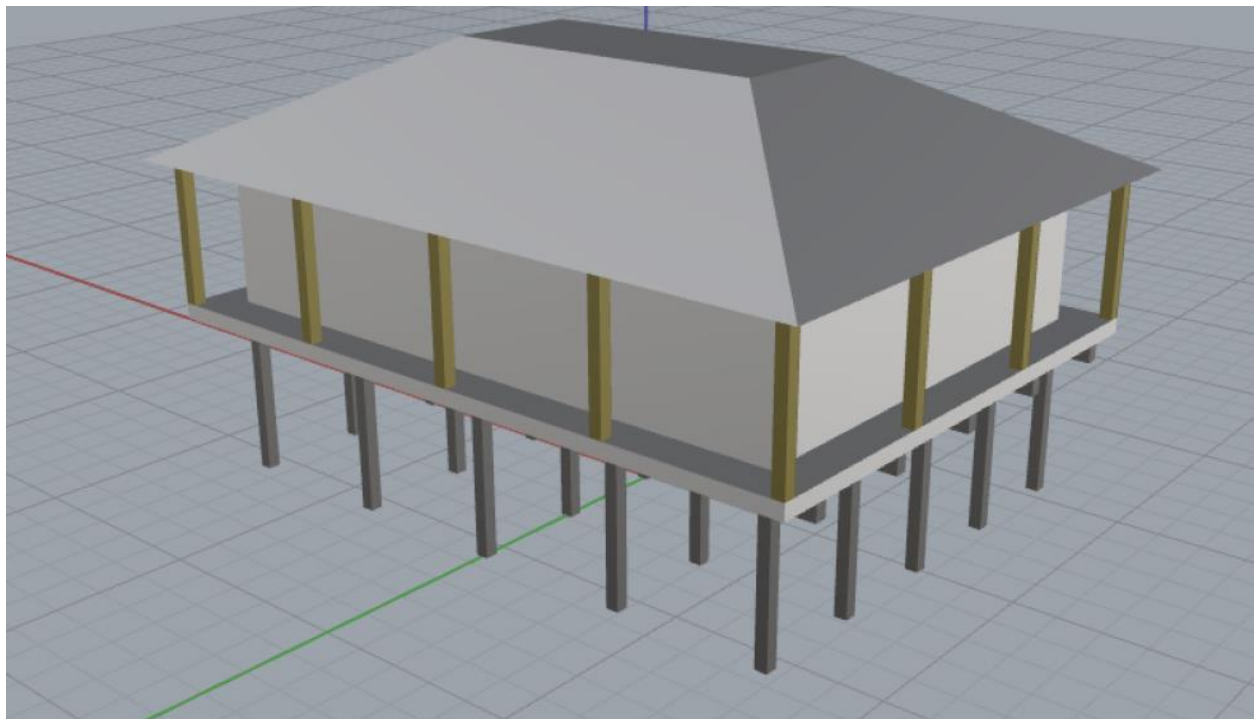
Figure 2-33. CAD approximation of 1101 FL-30/US-98 showing detailed isometric view

3   ENVIRONMENTAL LOADING

3.1 Elevation Data

Prior to both the first level and a CFD analyses, Mexico Beach was mapped using beach profile data that were collected from the FLDEP from December 2018. The elevation contours are presented below in Fig. 1-1. Included in this figure is the location associated with 1101 FL-30/US-98.
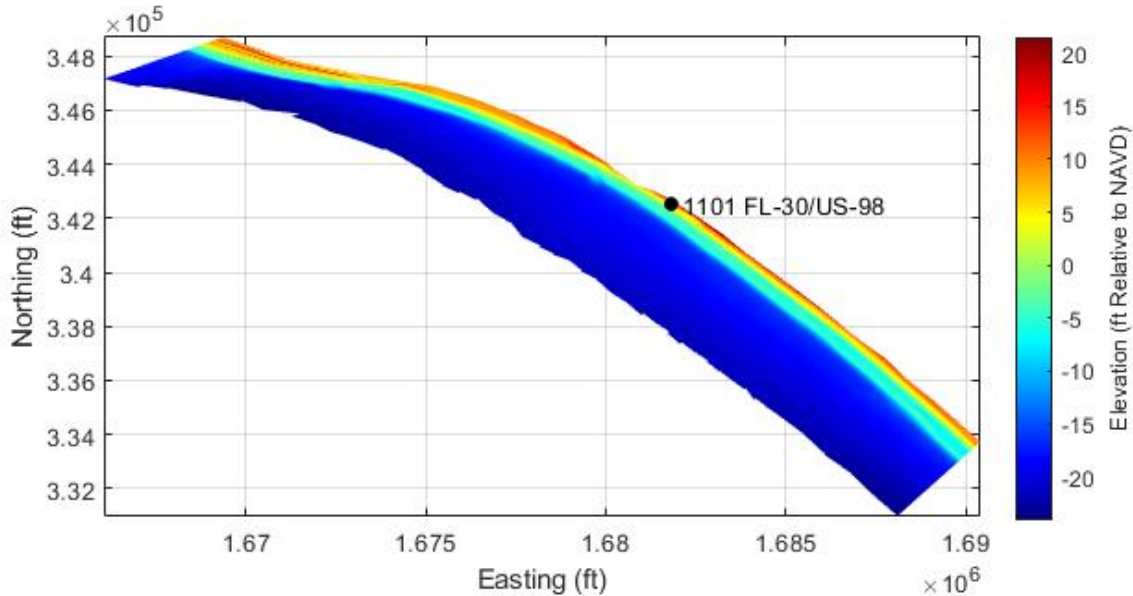
Figure 3-1. Beach elevation data after Hurricane Michael showing location of 1101 FL-30/US-98

Next, the structure's elevation was approximated along with reported water levels near the structure during Hurricane Michael. The sketch below (Fig. 3-2) shows a cross-section with the assumed structural elevation and various reported water level elevations during Hurricane Michael. As shown in the sketch, there is some ambiguity about the water levels near and around the structure during the storm. Hindcast calculations from Taylor Engineering estimate that the water elevation near the structure was +15.6 ft NAVD while data from the FEMA MAT report indicated that worst-case surge elevations may have been as high as +21.2 ft NAVD. As will be shown in the discussion on Task 3, these somewhat subtle changes in water elevation appear to have a large effect on structural forcing due to wave/surge action. In addition, it should be noted that in either case (i.e., +15.6 ft NAVD or +21.2 ft NAVD), the water elevations represent a return period greater than a 500-year storm. This is greater than the 100-year storm required for residential structures according to the Florida Building Code and greater than the Florida Building

Code's reference to ASCE24 (see Flood Resistant Provisions in the 7th Edition of the Florida Building Code 2020).
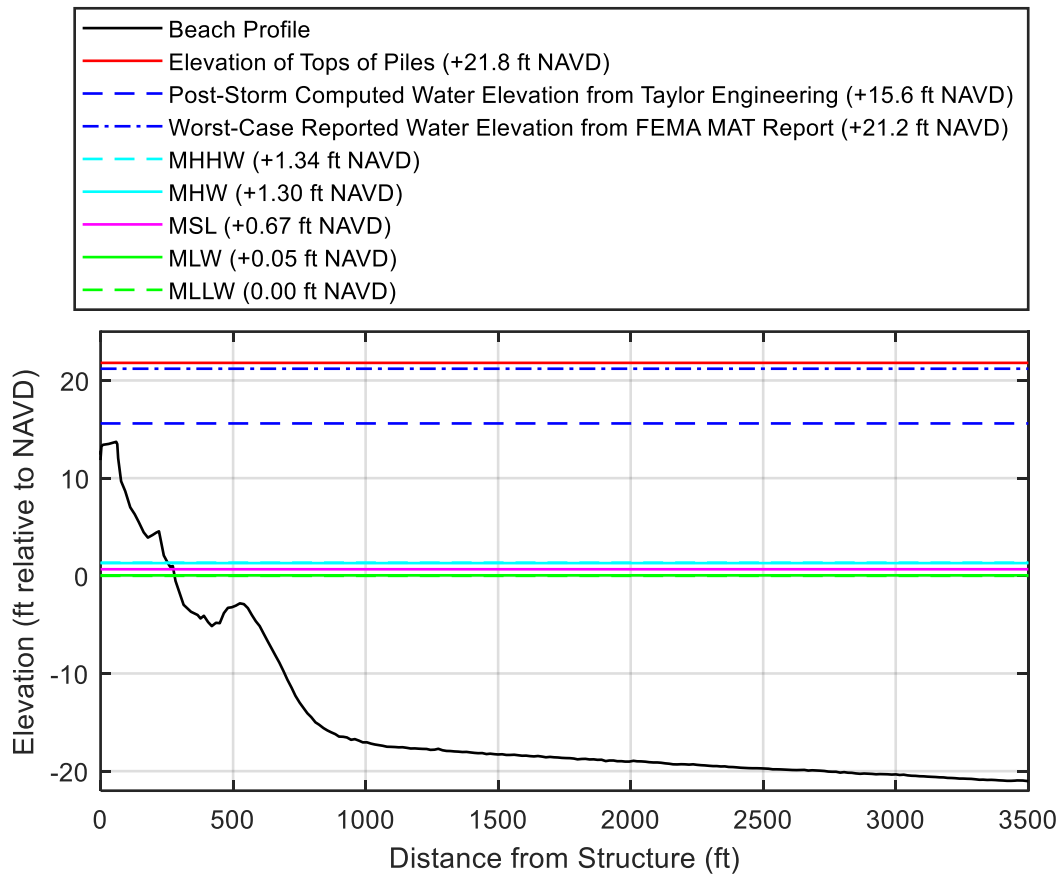
Figure 3-2. Beach profile near 1101 FL-30/US-98

3.2 First-Level Analysis – Wind Loading

Wind loads were computed on the structure located at 1101 FL-30/US-98 using the procedure illustrated in ASCE 7, Minimum Design Loads and Associated Criteria for Buildings and Other Structures (ASCE 2017). Computations associated with this were as follows:

3.2.1 Risk category

The structure is Risk Category II (Table 1.5-1)

3.2.2 Basic wind speed

Fig. 26.5-1C in ASCE (2017) shows that the basic wind speed, V is 140 mph.

3.2.3 Wind load parameters

- Table 26.6-1 in ASCE (2017) shows that the wind directionality factor, $K_d = 0.85$.

- Section 26.7.2 in ASCE (2017) indicates that the structure is in exposure category D because upwind of the structure is a flat open surface (i.e., the Gulf of Mexico).

- To compute the topographic factor, K_{zt}, it was assumed that the dune on which the structure was built constituted an escarpment. The dune height, H, was assumed to be 11 ft above mean sea-level. This led to a distance halfway up the escarpment, L_h equal to 250 ft. For an escarpment in in exposure category D:

$$\frac{K_1}{(H/L_h)} = 0.95 \tag{3-1}$$

Substituting and solving for K_1 yields $K_1 = 0.0418$. Then, from Fig. 26.8-1 in ASCE (2017):

$$K_2 = (1 - |x|/(\mu L_h)) \tag{3-2}$$

where x is the distance upwind from the crest to the site of the building and μ is the horizontal attenuation factor, which equals 4 for a two-dimensional escarpment. x was assumed to be equal to zero – i.e., the structure was built at the top of the dune. Solving for K_2 yields $K_2 = 1$. Next, K_3 is given as:

$$K_3 = \exp\left(-\frac{\gamma z}{L_h}\right) \tag{3-3}$$

where $\gamma = 2.5$ and z is the heigh of the building above the ground surface. Based upon results from the site visits, it appears that $z = 9$ ft. Substituting and solving yields $K_3 = 0.91$. To compute Kzt:

$$K_{zt} = (1 + K_1 K_2 K_3)^2 \tag{3-4}$$

Substituting and solving yielded $K_{zt} = 1.08$.

- Section 26.9 in ASCE (2017) indicated that $K_e = 1.0$ for structures less than 1,000 ft in elevation.

- The gust factor, G was determined from ASCE (2017) Section 26.11 which says that to be conservative, using $G = 0.85$ is acceptable.

- Determination of the enclosure classification was ambiguous. If the structures windows broke during the storm, then the structure would be considered partially enclosed and

$GC_{pi} = \pm0.55$. If the windows did not break during the storm, then the structure would be enclosed and $GC_{pi} = \pm0.18$. To be conservative, it was assumed that $GC_{pi} = \pm0.55$.

3.2.4 Pressure coefficients

To determine the pressure coefficient , K_z Table 26.10-1 in ASCE (2017) was used. According to the table, if z is less than 15 ft, then

$$K_z = 2.01 \left(\frac{15}{z_g}\right)^{(2/\alpha)} \tag{3-5}$$

where for exposure category D, $\alpha = 11.5$ and $z_g = 700$. If z is greater than 15 ft, then:

$$K_z = 2.01 \left(\frac{z}{z_g}\right)^{(2/\alpha)} \tag{3-6}$$

Values of K_z were computed as a function of z using a step-size of 0.1 ft starting at a structural elevation of 9 ft above the dune-level and ending at a structural elevation of 25 ft above dune level. This led to a maximum K_z value of 1.12 and a minimum K_z value of 1.03.

3.2.5 Velocity pressure

The velocity pressure, q_z was computed as a function of z using the following expression:

$$q_z = 0.00256 K_z K_{zt} K_d K_e V^2 \tag{3-7}$$

The maximum q_z was 49.34 psf and the minimum q_z was 47.36 psf.

3.2.6 External pressure coefficients

According to Fig. 27.3-1 in ASCE (2017), the structure of interest had a Mansard roof. Based upon the structure's length-to-width ratio (which was measured during the site visit), this led to the following values for wall pressure coefficients, C_p:

- Windward wall $C_p = 0.8$
- Leeward wall $C_p = -0.5$
- Sidewall $C_p = -0.7$

The roof was assumed to be 10 ft above the top-floor elevation (this was based upon images from the Google Earth ® search), and the roof was assumed to be at a 22-degree angle. This led to the following roof pressure coefficients:

- Windward roof $C_p = 0.3$

- Leeward roof $C_p = -0.6$

3.2.7 Pressure on building surfaces

Pressures on the building surfaces were computed using Eq. 27.3-1 assuming a rigid building:

$$p = qGC_p - q_i(GC_{pi})$$ (3-8)

where q is denoted as either q_z for windward walls or q_h for leeward walls and the roofs in which q_h is q evaluated at pre-specified height, h, which is either the mean roof or wall height. In this study, the pressures of interest were pressures in the x-direction (i.e., perpendicular the road and dunes). In the x-direction, computed pressures were as follows:

- $\max(p_{windward}) = 59.60$ psf; $\min(p_{windward}) = 58.25$ psf
- $p_{leeward} = 5.92$ psf
- $p_{roof_{windward}} = 38.12$ psf
- $p_{roof_{leeward}} = 1.89$ psf

Once pressure forces had been computed, they were used to find the total force on the structure due to wind in the x-direction by multiplying the pressures by the building dimensions (i.e., the height times the building length times the cosine of the appropriate angle for the cases of roofs). Then, the forces on the structure were added to find the total force on the structure. This led to a total computed force due to wind on the structure of approximately 68 k.

3.3 First-Level Analysis – Forces Due to Wave and Surge

Three methods were used to compute forces due to wave action and storm surge. First, a Morison-style approach was used. Then, linear wave theory was used to integrate pressures around the structure. Finally, guidelines from the FEMA Coastal Construction Manual (Volume II, Chapter 7) were applied to the structure.

3.3.1 Morison-style approach

The Morison Equation for forces on any submerged or partially submerged body is as follows:

$$F = F_D + F_I$$ (3-9)

where F_D are the drag forces on the object given by:

$$F_D = 0.5\rho C_D A u |u| \tag{3-10}$$

where C_D is the drag coefficient; A is the cross-sectional area; ρ is the density of water (assumed to be saltwater with a density of 64 pcf); and u are the water velocities in the x-direction. Assuming linear (i.e., Stokes) wave theory:

$$u = \frac{H}{2}\sigma \frac{\cosh\,(k(h+z))}{\sinh\,(kh)}\cos\,(kx - \sigma t) \tag{3-11}$$

where H is the wave height (distance from crest to trough or half the wave amplitude); h is the water depth, k is the wave number (i.e., $2\pi/L$; L is the wavelength); $\sigma = 2\pi/T$; T is the wave period; and z is an axis from the water surface upward. In Eq. 3-9, F_I represents the intertial forces and is given by:

$$F_I = \rho C_m V \frac{\partial u}{\partial t} \tag{3-12}$$

in which C_m is the inertial coefficient; V is the affected volume; and $\frac{\partial u}{\partial t}$ are the accelerations in the x-direction given by:

$$\frac{\partial u}{\partial t} = -\frac{H}{2}\sigma^2 \frac{\cosh(k(h+z))}{\sinh(kh)}\sin\,(kx - \sigma t) \tag{3-13}$$

Based upon the hindcast calculations from Taylor Engineering, the water surface elevation was assumed to be 15.6 ft above MSL; wave heights were assumed to be 26 ft; and the wave periods were assumed to be 10 s. Note however that 26-ft waves would have broken due to depth-limited conditions prior to reaching the structure. As such, a breaking criterion was used to limit the computed wave height. The breaking criterion was:

$$H_b = \kappa h$$

where $\kappa = 0.78$ and the computed water depth at the superstructure was 8 ft. The linear dispersion relationship was used to compute the wave number associated with this water depth/wave period combination and is given by:

$$\sigma^2 = gk \tanh(kh) \tag{3-14}$$

where g is the acceleration due to gravity (i.e., 32.2 ft/s^2). At the front face of the structure, the water surface elevation, η_1 was assumed to be given by:

$$\eta_1 = \frac{H}{2}\cos\,(kx - \sigma t) \tag{3-15}$$

And, at the far face of the structure, the water surface, η_2 was assumed to be given by:

$$\eta_2 = \frac{H}{2}\cos\,(kx_1 - \sigma t) \tag{3-16}$$

where x_1 is the structural dimension in the x-direction and x was assumed to be zero (i.e., space was fixed, and the wave was analyzed only as a function of time). Two scenarios are possible under these circumstances. First, below the elevation of the superstructure, water would not impact the superstructure and there would be no forces upon it (only forces would exist on the piles). But, when water elevations were above the elevation of the superstructure, both pile forces and superstructure forces needed to be considered. A Boolean logic sequence was written in MATLAB (Mathworks 2022) to address each of these scenarios.

One of the limitations of linear wave theory is that depth-dependent quantities (i.e., u, $\partial u/\partial t$, etc.) should only be integrated to the water surface because the solutions associated with linear wave theory are only valid in the domain bound by the water surface. But the scenario of interest is such where the initial water surface is always just below the elevation of the superstructure. As such, the depth-dependent quantities at the surface (i.e., $z = 0$) were computed and integrated upward over the inundated portion of the superstructure to develop a formulation for total superstructure force. The result of this computation is shown below in Fig. 3-3:
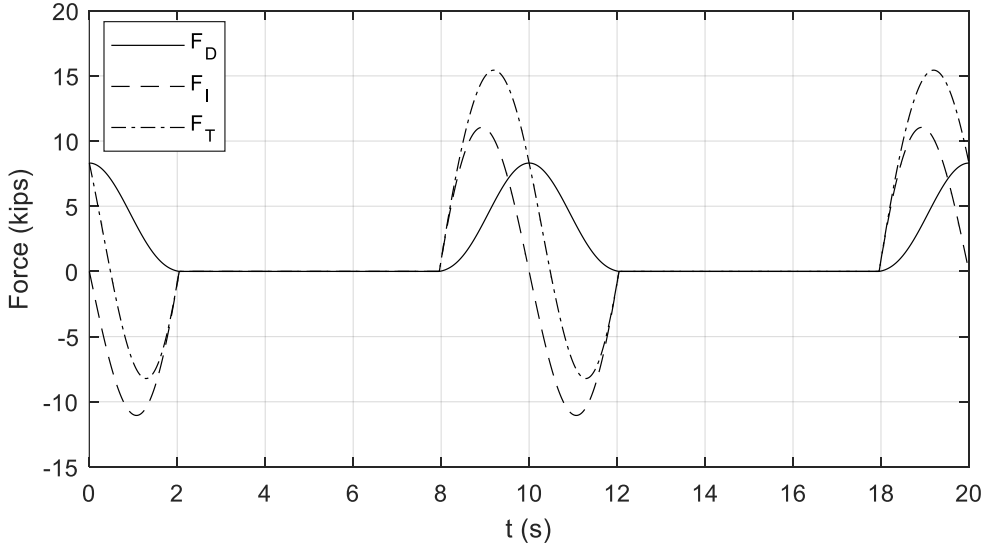
Figure 3-3. Wave loading on the superstructure as a function of time

As shown, the maximum total force on the structure appears to be a scenario that is both drag and inertially dependent and is approximately 15 k. Of course, the weakness to any Morison-style approach is that its results are entirely dependent upon assumed values for drag and inertial coefficients. During the computations, it was assumed that the drag coefficient was equal to 1.0 and the inertial coefficient was equal to 0.5. These were best guesses based upon experience, but

unfortunately, drag or inertial coefficients for a relatively long wave impacting a relatively wide-bodied structure are poorly established. Thus, while Fig. 3-3 gives an order-of-magnitude sort of check for forces upon the superstructure, these results should be treated skeptically. It is possible that actual forces on the superstructure could be as much as double (or as little as half) the values shown in Fig. 3-3.

Computation of wave forces on the piles also followed a Morison-style approach. Unlike the superstructure computation, however, drag and inertial coefficients for flow around square inundated piles is very well established and, in both drag and inertial scenarios, assuming coefficients of 1.0 should be acceptable. To compute the drag and inertial forces, velocity and acceleration were computed as a function of depth; these values were used to compute forces as a function of depth; and the force as a function of depth was summed over the inundated pile length. Finally, force was multiplied by the number of piles associated with the structure (i.e., 25 piles). The result of this computation is shown below in Fig. 3-4:
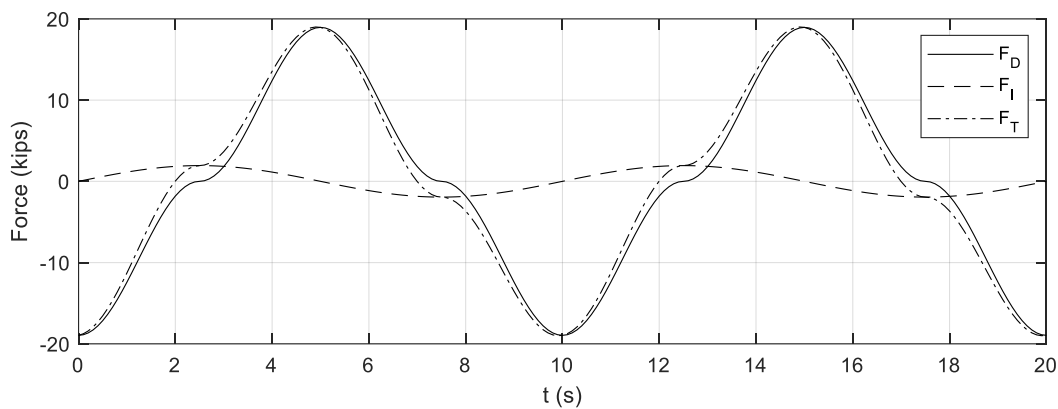
Figure 3-4. Wave loading on piles as a function of time

As shown, the maximum force on the structure due to piles was approximately 19 k.

3.3.2 Pressure integration approach

As discussed in Dean and Dalrymple (1991) assuming linear wave theory, the pressure force on a partially submerged structure is:

$$P = \frac{l_2 \rho g H \cos(kx - \sigma t)}{2 \cosh(kh)} \int_{z_1}^{z_2} \cosh\big(k(h + z)\big) \, dz \qquad (3\text{-}17)$$

where z_1 and z_2 represent the water elevations associated with the beginning and end of inundation; and l_2 is the width of the structure. As in the Morison-style approach, one cannot integrate linear wave theory above the water surface. Thus, like the previous set of computations,

z was assumed to equal zero and the integral with respect to *z* in Eq. 3-17 was evaluated using the water surface and superstructure elevation as limits. Under the pressure integration approach, four scenarios are possible:

- The crest of the wave is moving through the structure, and as such, both the front face and the back face of the structure are inundated. Thus, a positive pressure is exerted on the front face of the structure while a negative pressure is exerted on the downstream face.

- The crest of the wave is just approaching the structure, and as such, the front face of the structure is inundated, but the back portion of the structure is not inundated. Thus, a positive pressure is exerted on the front face of the structure, but there is no counteracting pressure acting in the negative direction.

- The crest of the wave has moved through most of the structure, and as such, the back portion of the structure is inundated but the front portion of the structure is not inundated. Thus, only a negative pressure is exerted on the structure.

- None of the structure is inundated. Thus, the superstructure experiences no pressure due to wave action.

Again, a Boolean logic sequence was coded using MATLAB (Mathworks 2022) to model these four scenarios; the same values for wave parameters (i.e., *H*, *h*, *T*, etc.) were used; and Eq. 3-16 was solved. The result of this computation is shown below in Fig. 3-5:
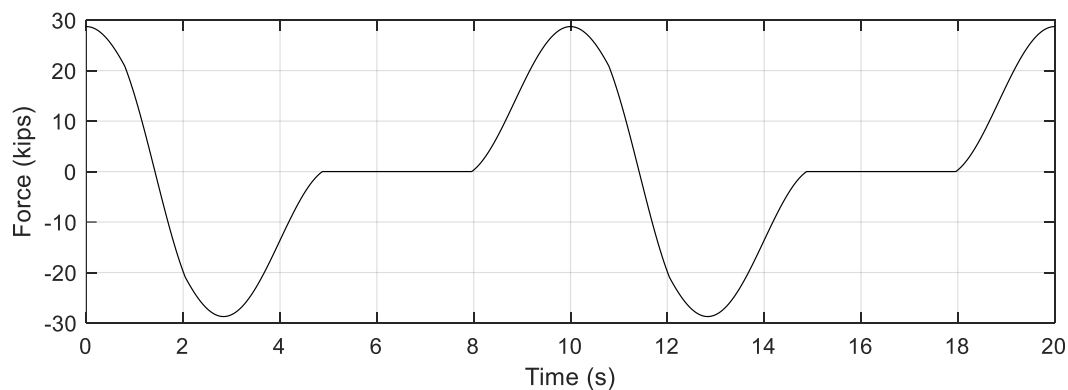
Figure 3-5. Wave forces on the superstructure using a pressure integration approach

As shown, using this approach, the total force on the structure due to surge/wave action was approximately double the computed force using the Morison-style approach. But, when one considers that the Morison-style approach is entirely based upon assumed, poorly understood

values for drag and inertial coefficients, these results appear to be relatively comparable. Fig. 3-5 shows that the maximum force upon the superstructure was approximately 29 k.

Since a Morison-style approach for computing wave loads on inundated piles is very well established, there was no need to use a pressure integration approach to compute the forces upon the structure's piles. In fact, using a pressure integration approach to compute forces upon the piles likely would have been incorrect because the pressure integration approach assumes that a very small wake develops downstream from the wave, and this is known to be incorrect around relatively slender piles.

3.3.3 FEMA Coastal Construction Manual

According to the FEMA Coastal Construction Manual, for an elevated foundation like the foundation at 1101 FL-30/US-98, the total load on the structure is given as the sum of the wave slamming force, F_s, the hydrodynamic load on the structure, F_{dyn}, and the debris load, F_i; or a load factor combination among F_{dyn}, F_i, and F_{brkp}, which is the force due to breaking waves on piles if slamming force is not an issue. The equations for computing these quantities are as follows:

$$F_s = 0.5\gamma_w C_S d_s hw \tag{3-18}$$

$$F_{dyn} = 0.5C_{dr}\left(\frac{\gamma}{g}\right)V^2A \tag{3-19}$$

$$F_i = WV C_D C_B C_{Str} \tag{3-20}$$

$$F_{brkp} = 0.5C_{db}\gamma_w DH_b^2 \tag{3-21}$$

where γ_w is the density of seawater (64 pcf); C_s is the slamming coefficient (2.0); d_s is the stillwater depth; h is the portion of the structure inundated due to waves; w is the structure width; C_{dr} is the drag coefficient for piles (2.0 for square piles); V is the velocity of the wave (i.e., $\sqrt{gd_s}$ for shallow-water waves); A is the inundated area of the piles; W is the weight of debris; C_D is the depth coefficient (1.0 for this case); C_B is the blockage coefficient (1.0 for this case); C_{db} is the breaking wave drag coefficient (2.25 for square piles); and C_{Str} is the building structure coefficient which was computed as:

$$C_{Str} = \frac{3.14C_I C_0 R_{max}}{2g\Delta t} \tag{3-21}$$

where C_I is the importance factor (1.0); C_0 is the orientation coefficient (0.80); Δt is the duration of impact (0.03 s); and R_{max} is the maximum response ratio which is 0.35 s for concrete piles. Substituting the approxpriate pile dimensions (i.e., 1-ft by 1-ft) and water elevations (+15.6 ft

NAVD means that the piles were inundated, and the structure was subjected to approximately 4.5-ft of slamming force. This means that the governing load combination is $F_{dyn} + F_s + F_i$, which was computed to be over 200 k. This is much greater than the forces computed via either the Morison-style method or the quasi-static pressure integration approach, but the FEMA approach is known to be very conservative. As such, the next step was to compare these results with results from CFD.

3.4 The CFD Model

As noted in Introduction, Siemens' Star-CCM+ was used for all CFD modeling. Also as noted, at first, investigators initially attempted to utilize k-ϵ RANS turbulence closure. However, the result from these computations led to results that were believed to be inaccurate. Use of RANS modeling led to residuals that were unreasonably high; computed sporadic high frequency forcing that made no sense physically; discontinuities in the water surface that were physically nonsensical; and hypersensitivity to initial water elevations. As such, investigators switched to LES modeling shortly after the Interim Report was presented.

3.4.1 Turbulence Closure

As discussed extensively by Siemens' (2021), LES modeling is a transient technique whereby large eddy turbulence scales are directly resolved everywhere in the flow domain, and then the small-scale motions are modeled. The advantage to an LES model when compared to a RANS model is that by modeling "less" turbulence while explicitly solving for more of it, the error associated with turbulence assumptions is not as consequential. On the other hand, a RANS model essentially assumes a relative balance between turbulent production and dissipation. In the case of a wave approaching a beach, significant unbalanced turbulence is produced via wave breaking, and this tends to lead to computational errors. The disadvantage to a LES model when compared to a RANS model is that it requires more computational time, but investigators were able to complete sufficient modeling in the allotted time to draw conclusions about forcing on the structure.

Unlike a RANS model, the LES equations are obtained by spatial filtering rather than an averaging process. Each solution variable ϕ is decomposed into a filtered value $\tilde{\phi}$ and a sub-filtered (i.e., subgrid) value ϕ':

$$\phi = \tilde{\phi} + \phi' \tag{3-22}$$

where ϕ representes some quantity – i.e., velocity components, pressure, or energy. The decomposed solution is inserted into the standard Navier-Stokes equations, and this results in equations for filtered quantities. The filtered equations are rearranged into a form that looks identical to the unsteady RNAS equations, but the turbulent stress tensor is now represented by the subgrid scale stresses that result from the interaction between the larger, resolved eddies. Meanwhile, the smaller, unresolved eddies are modeled using the Boussinesq approximation:

$$T = 2\mu_t S - \frac{2}{3}(\mu_t \nabla \tilde{v})I \tag{3-23}$$

where S is the mean strain rate tensor and $\tilde{v}$ is the filtered velocity. The turbulent viscosity μ_t is modeled using a subgrid scale model. While three subgrid scale models are available in Star-CCM+, the Wall-Adapting Local-Eddy Viscosity (WALE) subgrid model was used throughout this study (Nicoud and Ducros 1999). The advantage to this model when compared to other subgrid models is that it not as sensitive to its non-universal model coefficient. In addition, it does not require any wall dampening as it automatically accurately scales at walls (Siemens 2021).

3.4.2 Volume of Fluid Model

To simulate the properties of the multicomponent, multiphase flow, a volume of fluid (VOF) model was used to capture the differences in fluid properties between water and air. The assumption of the VOF model is that both fluids share the same field values when evaluating velocity, pressure, and temperature terms. The assumption behind the use of this model is that a sufficiently fine mesh is used so that discretization errors associated with mixing are minimized. The equations governing the volume of fluid model of the phase are:

$$\rho = \sum_i \rho_i \alpha_i \tag{3-24}$$

$$\mu = \sum_i \mu_i \alpha_i \tag{3-25}$$

$$c_p = \sum_i \frac{(c_p)\rho_i}{\rho} \alpha_i \tag{3-26}$$

$$\alpha_i = \frac{V_i}{V} \tag{3-27}$$

where c_p is the fluid's specific heat (if calculating heat flux), and α is the phase volume fraction. The modified parameters are then used to create the new governing transport equation for multiphase flow as:

$$\frac{d}{dt} \int \alpha_i dV + \int \alpha_i (\boldsymbol{v} - \boldsymbol{v_g}) \cdot da = \int \left(s_{\alpha_i} - \frac{\alpha_i}{\rho_i} \frac{D\rho_i}{Dt} \right) dV \quad\quad\quad (3\text{-}28)$$

where s_{α_i} is the phase source or sink term, and $\frac{D\rho_i}{Dt}$ is the material derivative of the phase densities, which was assumed to be zero because flow was assumed to be incompressible.

3.4.3 Wave Generation and Damping

Star-CCM+'s fifth order Stokes waves were specified at the incoming boundary (see below) in an effort to model realistic water surface elevations. For details about the Star-CCM+ fifth order Stokes wave model, please refer to Fenton (1985). At the boundary closet to the structure, wave damping was used using the built-in Star-CCM+ wave damping option by adding a resistance term to the equation for velocity in the z-direction.

3.4.4 Eulerian Multiphase Models

Two fluid phases were defined – water and air. Water was assumed to have a constant density, ($1,025 \ kg/m^3$), dynamic viscosity ($8.89 \times 10^{-4} \ Pa \cdot s$), molecular weight $\left(18 \frac{kg}{kmol} \right)$, specific heat $\left(4782 \frac{J}{kg \cdot K} \right)$, sound speed transmission velocity ($1500 \ m/s$), and thermal conductivity $\left(0.62 \frac{W}{m \cdot K} \right)$. Air was assumed to have a constant dynamic viscosity ($1.85 \times 10^{-5} Pa - s$), molecular weight $\left(29 \frac{kg}{kmol} \right)$, specific height $\left(1004 \frac{J}{kg \cdot K} \right)$, and thermal conductivity $\left(0.026 \frac{W}{m \cdot K} \right)$. An ideal gas law was used to model the air's compressibility:

$$\rho = \frac{p}{RT} \quad\quad\quad (3\text{-}29)$$

in which R is the specific gas constant defined by:

$$R = \frac{R_u}{M} \quad\quad\quad (3\text{-}30)$$

where R_u is the universal gas constant and M is the molecular weight.

3.4.5 Geometrical Configuration and Meshing

The representative beach in Fig. 3-1 was imported into CAD and converted to a surface mesh. Next, the structure was geo-located onto this surface mesh and an approximately 800-ft "strip" of this mesh was cut so that the structure was approximately centered in the y-direction

with approximately 400-ft of undisturbed beach on either side. The strip of beach was projected upward approximately 75-ft and the gaps between the beach and the upward projection were filled with vertical planes to yield a closed flow domain (see Fig. 3-6 below).
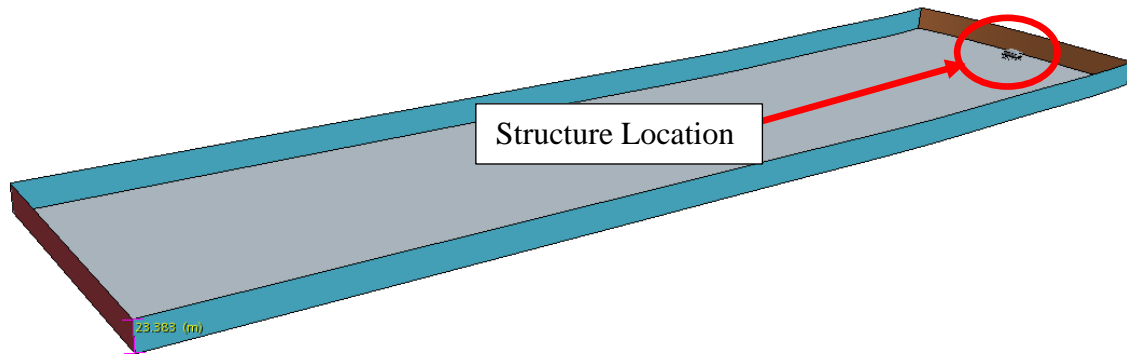
Figure 3-6. CFD flow domain (top hidden for clarity)

The dimensions of the flow domain were approximately 800-ft in the y-direction (i.e., parallel to the dunes) and approximately 3,500 ft. in the x-direction (i.e., perpendicular to the dunes). Once the flow domain had been established, an anisotropic meshing algorithm was developed using Star-CCM+'s built-in hexahedral meshing scheme (called the "trimmer" in Star-CCM+). Far from the free-surface, cell length was approximately 50 ft in the x and y directions; and approximately 6.5 ft in the z-direction. Closer to the free surface (i.e., plus or minus two wave heights), the x and y resolutions were reduced to approximately 25 ft in the x and y directions; and approximately 3 ft in the z-direction. Even closer to the free surface (i.e., plus or minus a wave height), the resolution was even further improved by reducing the x and y mesh dimensions to approximately 13 ft and by reducing the z mesh dimensions to approximately 1.5 ft. Then, close to the structure, two more refinement regions were added. Approximately half a structure width away from the structure, uniform mesh dimensions of 10 in. were used; and around the structure itself and approximately one-quarter of the structure width away from the structure, uniform mesh dimensions of approximately 5 in. were used. Because of the elevation change in the beach, the free surface refinement had the net effect of also continually improving resolution along the ground surface. In addition to this, a 7-cell thick prism layer was included throughout the domain using a minimum resolution of approximately 3 ft (adjusted proportionally in the refinement regions) Please see Fig. 3-7 through Fig. 3-9 for images associated with the mesh.
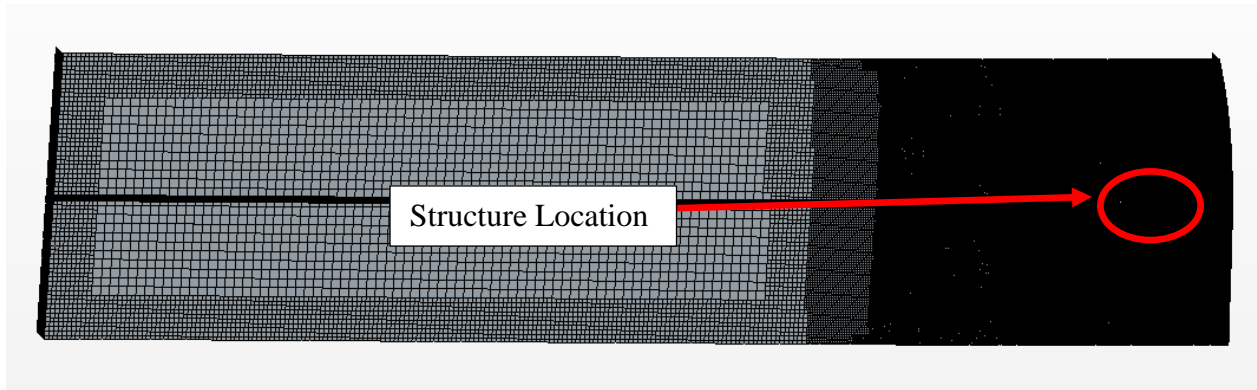
Figure 3-7. Top view of the mesh showing the entire flow domain
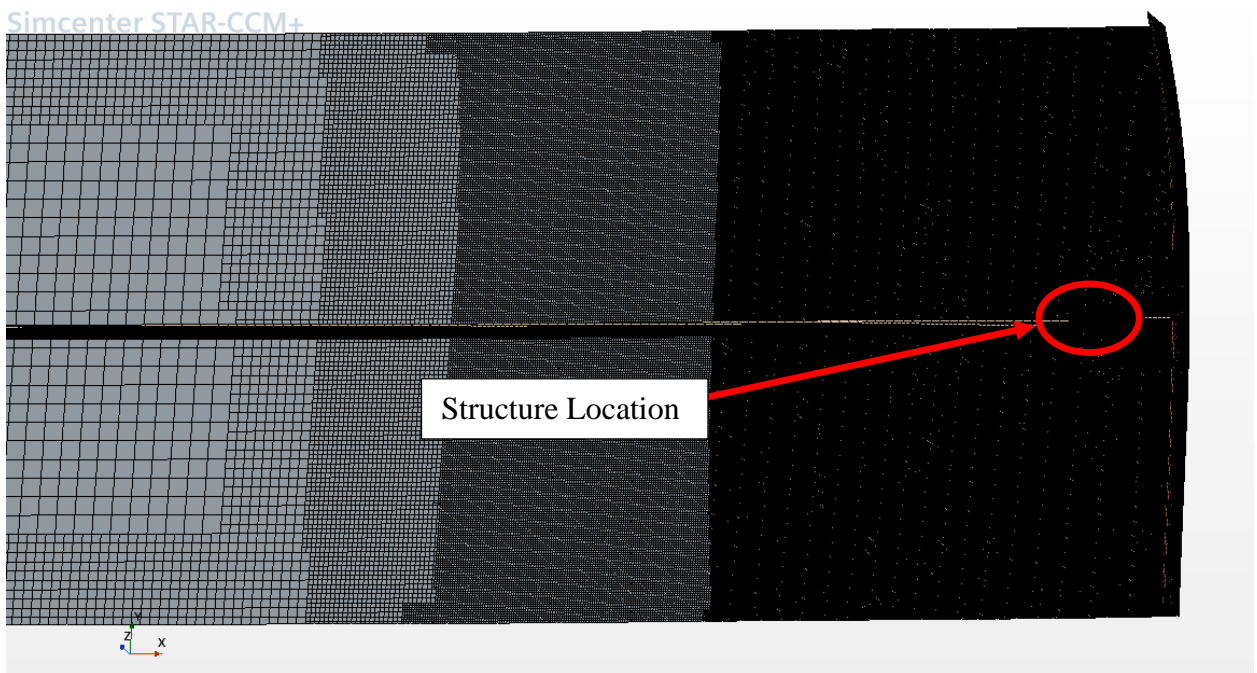
Figure 3-8. Top view of mesh zoomed in closer to the structure

The resultant mesh contained approximately 8.2 million cells. During the mesh convergence studies (please see below), meshes with approximately 4.4 million and 2.6 million cells were tested by proportionally enlarging each refinement area by 25% and 50% respectively.
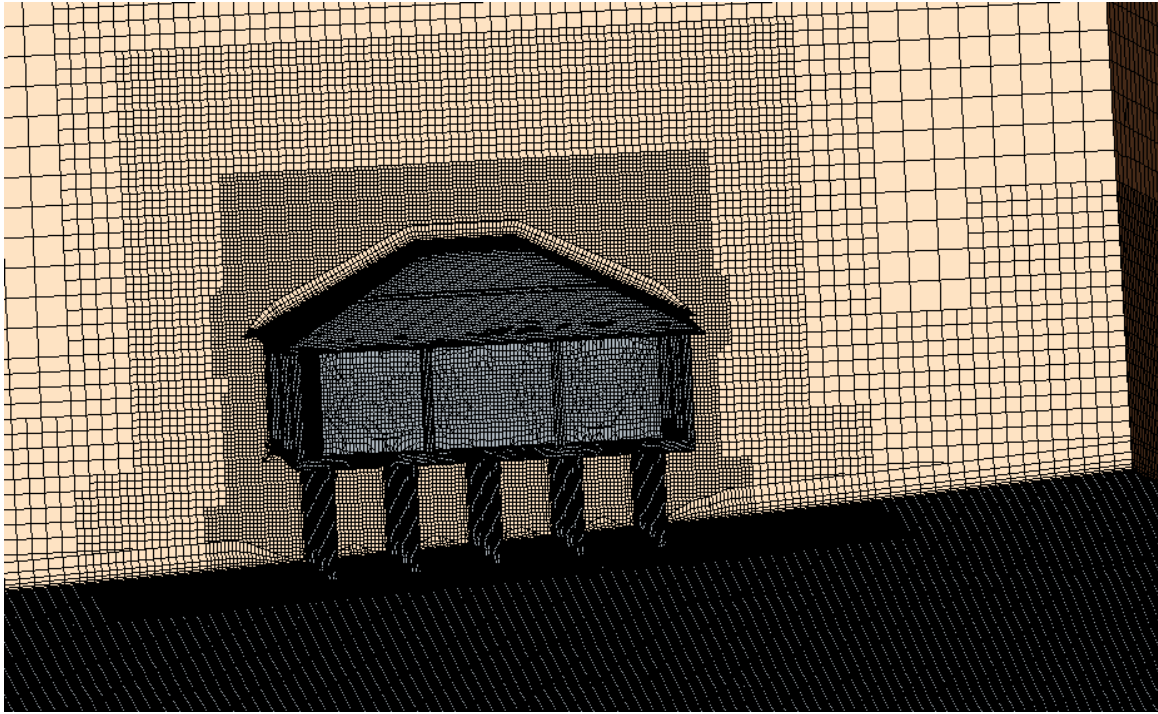
Figure 3-9. Side-view of mesh around structure

3.3.6 Boundary Conditions

The domain's vertical face on the left-hand-side of Fig. 3-6 (i.e., the vertical plane far from the structure) was specified as a "velocity inlet" where fifth-order wave boundary conditions were defined. The structure and bottom of the flow domain were considered "walls" where velocity components were set equal to zero and stresses were computed via the aforementioned all y+ wall treatment. The vertical face on the right-hand side of Fig. 3-6 (i.e., vertical plane close to the structure) was considered a "pressure outlet" where wave damping was specified. The planes of the domain perpendicular to the dune line were considered symmetry planes.

Along the top of the domain, several configurations were tested. First, investigators used a symmetry plane, but this led to unreasonable results in the sense that large computational errors were observed. The top of the domain was switched to a pressure outlet "vent" where atmospheric pressure was assumed. While this was effective from a wave forcing standpoint, its disadvantage was that any wind imparted onto the model also vented toward this artificial outlet. To account for this, the top of the domain was switched to a wall. While this technique prevented the wind from improperly "venting," its disadvantage was that wave production induced wind around the structure (due to continuity/conservation of mass) that tended to be significant. This could have been mitigated by extending the flow domain upward and downstream but doing so would have

significantly increased computational time. Instead, investigators ran two sets of models instead. The first set of models focused on wind forcing only while the second set of models focused upon wave forcing only and only forces on parts of the structure impacted by water were analyzed. The added advantage to this approach was that it allowed for a relatively straightforward comparison between the first-level wind/wave analyses and results from CFD.

The models with waves/no wind were initialized so that their front waves were approximately 300 ft from the structure – see Fig. 3-10 and Fig. 3-11.
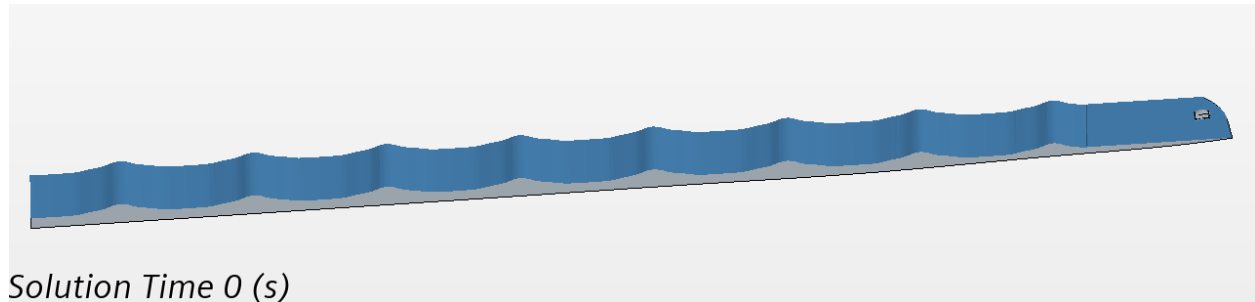
Figure 3-10. Model at initialization showing the entire flow domain
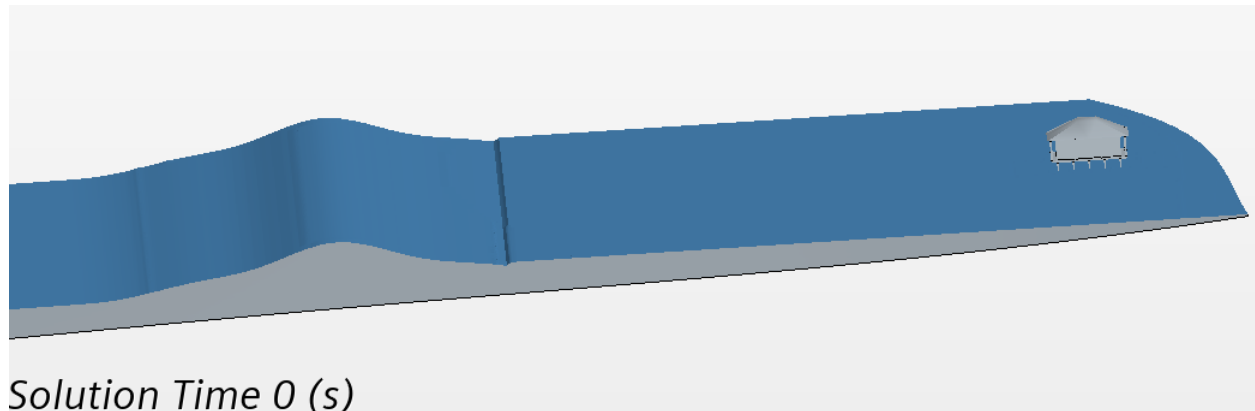
Figure 3-11. Model at initialization closer to the structure

Meanwhile, the models with wind/no waves were initialized with a steady (i.e., non-transient) wind both everywhere in the flow domain above the water surface and at the upstream velocity inlet.

3.4.7 Run Conditions

To provide a basis of comparison for the first-level analysis, the same conditions that were previously used in terms of wave periods, heights, water depths, etc. were used during CFD modeling. However, in an effort to simulate wind with respect to more storm-specific wind conditions, the wind speed was changed to 175 mph (compared to a 140-mph basic wind speed

from ASCE7). Star-CCM+'s implicit unsteady solver was used to solve the model using 10 iterations per timestep for a total of 60 second of total runtime per model. Results showed good residual convergence using an implicit timestep of 1 ms. A mesh sensitivity analysis was conducted using each model (i.e., wind/no wave and wave/no wind) to verify computational convergence.

3.4.8 Results Output

Forces were computed in the x, y, and z-directions on several subdivided portions of the structure. These portions were the:

- Floor
- Piles
- Roof
- 2nd Floor Columns
- Walls

These subdivisions are indicated below in Fig. 3-12 using Fig. 3-9 as a basis:
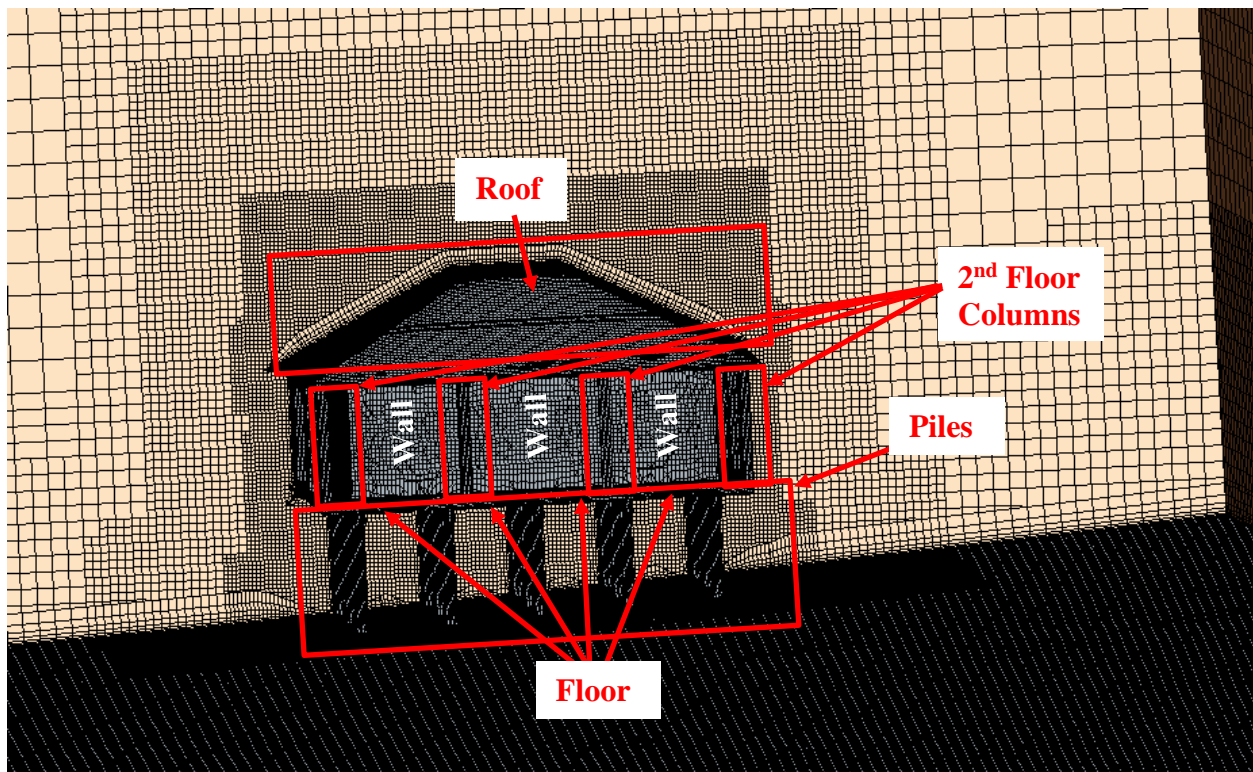
Figure 3-12. Force tracking subdivisions

3.5 CFD Results – Wind

Results for forces due to wind on the floor, roof, walls, and 2nd floor columns are shown below in Fig. 3-13 through Fig. 3-16 using each of the meshes studied during refinement. In addition, total force on the structure is presented in Fig. 3-17. As shown in these figures, lateral force (i.e., force in the x-direction), uplift force (i.e., force in the z-direction) on each component appeared to stabilize after approximately 30 seconds of modeled time. Likewise, total force on the structure in both the x and z directions appeared to become relatively stable after a similar period. As such, computational convergence was evaluated by plotting average total force on the structure as a function of cell resolution near the structure and fitting a best-fit regression line to the data of the form $y = ax + b$ where x is the cell resolution; y is the force on the structure; a and b are best-fit coefficients. The intercept associated with this line represents "perfect resolution." The error was computed as the percent difference between the best-fit regression line and total modeled force using the 8.2 million cell resolution. As shown in Fig. 3-18, computational errors were below 2 % in the x-direction and below 15% in the z-direction.
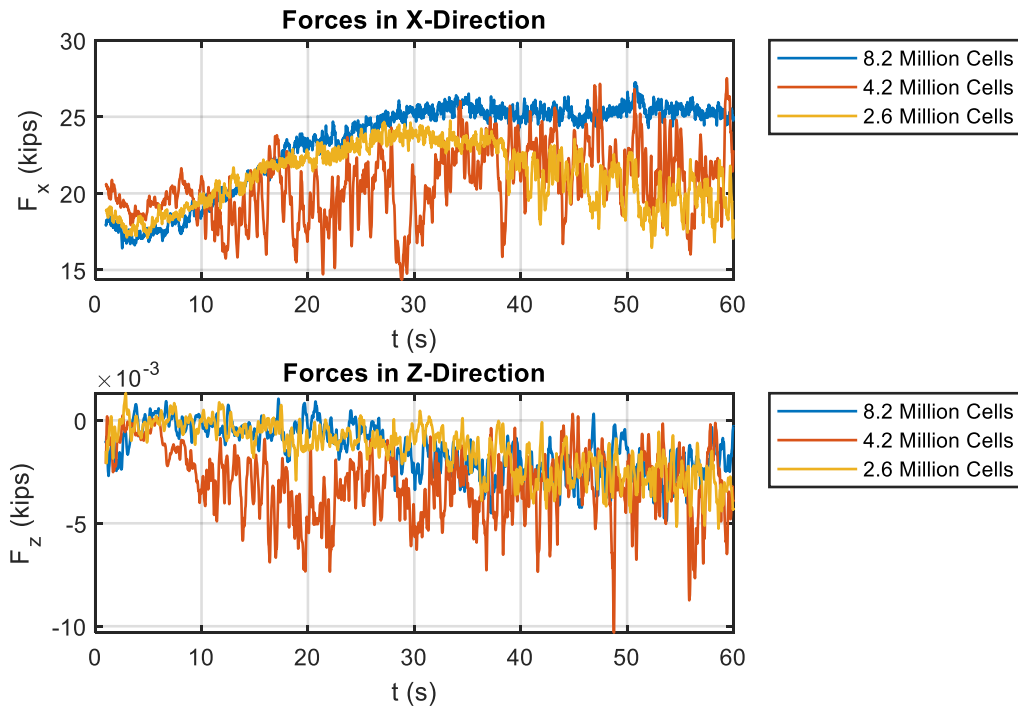
Figure 3-13. Results from CFD showing forcing on the wall due to wind

Figure 3-14. Results from CFD showing forcing on the roof due to wind

Figure 3-15. Results from CFD showing forcing on the 2nd floor columns due to wind

Figure 3-16. Results from CFD showing forcing the floor

Figure 3-17. Results from CFD showing total forcing on the structure due to wind
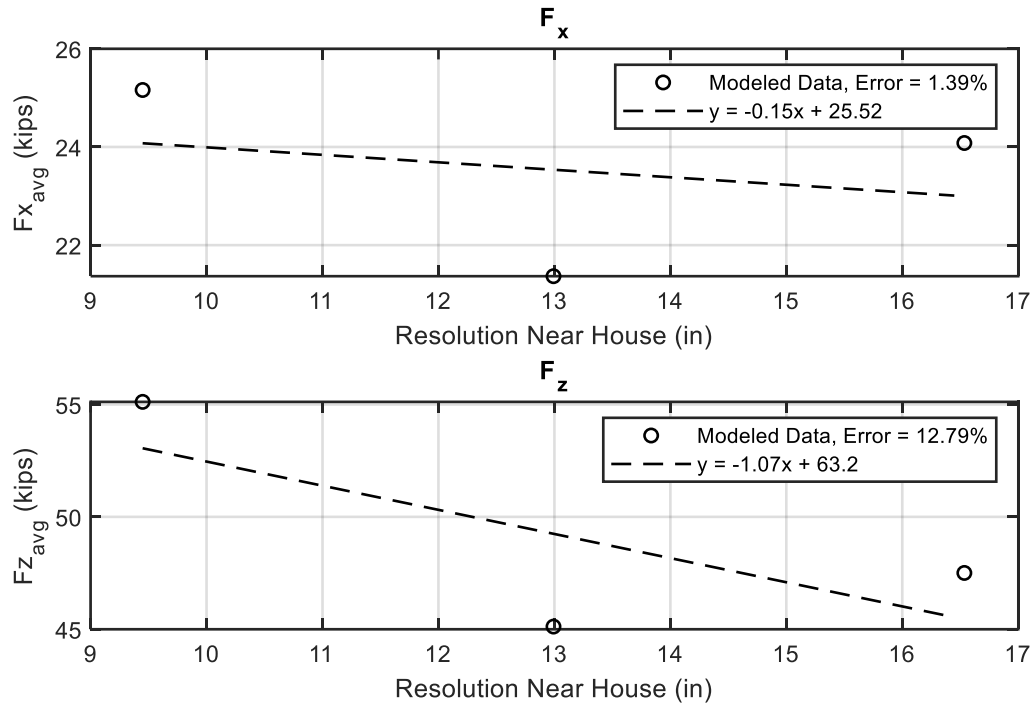
Figure 3-18. Results from CFD showing total averaged force after 30 s as a function of near-house mesh resolution

As shown in Fig. 3-18, the total force in the x-direction computed using CFD was approximately 25 k. This force is almost entirely due to the force on the walls as illustrated below in Fig. 3-19 and Fig. 3-20. Wall pressures compared well to wall pressures computed using first-level analysis. Furthermore, results indicated that ASCE7 computes a conservative value for the force on the structure. Recall that total pressure in ASCE7 is computed by adding the external pressures to the internal pressures. Since it is not possible to model internal pressures in CFD, the correct basis of comparison between the two methods is to compare the external pressure only. On the windward side of the structure, neglecting internal pressure, ASCE7 returns external pressures that range between 32 psf and 34 psf. On the windward structure face, CFD returns external pressures between approximately 25 psf and 36 psf. On the leeward side of the structure, ASCE7 returns a pressure of -20 psf compared to pressures ranging from -15 psf to -10 psf from CFD. Again, it is important to note that these results were obtained using a 175-mph wind speed compared to a 140-mph basic wind speed from ASCE7. Overall, then, for wall pressure, one may conclude that ASCE7 performs well/conservatively when compared to results from CFD.
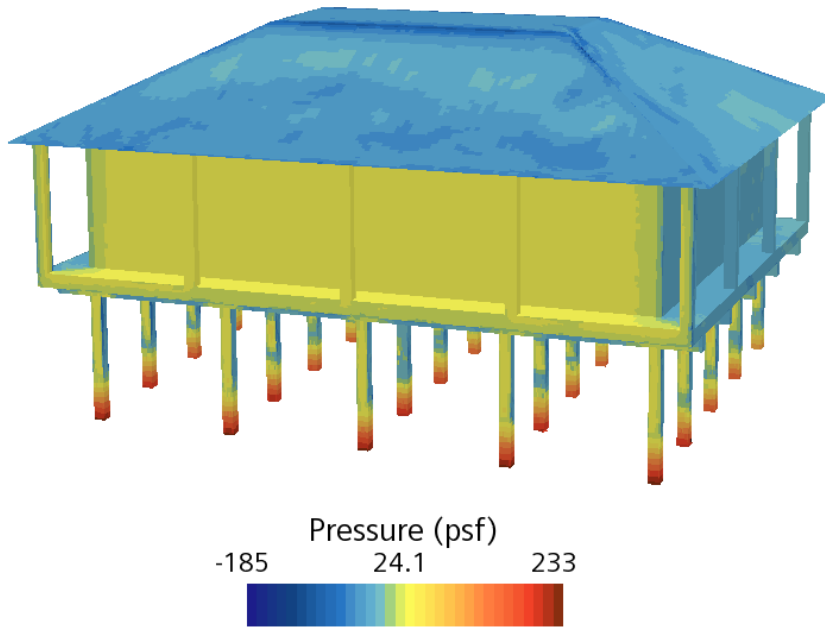
Figure 3-19. CFD pressure map on windward side of the structure
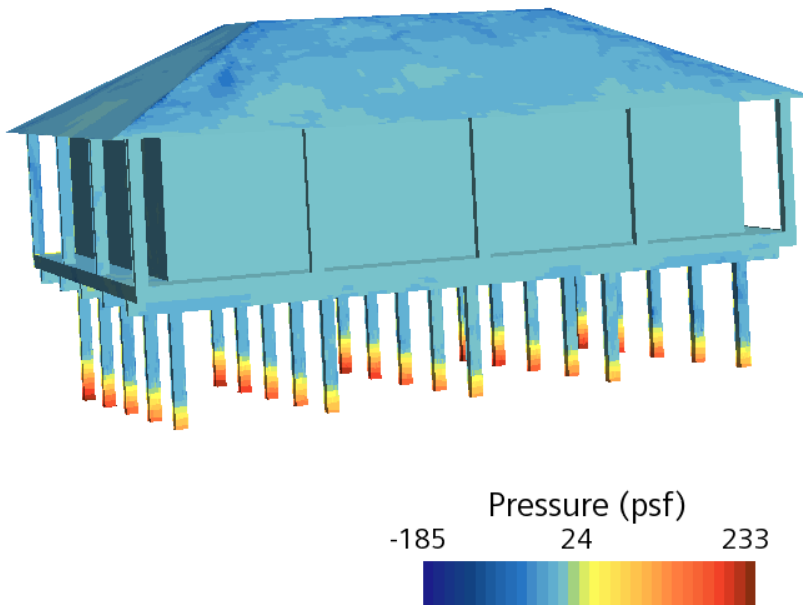
Figure 3-20. CFD pressure map on leeward side of the structure

A close-up of the structure's roof (Fig. 3-21) shows that CFD predicted the wind forcing on the structure to consist of an uplift force that acted in the net negative direction away from the structure. This contrasts with results from ASCE7 in the sense that ASCE7 predicted that the roof forcing would add to the lateral force on the overall structure (i.e., act in the positive x-direction). As such, the data suggest that ASCE7 performs well/conservatively for this structure when compared to results from CFD in the context of lateral loading on the structure.
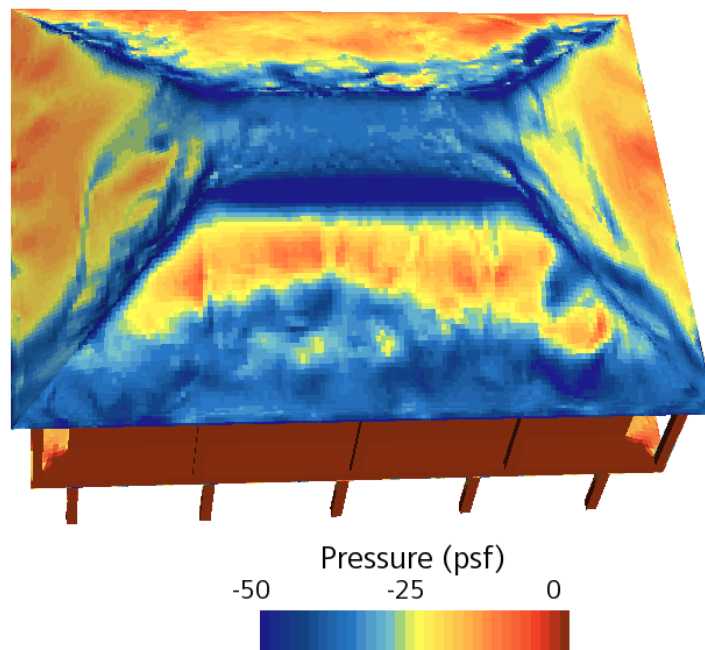
Figure 3-21. Close-up pressure map on structure roof (wind speed was from top-to-bottom)

3.6 CFD Results – Waves and Surge

3.6.1 Initial Water level

Results for forces due to wave on the floor, walls, 2nd floor columns, and ground-level piles are shown below in Fig. 3-22 through Fig. 3-25 using each of the meshes studied during refinement. In addition, a plot that shows total forcing on the structure is presented in Fig. 3-26.
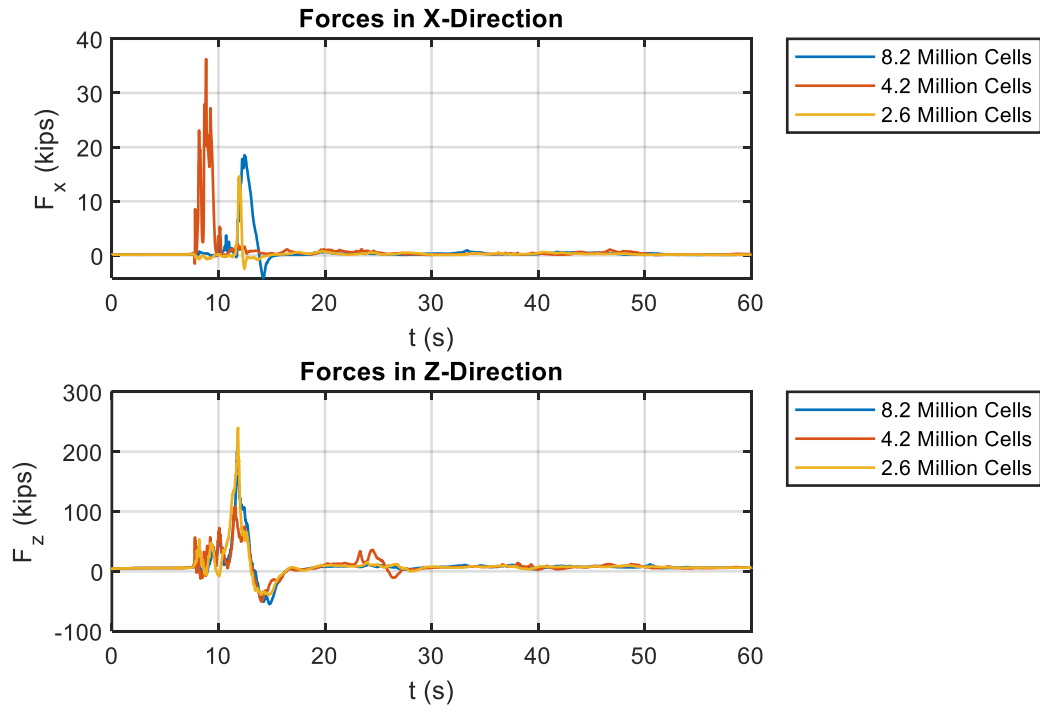
Figure 3-22. Results from CFD showing forcing on the floor due to waves
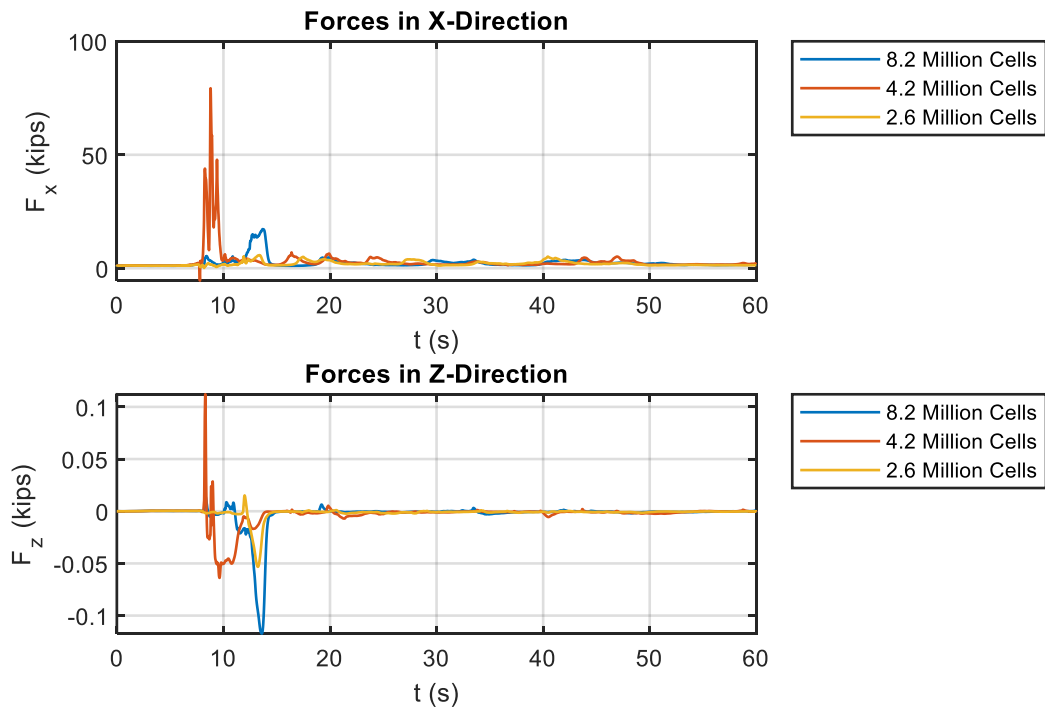
Figure 3-23. Results from CFD showing forcing on the walls due to waves
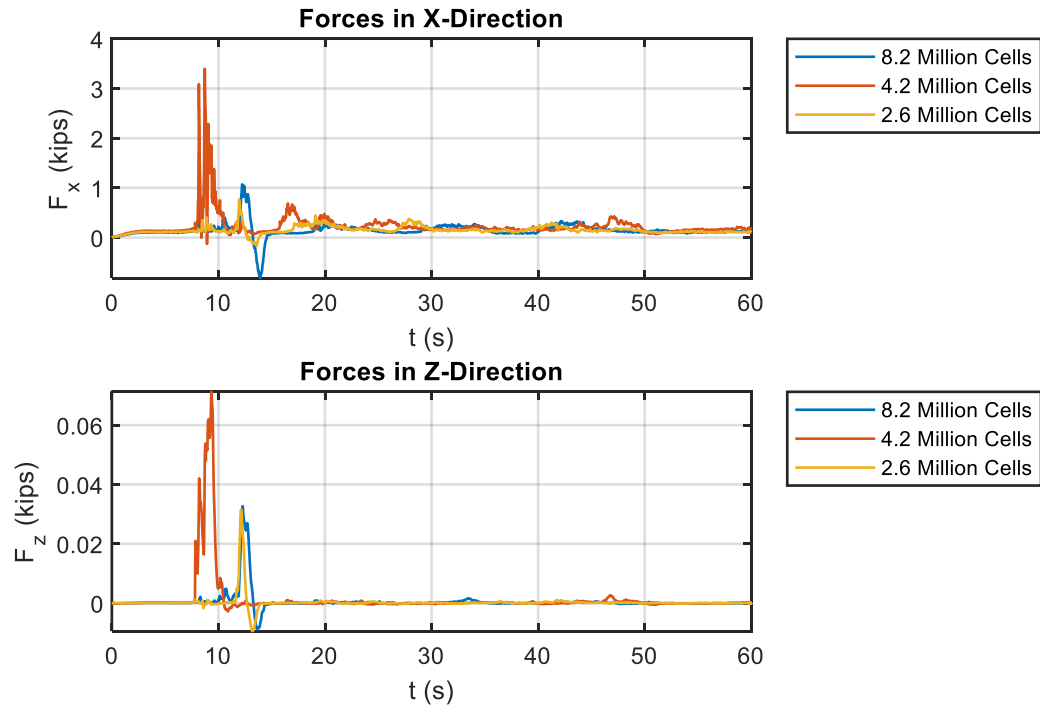
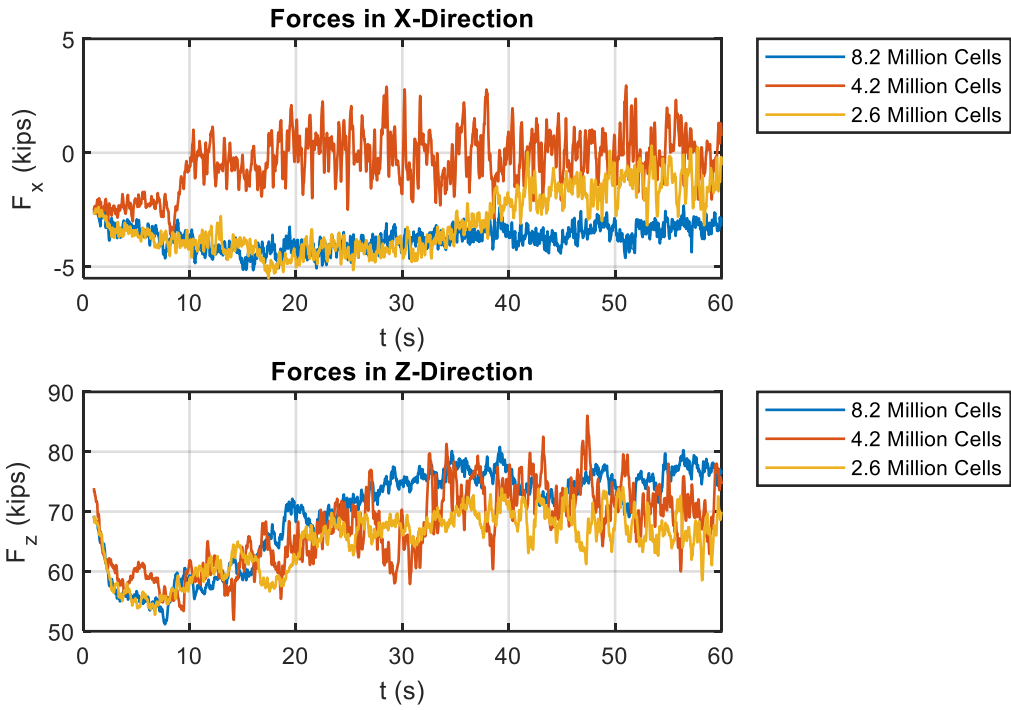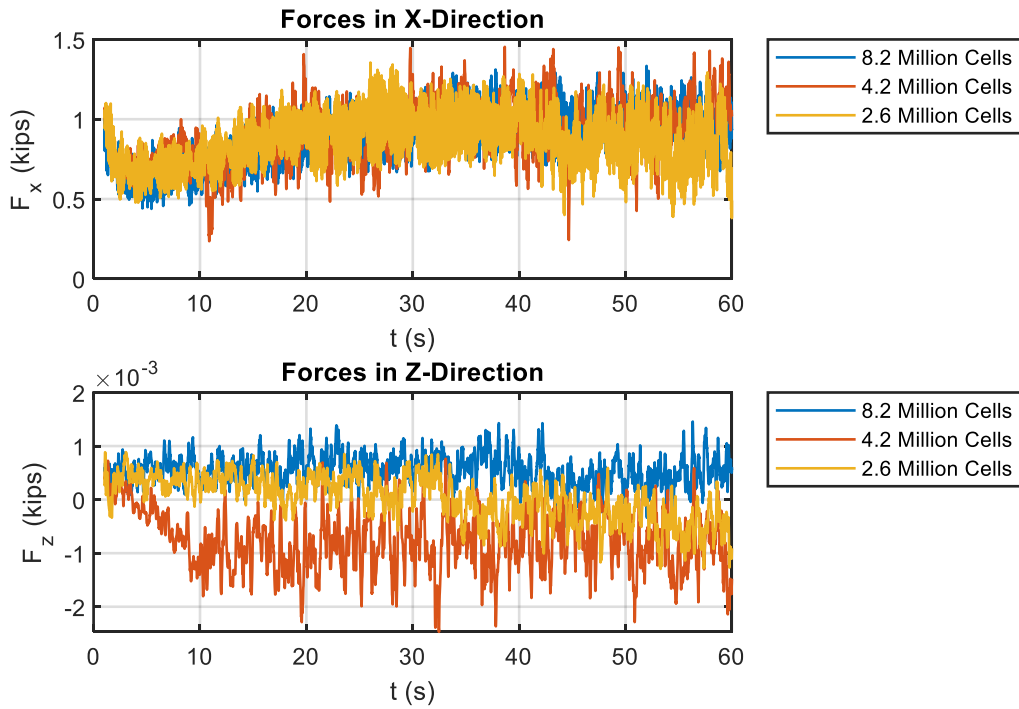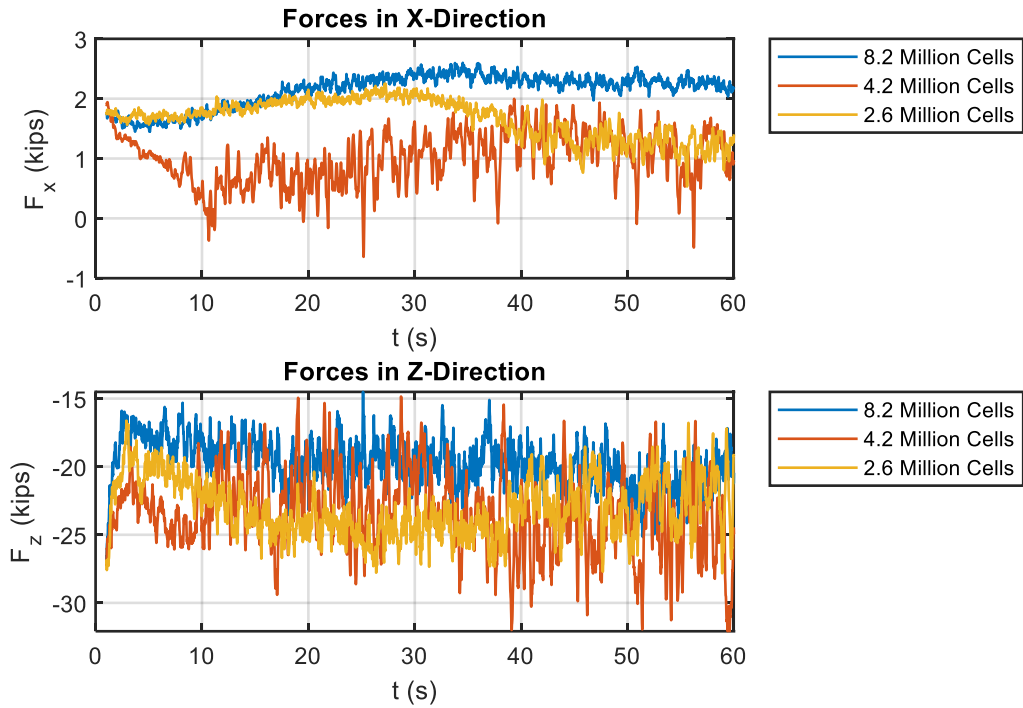Figure 3-24. Results from CFD showing forcing on the 2nd floor columns due to waves
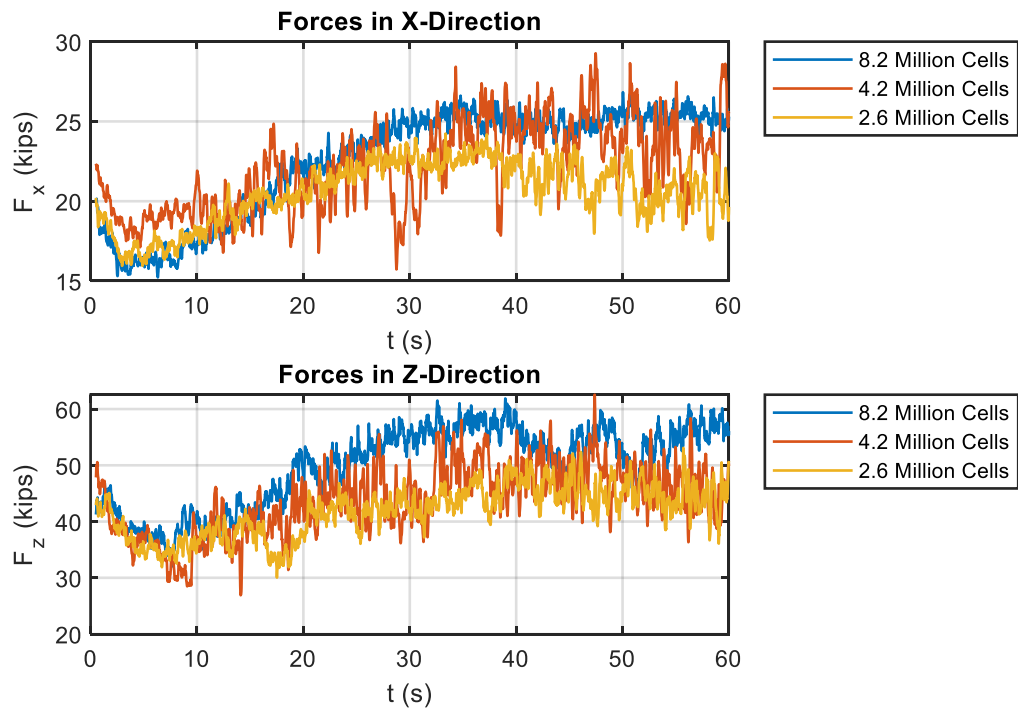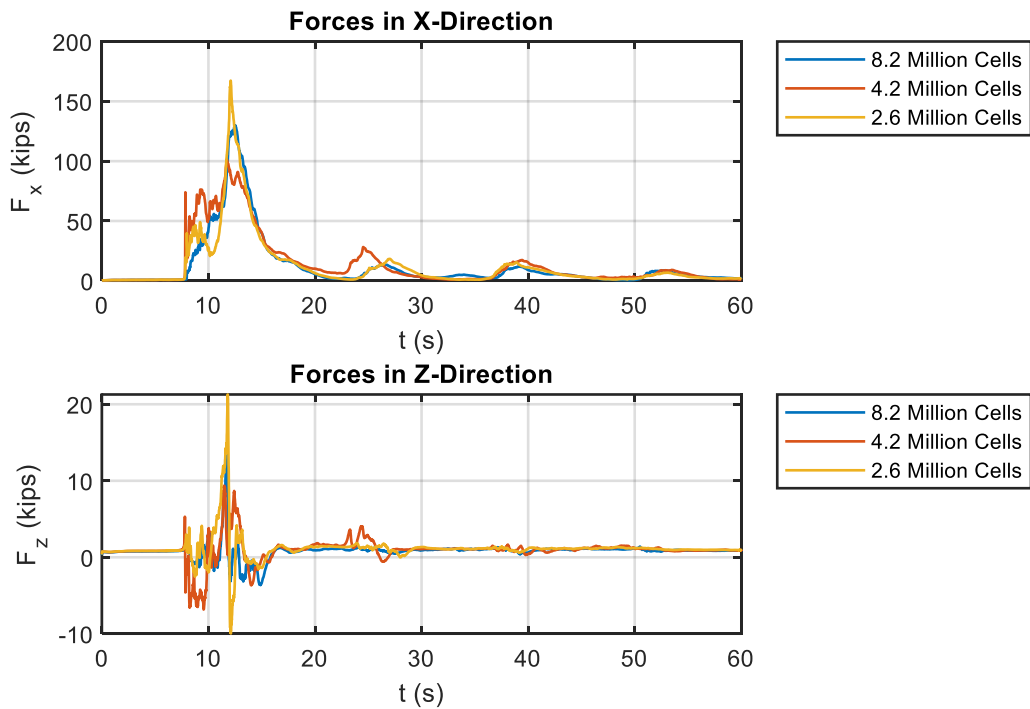

Figure 3-25. Results from CFD showing forcing on the piles due to waves
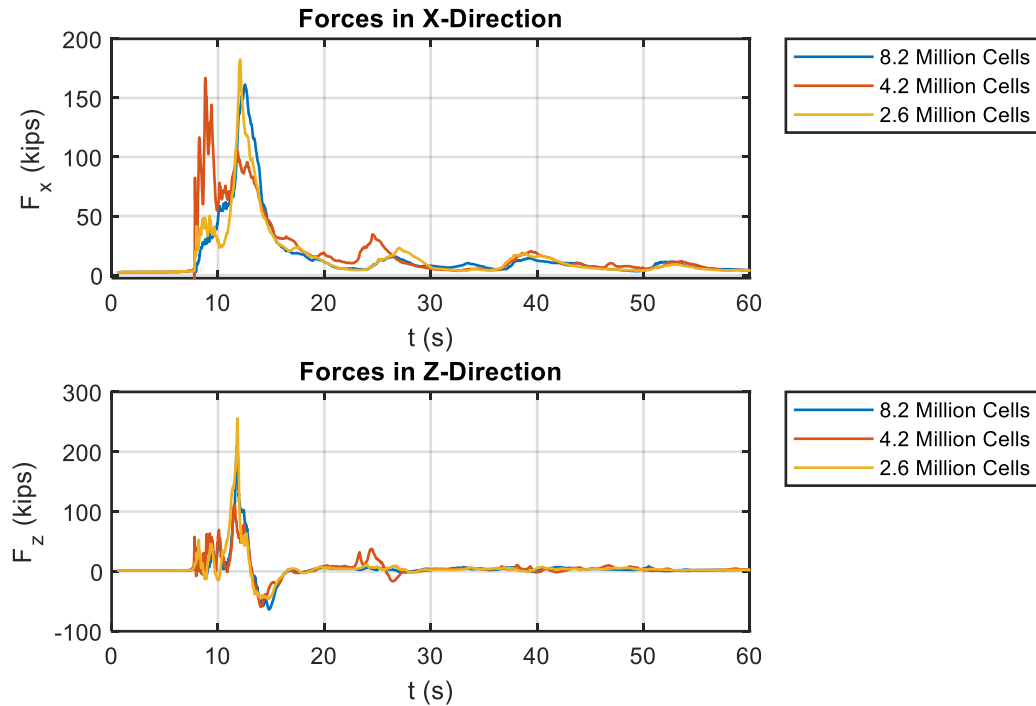
Figure 3-26. Results from CFD showing total forcing on the structure due to waves

Upon first glance, results appear to indicate that the Morison-style and quasis-static pressure integration approaches for computing lateral wave loading on the structure significantly underrepresented results from CFD because forces due to the first wave through the structure are almost an order of magnitude higher than were computed using these analyses. One might further conclude that the FEMA method was more accurate. However, one must consider how the model was initialized. In modeled time, at $t = 0$, the first wave was positioned approximately 300 ft from the structure. This wave was "fully formed" in the sense that its prespecified wave height wave was fully realized in the flow domain. In reality though, waves are depth-limited and will tend to break when their wave height exceeds approximately 78% of the water depth. As such, the first three waves in the wave train should be treated skeptically since they probably should not physically exist. On the other hand, the 4th wave in the wave train had the opportunity to fully runup the beach and begin the breaking process before they reached the structure. This would be much more indicative of conditions in the field during Hurricane Michael. As such, subsequent analysis involved using the 4th wave from the wave train (i.e., when t was greater than 30 seconds). Close-ups of wave forcing due to the 3rd and 4th wave of the wave train are presented below in Fig. 3-27 through Fig. 3-31. Maximum fourth wave data from Fig. 3-31 were used to develop a plot

between mesh resolution and forcing; and computational error was computed using the same method described earlier for wind (Fig. 3-32). As shown below, computational error was low (less than 2%) in the x-direction and was reasonably low (less than 15%) in the z-direction.
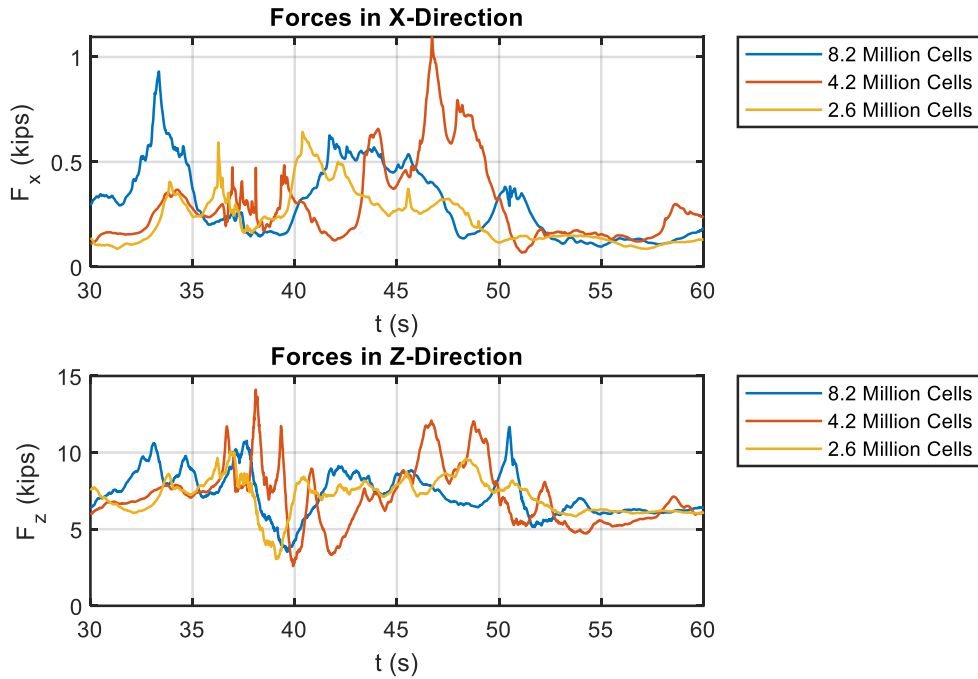
Figure 3-27. Results from CFD showing forcing on the floor due to waves (3rd and 4th wave only)
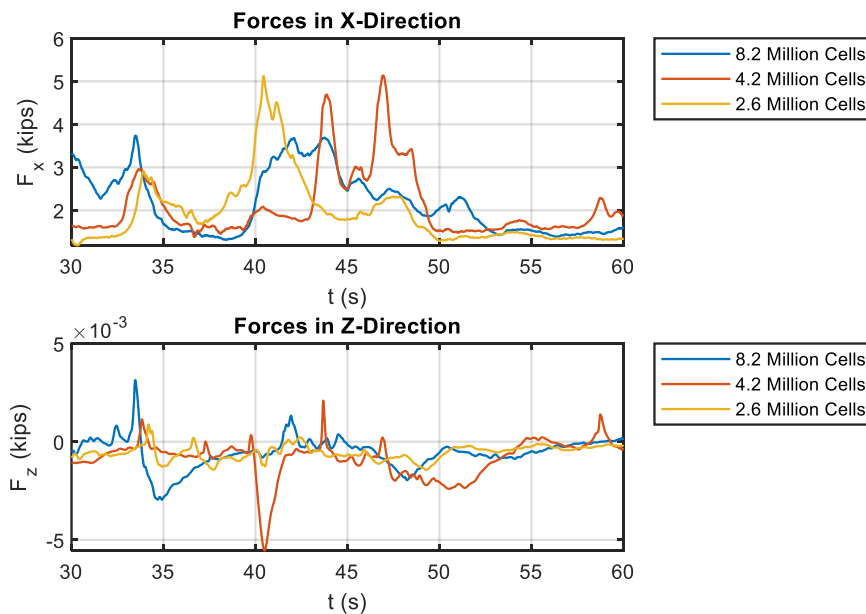
Figure 3-28. Results from CFD showing forcing on the wall due to waves (3rd and 4th wave only)
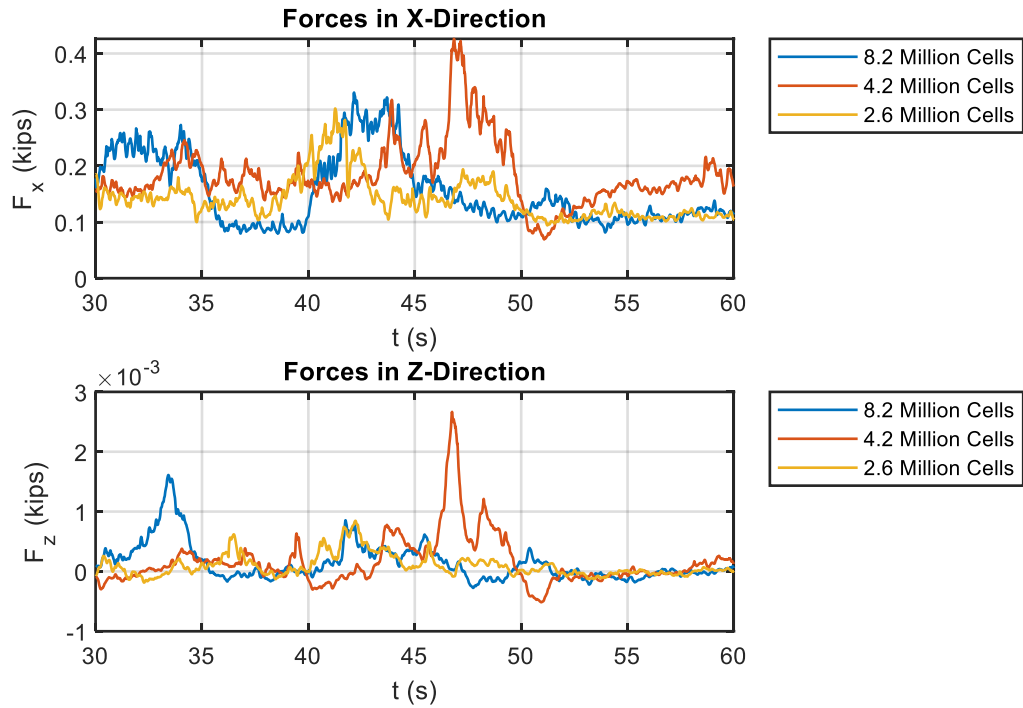
Figure 3-29. Results from CFD showing forcing on the 2nd floor columns due to waves (3rd and 4th wave only)
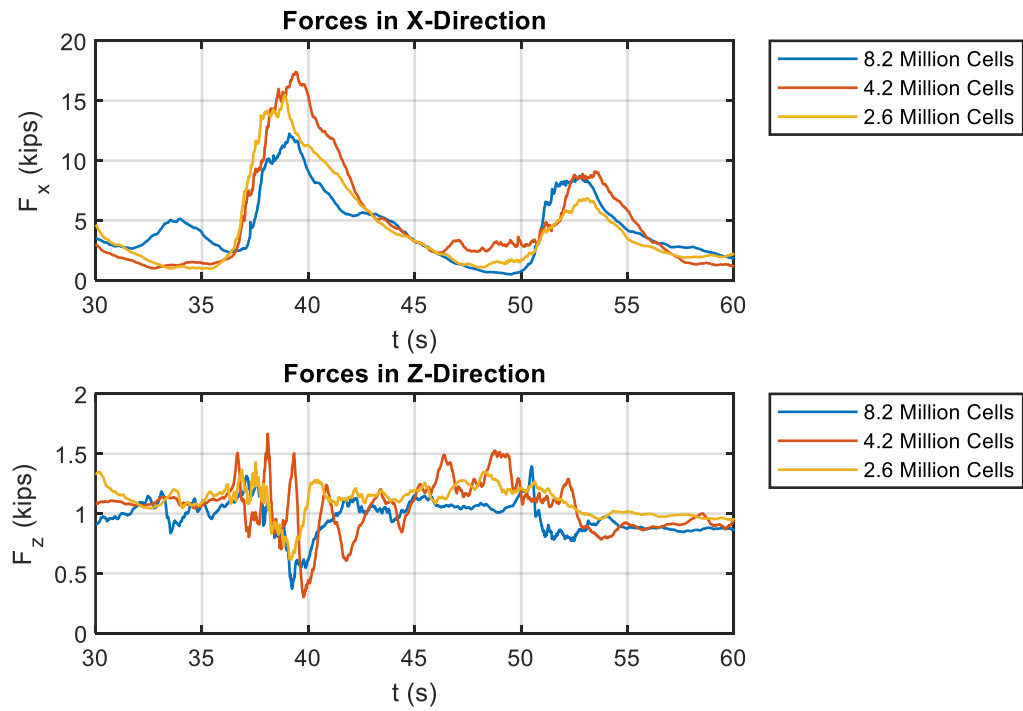
Figure 3-30. Results from CFD showing forcing on the piles due to waves (3rd and 4th wave only)
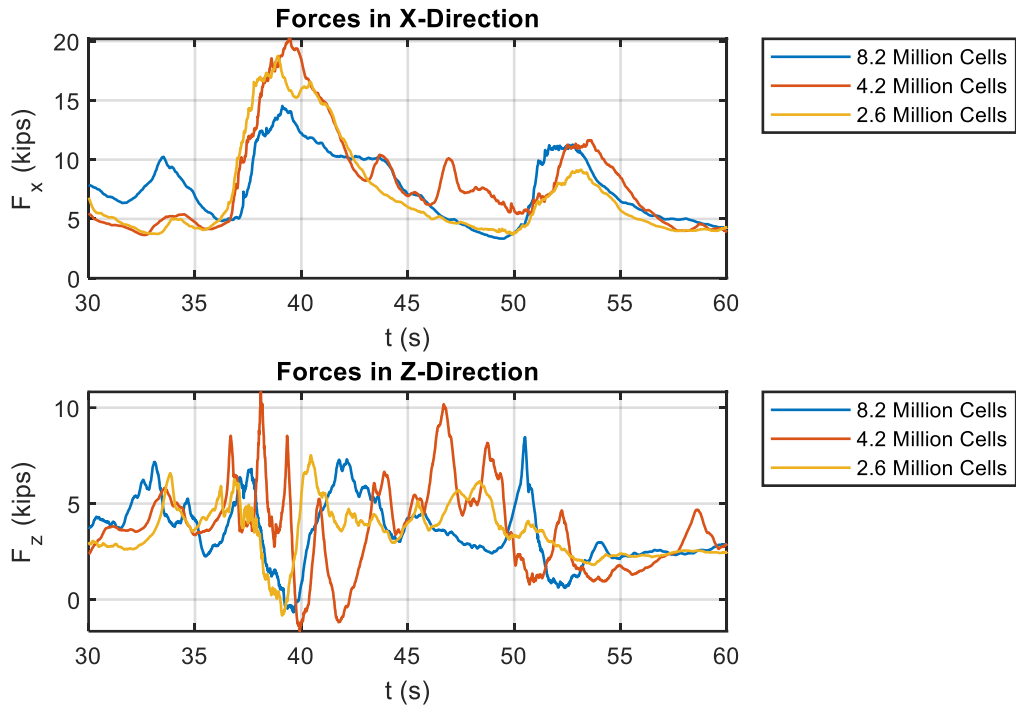
Figure 3-31. Results from CFD showing total forcing on the structure (3rd and 4th wave only)
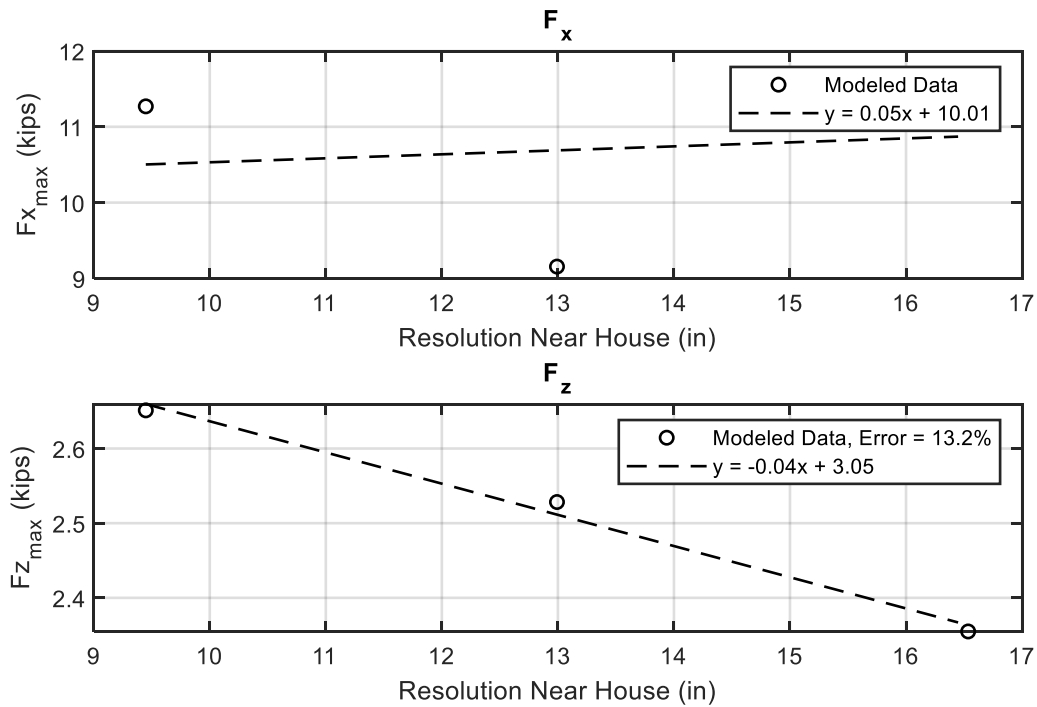
Figure 3-32. Results from CFD showing maximum fourth wave force as a function of near-house mesh resolution

Overall, results suggest that the quasi-static pressure integration and Morison-style methods for computing lateral loading due to waves on the structure performed well in the sense that these first-level analysis results were very conservative when compared to CFD. CFD results suggest that lateral loading due to waves was between 12 k and 13 k. Meanwhile, first-level results suggested that the wave forcing on the structure was approximately 30 k using a pressure integration approach and approximately 20 k using a Morison-style approach with assumed drag and inertial coefficients. Results from the FEMA method were closer to first-wave results, and as disussed, these waves would likely have broken before they reached the structure.

3.6.2 Additional Water levels

Data suggested that for environmental loading, methods outlined by the Florida Building Code perform well/conservatively. As will be discussed below in Chapter 4, using the first-level loads on the structure may produce pile failure below the ground surface. However, finite element analysis (FEA) results did not produce failure *above* the ground surface like the failures that were observed at Mexico Beach after Hurricane Michael. As such, additional water levels were modeled whereby the initial still-water elevation was increased in 1.6-ft (0.5-m) increments from its presumed position (i.e., +15.6 ft NAVD). Since the 8.2-million cell model had already been established to be relatively computationally accurate, it was used for all these additional runs. As before, force was computed on each structural sub-area (i.e., floor, walls, etc.), and these forces were added together to compute the total force on the structure in both laterally and upward. Plots of these results are presented below for each water level (Fig. 3-33 through Fig. 3-38). Zoomed-in plots are presented for the 3rd and 4th wave Fig. 3-39 through Fig. 3-44) while a plot showing maximum force of the 4th wave as a function of water-elevation is presented in Fig. 3-45. Included in Fig. 3-45 are best-fit regression curves through the data. As shown in the figure, lateral force appeared to increase linearly with initial water depth while a 2nd order polynomial trend was observed for uplift force as a function of depth.
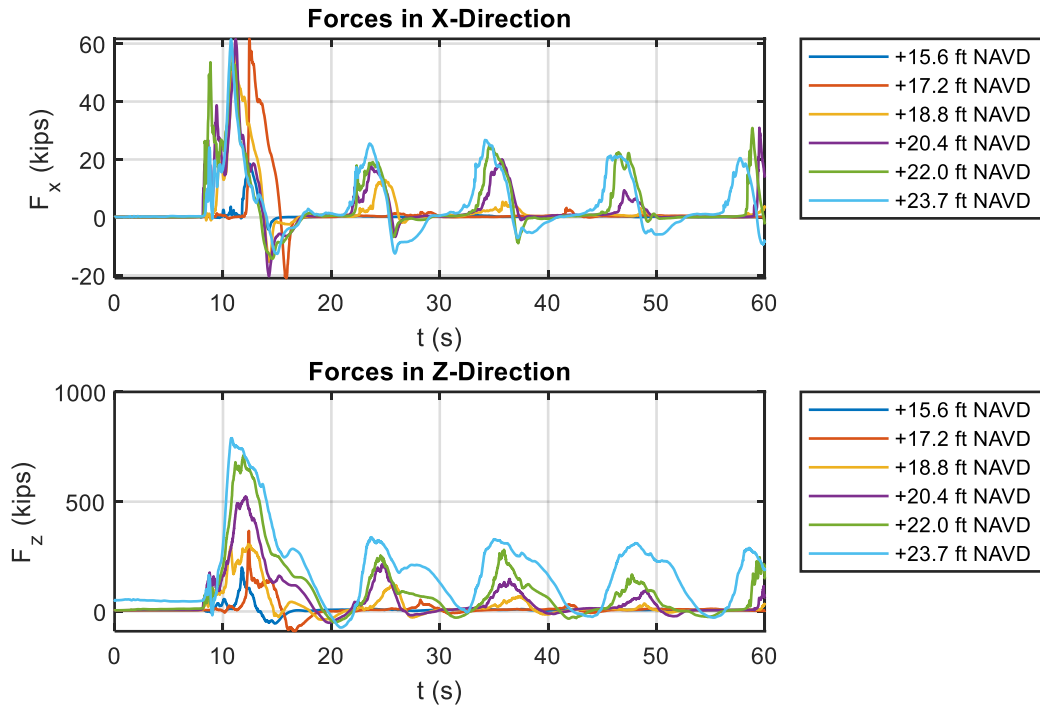
Figure 3-33. Results from CFD showing forcing on the floor due to waves for several initial water-elevations
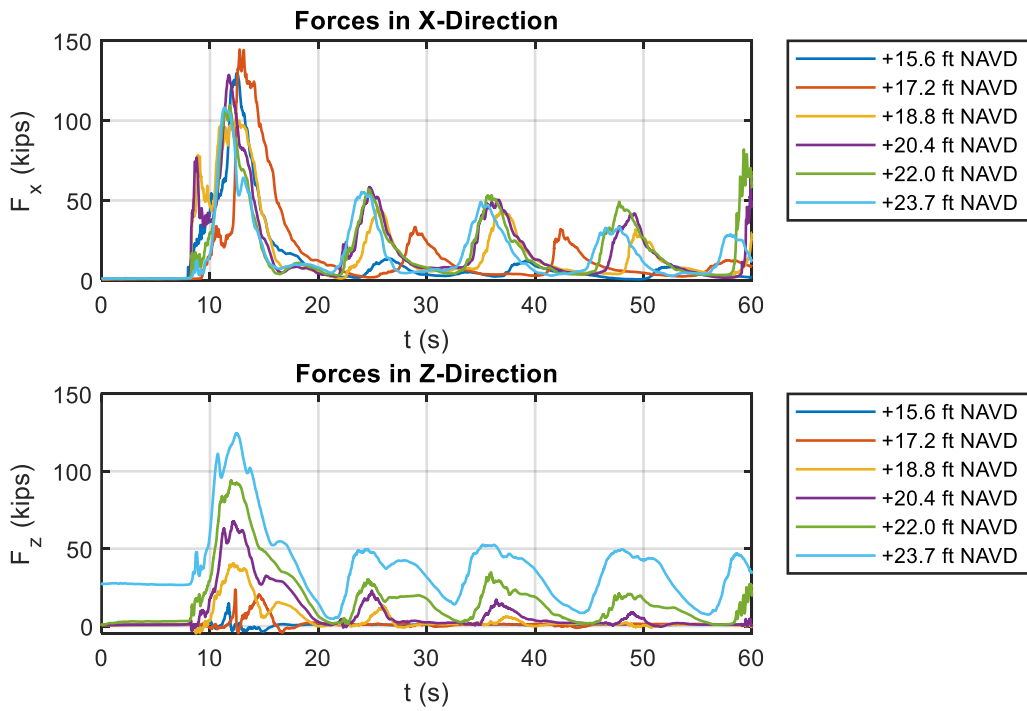
Figure 3-34. Results from CFD showing forcing on the piles due to waves for several initial water-elevations
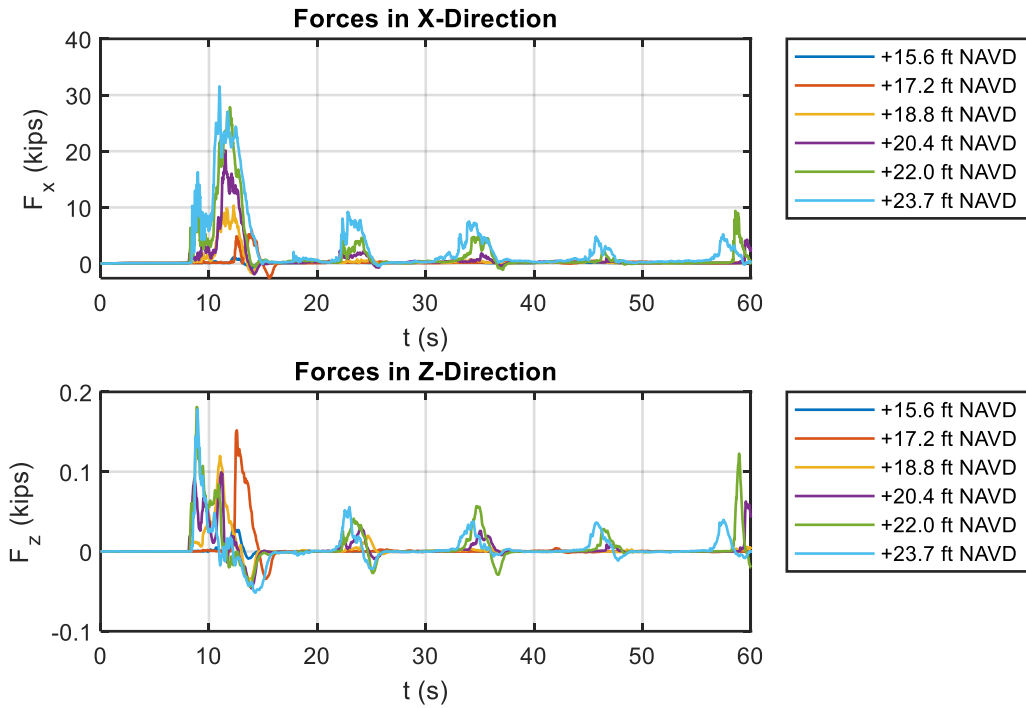
Figure 3-35. Results from CFD showing forcing on the 2nd floor columns due to waves for several initial water-elevations
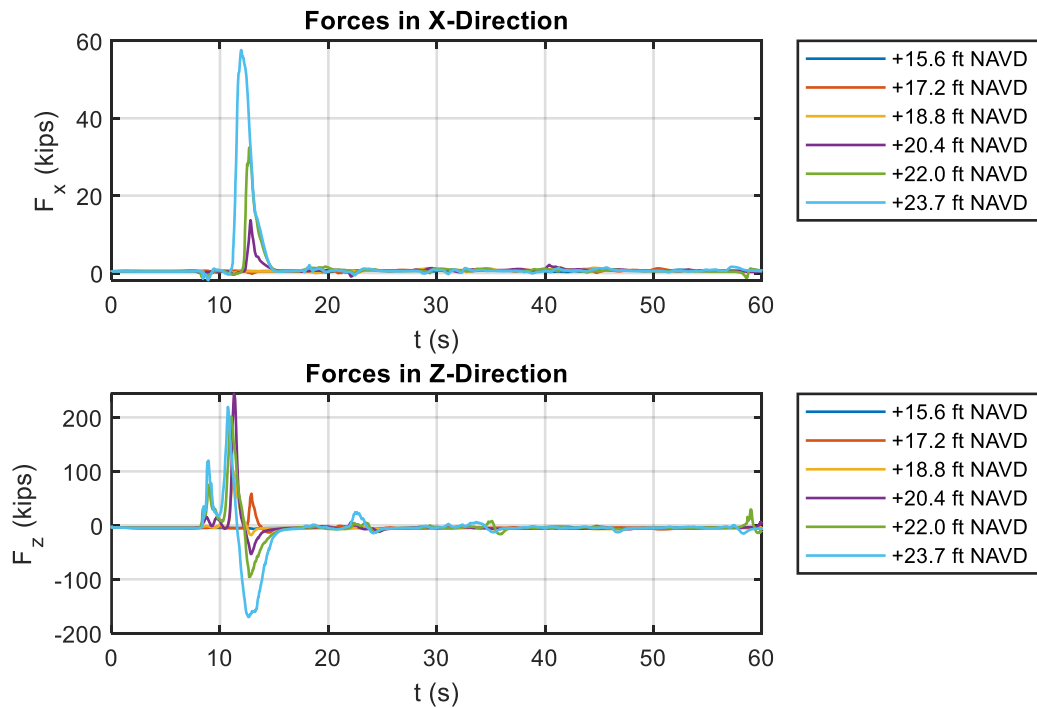
Figure 3-36. Results from CFD showing forcing on the roof due to waves for several initial water-elevations
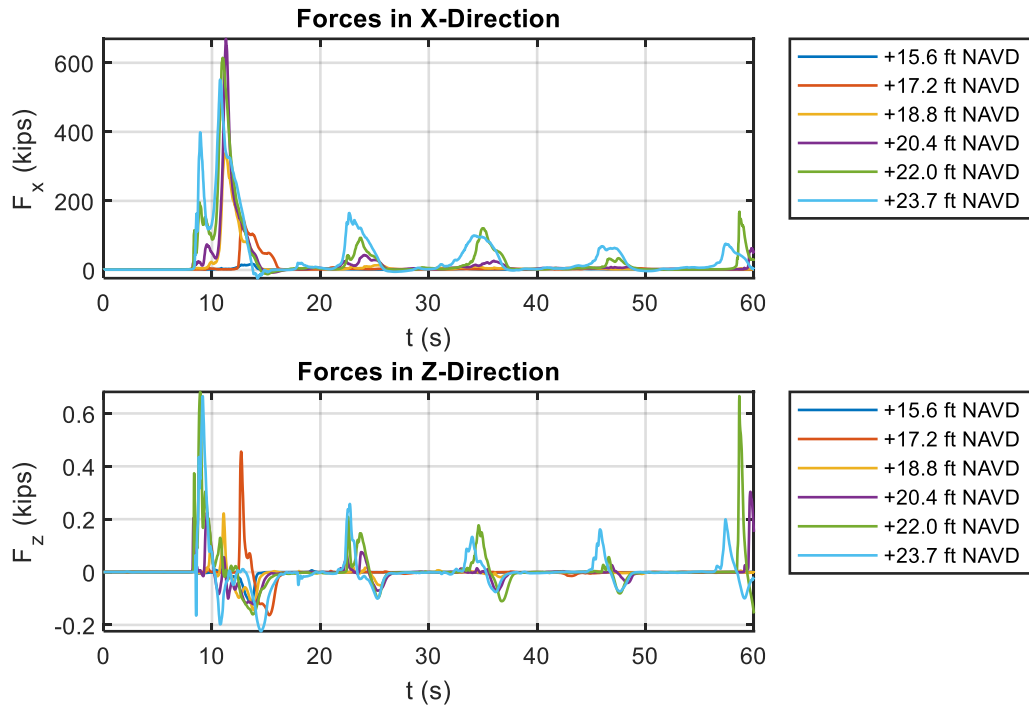
Figure 3-37. Results from CFD showing forcing on the walls due to waves for several initial water-elevations
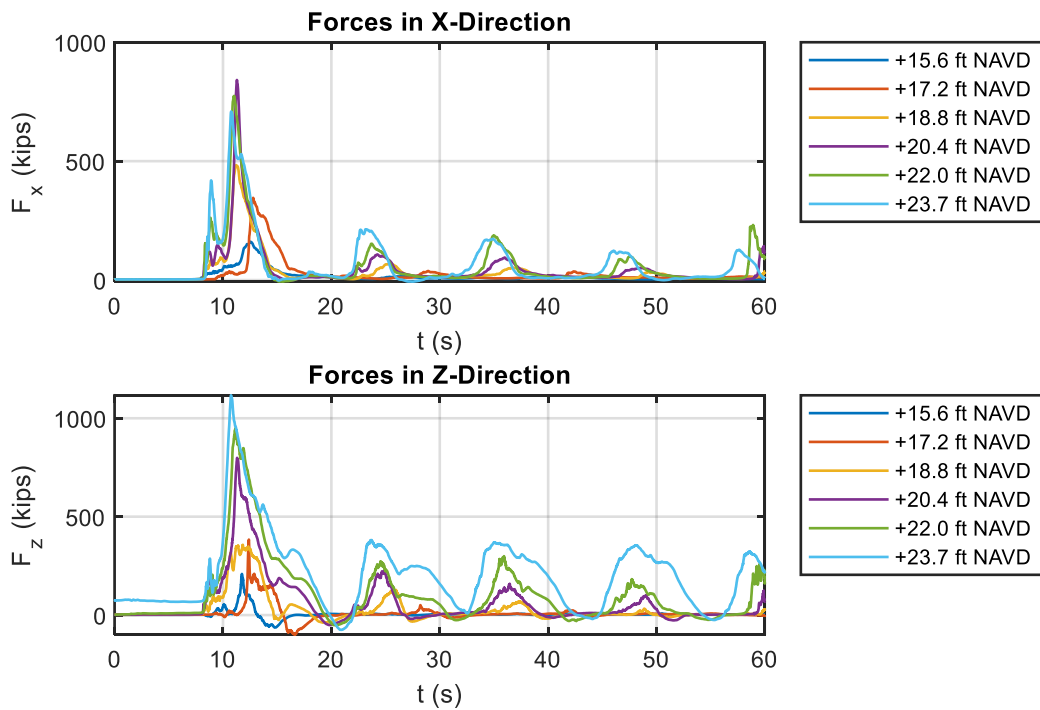
Figure 3-38. Results from CFD showing total forcing on the structure due to waves for several initial water-elevations
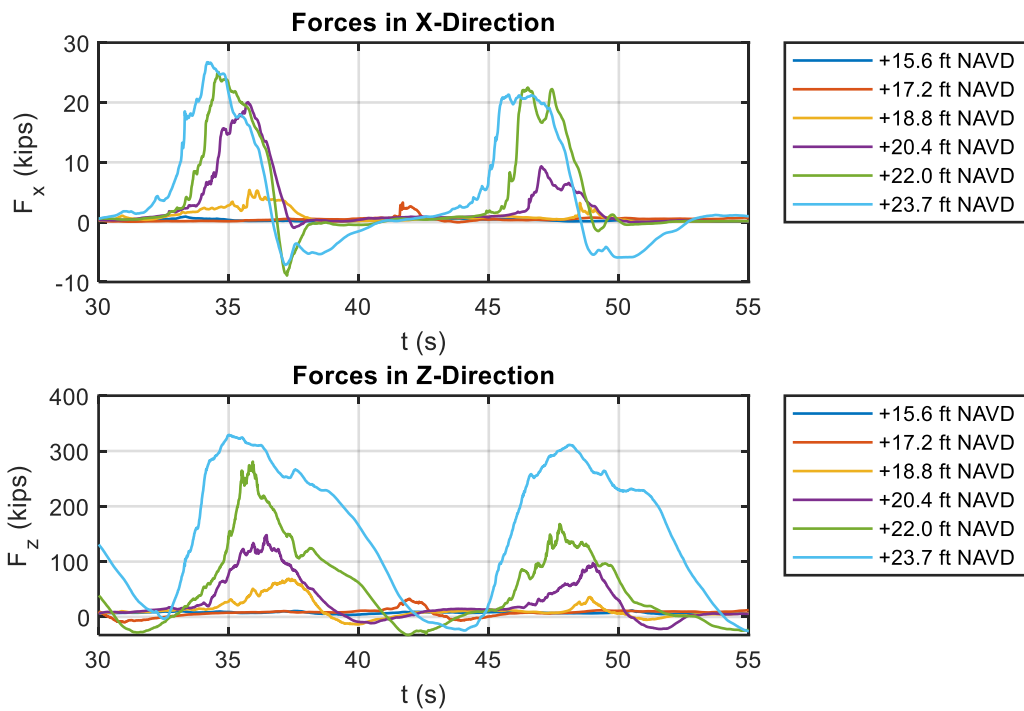
Figure 3-39. Results from CFD showing forcing on the floor due to waves for several initial water-elevations (3rd and 4th wave only)
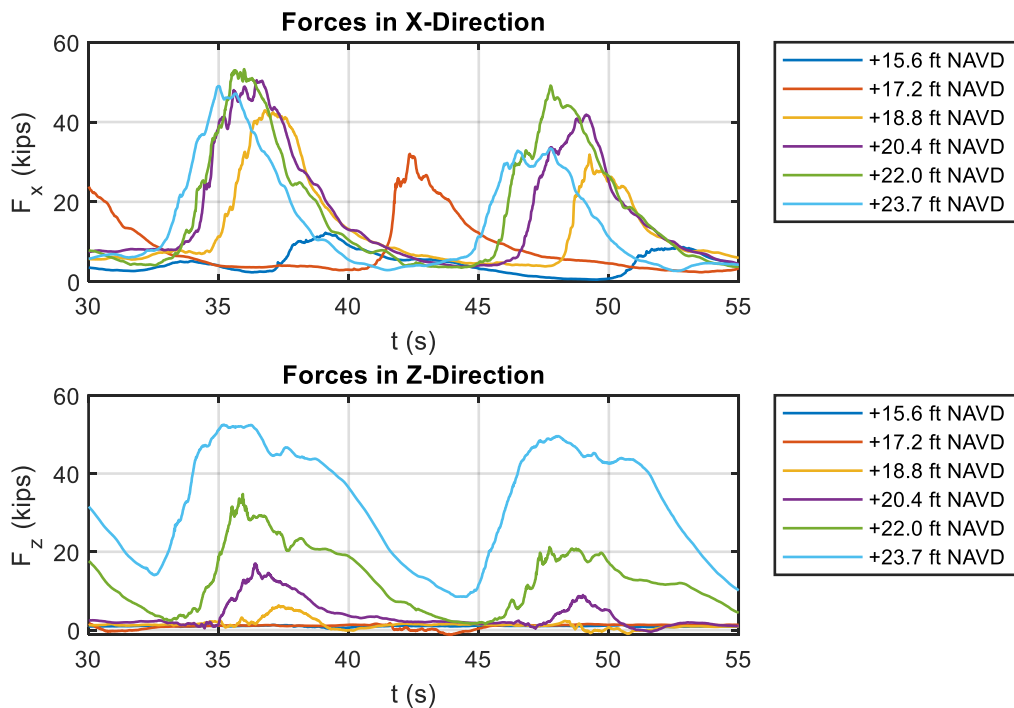
Figure 3-40. Results from CFD showing forcing on the piles due to waves for several initial water-elevations (3rd and 4th wave only)
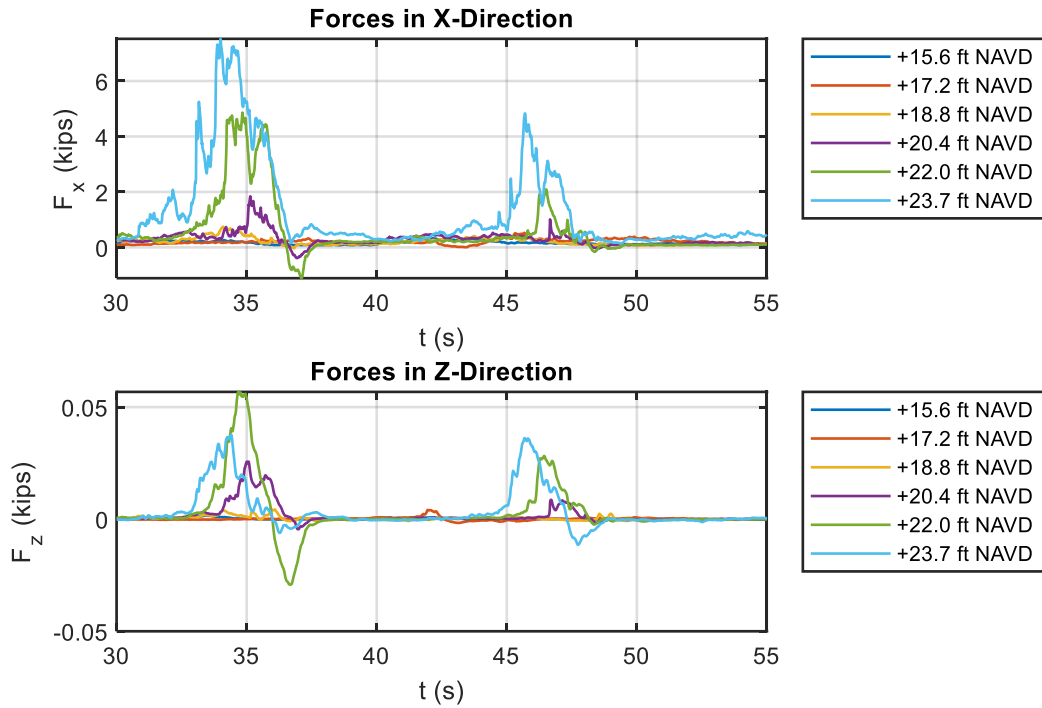
Figure 3-41. Results from CFD showing forcing on the 2nd floor columns due to waves for several initial water-elevations (3rd and 4th wave only)
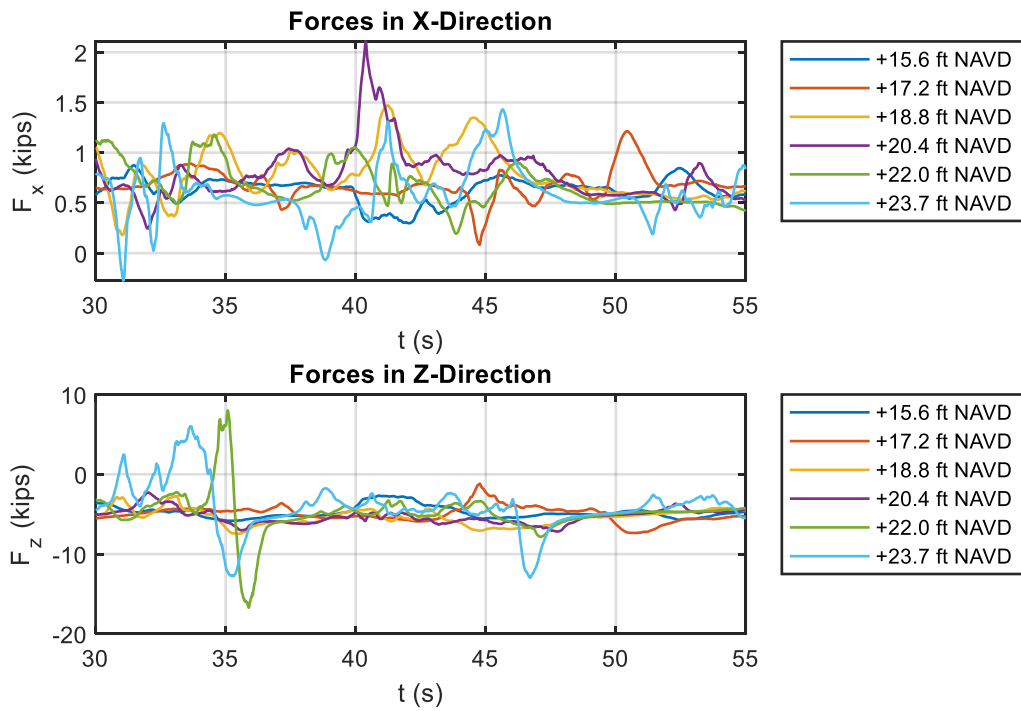
Figure 3-42. Results from CFD showing forcing on the roof due to waves for several initial water-elevations (3rd and 4th wave only)
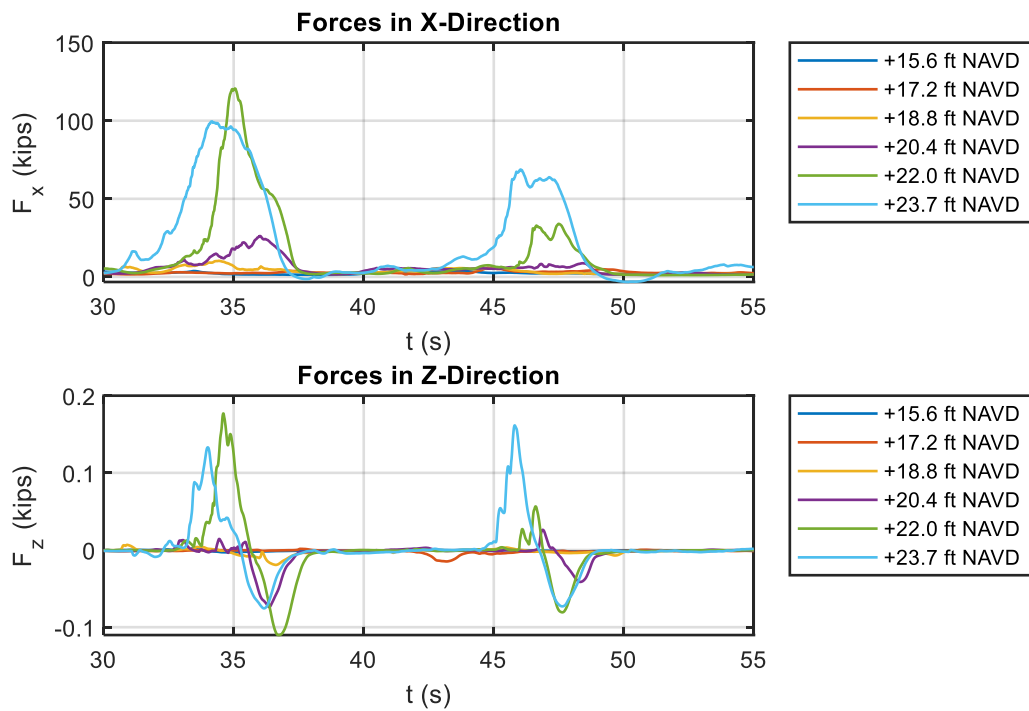
Figure 3-43. Results from CFD showing forcing on the wall due to waves for several initial water-elevations (3rd and 4th wave only)
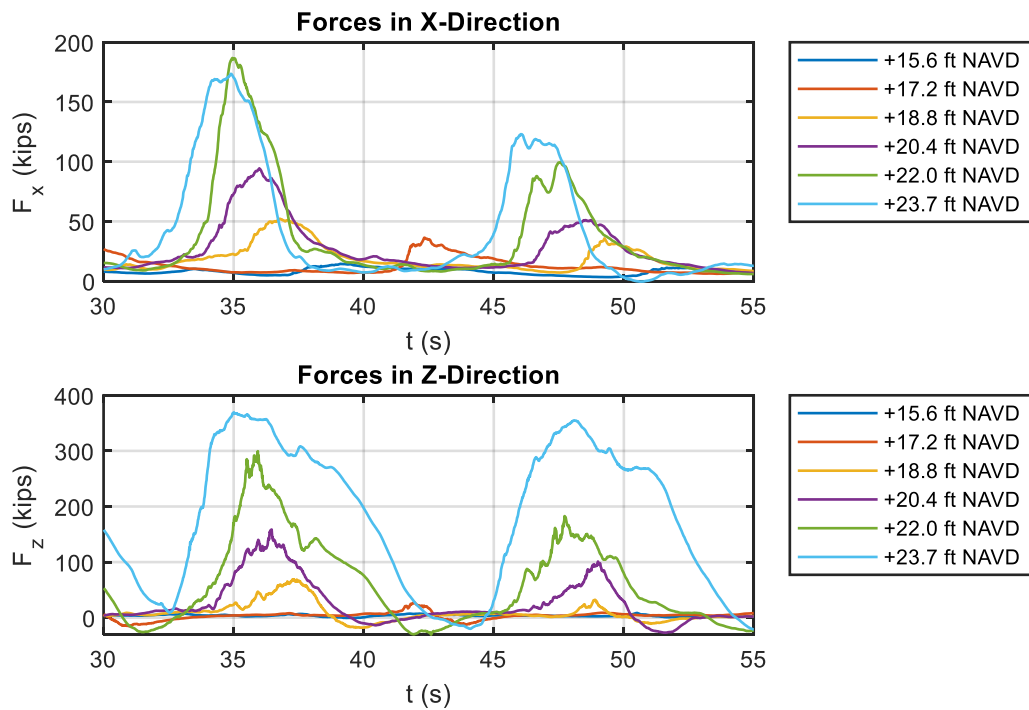
Figure 3-44. Results from CFD showing total forcing on the structure due to waves for several initial water-elevations (3rd and 4th wave only)
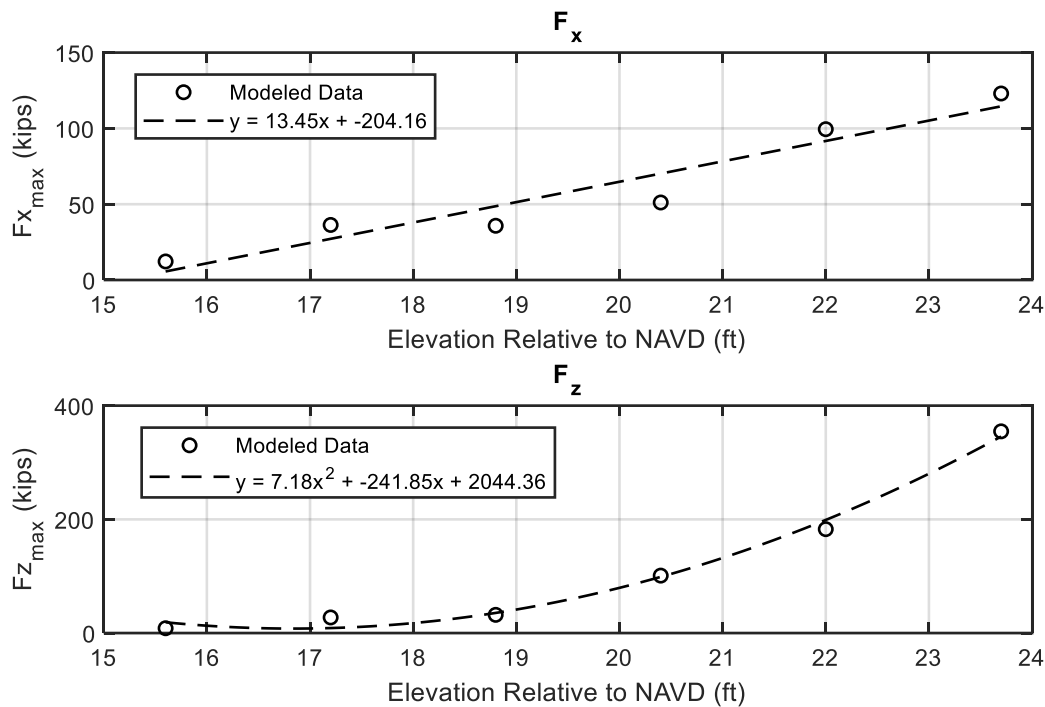
Figure 3-45. Results from CFD showing total maximum 4th wave forcing on the structure as a function of initial water elevation

These data suggest that if the initial water level was higher than originally estimated, significant additional lateral and uplift forcing would be experienced by the structure when compared to forcing computed using the reported water level. Recall from Section 2.1 that FEMA's MAT report indicated that water levels may have reached as high as +21.2 ft relative to NAVD. As such, it is likely that the previously computed first-level data were too low for wave and surge on the structure. However, this does not mean that a first-level analysis would not be effective for increases in water-elevation beyond the reported water elevation. The Morison-style analysis was repeated using an additional 6-ft of water elevation, and results are presented below in Fig. 3-46. Note that wave loading was still conservative relative to CFD. This is likely because in all cases, loading was observed to be mostly quasi-static with very few (if any) high-frequency oscillatory forces affecting the structure.

Overall, data suggest that using a combination of ASCE7 for wind load with typical first-level storm/wave load analyses should yield conservative design estimations for environmental loading on a structure like the structure at 1101 FL-30/US-98. And, if the FEMA method is used to compute wave loading, results would be very conservative when compared to results from CFD.
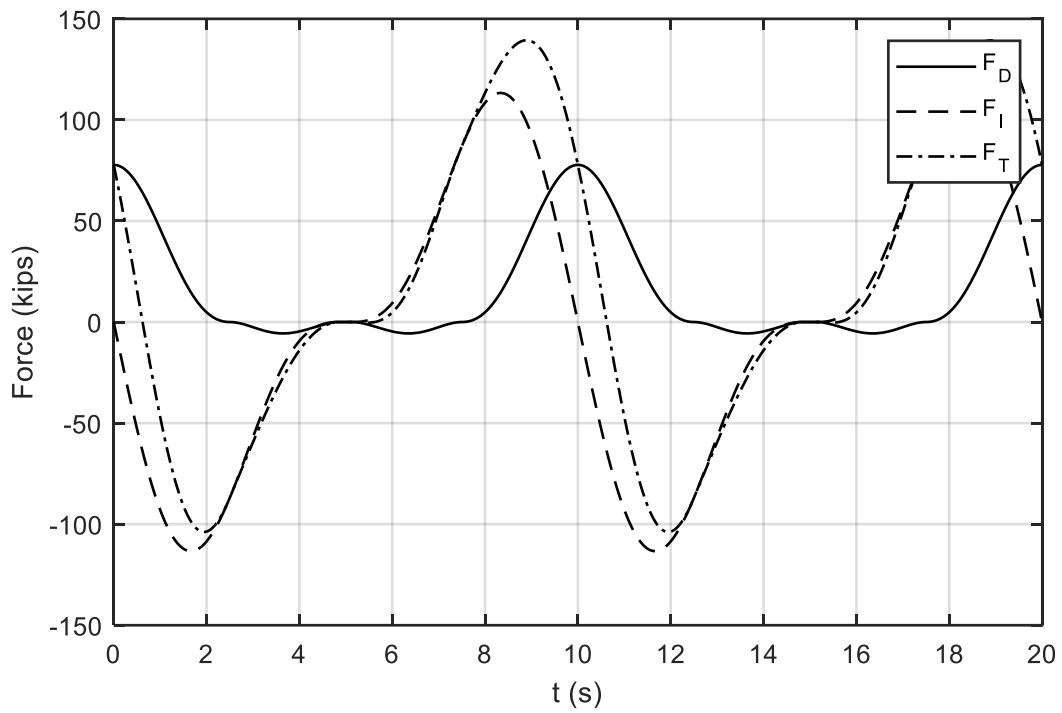
Figure 3-46. Repeat of Morison-style wave analysis using an initial water elevation of +22.16 ft relative to NAVD

4 STRUCTURAL RESPONSE

4.1 Moment Capacity – First-Level Analysis

Since the piles at 1101 FL-30/US-98 were observed to have failed due to overturning moments, first-level concrete capacity analysis focused upon computing these piles' moment capacities. Field reconnaissance showed that the structure's piles were prestressed, as evidenced by broken prestressing strands showed in section on Task 1. The piles properties were assumed to be as follows:

- Compressive strength of concrete, $f_c' = 6$ ksi
- Prestressed strand strength, $f_{pu} = 270$ ksi
- Prestressed strand modulus, $E_p = 28{,}500$ ksi
- Prestressed strand area, A_{ps} – 7-strand groups, each with an area of 0.255 in^2 were used based upon measurements/site observations
- Depth of prestressed strands, $d_p = 9.25$ in
- Strand service strength, $f_{py} = 0.9 f_{pu} = 243$ ksi
- Width of pile (i.e., compression face), $b_f = 12$ in
- Since $\frac{f_{py}}{f_{pu}} \geq 0.9$, $\gamma_p = 0.28$

Then:

$$\rho_p = \frac{A_{ps}}{f_f d_p} = 0.0046 \tag{4-1}$$

$$\beta_1 = 0.85 - 0.05(f_c' - 4000\ psi) = 0.75 \tag{4-2}$$

Since no non-prestressing reinforcement was observed in the debris at 1101 FL-30/US-98, the stress strand at nominal moment capacity reduces to:

$$f_{ps} = f_{pu}\left(1 - \frac{\gamma_p}{\beta_1}\rho_p\frac{f_{pu}}{f_c'}\right) \tag{4-3}$$

Substituting the values from above yields $f_{ps} = 249$ ksi. Next:

$$a = \frac{A_{ps}f_{ps}}{0.85b_f f_c'} \tag{4-4}$$

Substituting leads to an *a*-value of 2.08 in. Solving for *c*, the distance to the neutral axis:

$$c = \frac{a}{\beta_1} = 2.78\ \text{in} \tag{4-5}$$

The nominal moment, M_n then is:

$$M_n = A_{ps}f_{ps}\left(d_p - \frac{a}{2}\right) = 87 \text{ kip-ft} \tag{4-6}$$

Then, a check was made to ensure that the strands were tension-controlled:

$$\epsilon_{cp} = 0.003\frac{(d_p-c)}{c} \tag{4-7}$$

$$\epsilon_{ty} = 0.002 \tag{4-8}$$

Because ϵ_{cp} was less than ϵ_{ty}, tension control was assumed. Thus, $\phi = 0.9$ and $\phi M_n = 78$ k-ft.

To compare with loading, it was assumed that the wind and wave loads imparted overturning moments about the tops of the piles using the distance from the tops of the piles to the appropriate load component as the moment arm. Likewise, it was assumed that the overturning moments upon the piles due to wave action was also equivalent to overturning moments about the pile cap. This was computed by integrating the depth-dependent forces on the piles multiplied by their corresponding moment arm between their depth and the distance to the pile cap. Furthermore, it was assumed that both the wave loads and wind loads were divided equally among the structure's 25 piles. Finally, it was assumed that scour was negligible, which as will be shown below, is a poor assumption. The result of this computation led to an apparent overturning moment of approximately 65 k-ft per pile. This is below the design moment of 78 k-ft per pile computed using ACI/PCI guidelines.

4.2 The Finite Element Model

4.2.1 Governing Equations

As noted in Chapter 1, ANSYS Workbench was used for all FEA modeling. Small deflection theory was used throughout this analysis whereby it was assumed that displacements, stresses, strains, and forces did not induce significant inertia or damping effects and that loading was relatively steady. Results from CFD showed that this assumption is likely sufficiently accurate in the sense that high-frequency oscillatory forces were not observed during wave forcing analysis. As such, steady response coefficients were assumed using ANSYS' built-in Static Structural package which uses the overall equilibrium equations for linear structural static analysis:

$$[K]\{u\} = \{F\} \tag{4-9}$$

where $[K]$ is the total stiffness matrix; $\{u\}$ is the nodal displacement vector; and $\{F\}$ represents the loads on an element. Strains are related to nodal displacements via:

$$\{\epsilon\} = [B]\{u\} \tag{4-10}$$

in which $[B]$ is the strain-displacement matrix based upon the element shape functions; and $\{\epsilon\}$ represents the strain. Then, strains are converted to stresses, $\{\sigma\}$, via:

$$\{\sigma\} = [D]\{\epsilon\} \qquad (4\text{-}11)$$

If an element has 6 degrees of freedom, internal moments may be computed via the typical relationship between stress and moment, $\sigma = Mc/I$ where M represents the internal moment; I, the moment of inertia; and c the distance to the neutral axis.

4.2.2 Importing the Model

The CAD structure at 1101 FL-30/US-98 that was used for CFD was converted to a format that was appropriate for FEA modeling. This conversion involved converting the "shell" associated with CFD into a structural drawing by framing floor and roof joists along the structure's interior. It was assumed that the structure's floor frame, wall frame, and roof trusses consisted of nominal 2-inch by 4-inch lumber spaced at 16-inches on-center. Once converted, the new CAD model was imported into ANSYS Workbench, and a grade-level slab with an assumed thickness of 6-in was added to the structure so that its effects could be analyzed. The structure's pile elements were converted to beams using the built-in conversion algorithm in Workbench's Spaceclaim. This step was not trivial; if not converted, the piles would have represented as solids (as opposed to beams). Solid elements in ANSYS only have three degrees of freedom (as opposed to 6 degrees of freedom for beams). Thus, while solid modeling will return results for elemental stresses, results from a solid portion of a model will not yield data for internal moments in a member that consists of multiple solids. Because the piles consisted of concrete, which is a brittle material, a moment analysis was deemed more appropriate than a stress/strain analysis.

4.2.3 Connections, Boundary Conditions, and the Grade-Level Slab

The piles were assumed to be fixed at their bases (i.e., the bottom of the mudline or bottom of the scour hole). For several runs, piles were connected to the grade-level slab manually using bonded connections between the slab "body" and the closest nearby node on each pile in conjunction with an 18-in "pinball." For other runs, it was assumed that the slab "broke away" or provided no connection to the piles, and as such, the slab was eliminated during these runs. When the slab was connected to the piles, two scenarios were tested. First, the slab was allowed to move with the structure. This produced maximum moment results that were identical to results when the

slab was excluded, which is logical in hindsight – the slab would just be another element that would move with the structure and provide no point of fixity for the piles. A second series of runs was performed whereby a displacement constraint was placed along the downstream slab faces – thereby assuming that the slab remained connected and was constrained by the dune. The point about the slab connection to the piles bears further discussion. According to the Florida Building Code, a space is supposed to be left between any grade-level slab and piles. However, investigators hypothesized that such a space was not properly included at the structure.

Three scour scenarios were studied – zero scour (with or without the slab would have made no difference, so only the "with slab" configuration was used), 3-ft of scour, and 6-ft of scour. The zero-scour scenario was analyzed as a baseline; the 3-ft scour scenario was chosen because measurements at Mexico Beach appeared to show 3-ft of exposed pile below where the grade-level slab had been located (i.e., approximately 3-ft of unpainted portions of the piles were observed on-site); the 6-ft scenario was chosen because during the storm, it is possible that more scour occurred that was obscured after the fact due to infilling.

4.2.4 Materials

As noted, the piles and grade-level slab consisted of concrete. These materials were assigned using the built-in concrete properties from ANSYS material database which assumes a density of 143 pcf; an ultimate tensile strength of 725 psi; and ultimate compressive strength of 5,947 psi. For the balance of the structure, lumber was assumed using properties from ANSYS' material database for wood where a density of 68 pcf; a tensile yield strength of approximately 7 ksi; and an ultimate strength of approximately 21 ksi were assumed.

4.2.5 Meshing

All meshing was performed using ANSYS' built-in meshing algorithm with element sizes of approximately 8-in; a growth rate of 1.85; and a maximum size of 16.4-in. This yielded a model between 502,444 nodes and 501,994 nodes; and 124,816 and 124,591 elements (depending on assumed scour depth). An example of a 6-ft scour scenario model is shown below in Fig. 4-1:
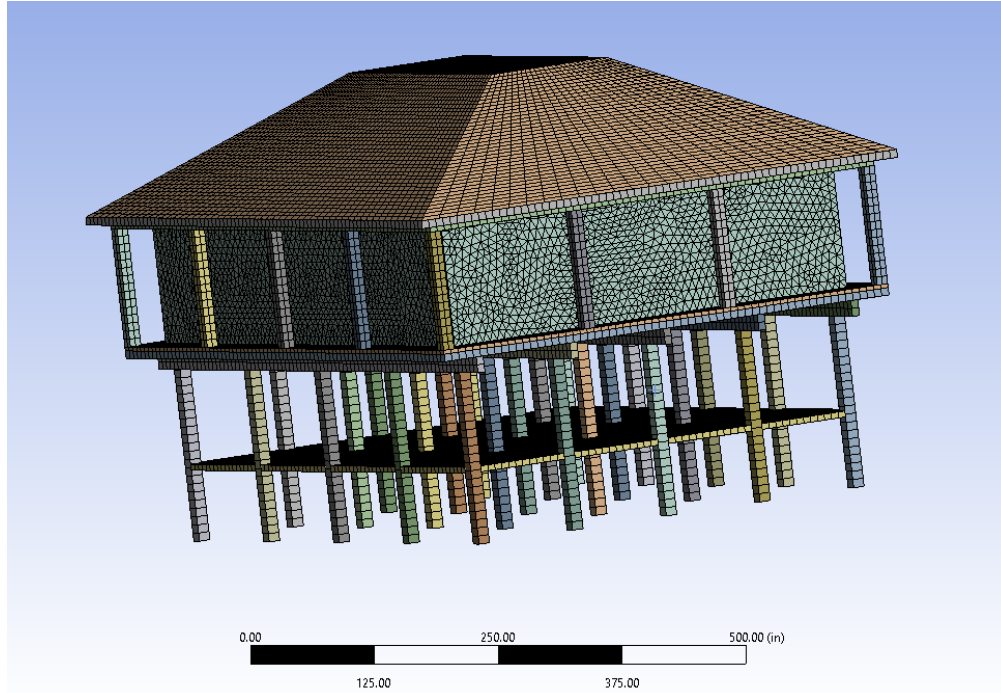
Figure 4-1. Meshed FEA model used during this study showing the 6-ft scour scenario

4.2.6 External Loading

External loads were applied to the structure in the following manners:

- The ASCE wind pressures were applied directly to the roof, leeward, and windward walls in an effort to understand response to the most conservative wind loading assumptions. This allowed investigators to account for the internal pressure forces that could not be modeled using CFD.

- Wave loads were applied to the piles by imparting line pressures along each of the pile lengths that corresponded to average results from CFD for forces on the pile divided by the pile lengths.

- Wave loads were applied to superstructure by imparting a point load upon the upstream (i.e., windward) wall. Like the wave loads on the piles, these loads were the result of computations in CFD.

- Prestressing on the piles was simulated by assuming axial forcing on the piles. This axial force's magnitude was computed by converting the prestress strands' assumed service stresses (i.e., 243 ksi) to strain using Hooke's Law combined with the prestressed strands' assumed modulus (i.e., 28,500 ksi). Then, the ACI equation (i.e., $57,000 \sqrt{f_c'}$) was used to

find the concrete modulus. Finally, the strain was converted to stress in the concrete by using Hooke's Law again with the concrete modulus. This stress was converted to a point load by dividing by each pile's concrete cross-section area.

A sketch that shows the forces on the structure is shown below in Fig. 4-2:
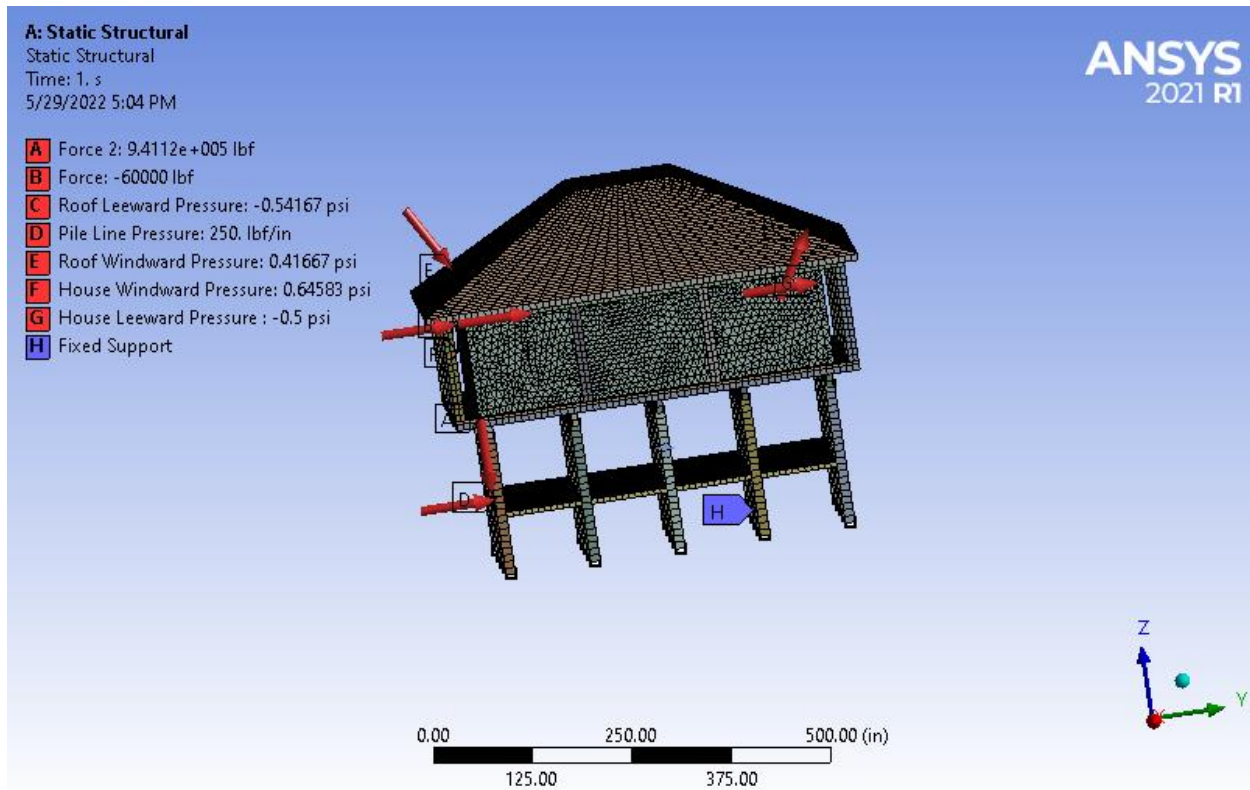
Figure 4-2. External loading on the structure

4.2.7 Testing Scenarios

As noted above, several model scenarios were examined that involved different combinations of scour and the grade-level slab. In addition, several different water levels were also examined by linearly interpolating results from CFD. A testing matrix that shows that different scenarios is presented below in Table 4-1.

Table 4-1. FEA Testing Matrix

Run No.	Test Name	Water level (ft relative to NAVD)	Scour Depth (ft)	Slab included?
1	FEA1	15.6	0	Yes
2	FEA2	15.6	3	Yes
3	FEA3	15.6	6	Yes
4	FEA101	21.2	0	Yes
5	FEA102	21.2	3	Yes
6	FEA103	21.2	6	Yes
7	FEA202	15.6	3	No
8	FEA203	15.6	6	No
9	FEA301	18.4	0	Yes
10	FEA302	18.4	3	Yes
11	FEA303	18.4	6	Yes

4.3 FEA Results and Discussion

Results from FEA modeling showing internal moment contours are presented below from Fig. 4-3 through Fig. 4-13. These results were compared with moment capacity computed in Section 3.1 (i.e., 78 k-ft). As shown in these figures, failure is dependent upon three variables – initial water level, scour depth, and whether the grade-level slab was connected to the piles. If the initial water level was presumed to be +15.6 ft NAVD, then the structure does not fail if the grade-level slab was connected to the piles (Fig. 4-3 through Fig. 4-5). On the other hand, when the same slab geometry was used and the water level was increased to the highest value reported by FEMA's MAT report (i.e., 21.2 ft NAVD), then the piles always fail due to insufficient moment capacities regardless of scour depth (Fig. 4-6 through Fig. 4-8). Particularly interesting about Fig. 4-3 through Fig. 4-5 is that the *magnitude* of the maximum moment did not change significantly for a given loading scenario regardless of scour depth. Rather, the *location* of the maximum moment changed relative to its position from the gradeline. In all cases from Fig. 4-3 through Fig. 4-8, the piles' maximum moment was experienced just above the grade-level slab, regardless of scour depth. In effect then, the grade-level slab provided a point of fixity for the piles.

However, when the grade-level slab was removed, scour played a larger role in terms of the maximum moment magnitude. Note in Fig. 4-9 and Fig. 4-10, results show that with an initial water-elevation of +15.6 ft NAVD and the grade-level slab "broken away," the structure survived 6 ft of scour but not 9 ft of scour. Likewise, results in Fig. 4-3 imply that the structure would have survived with no scour. But it is important to reiterate that under an initial water-elevation of +15.6 ft NAVD, the structure *also* survived the scenario when the grade-level slab was connected. When the midpoint water level was examined (i.e., Fig. 4-11 through Fig. 4-13), the structure failed under the zero-scour condition and was very close to failure under both the 3-ft and 6-ft scour conditions.

It is also interesting to note that with the grade-level slab scenarios, results show that an increase in scour led to a slight decrease in maximum internal moment in the piles. This is an artifact of the way in which the structure was modeled in the sense that worst-case line loads were applied to each pile as a function of depth. Inclusion of the slab connection tended to create a structural point of fixity. As more scour developed below this fixity point, its net effect was to expose more portions of the pile and provide an increase in the amount of righting (i.e., positive when using the right-hand rule) moment around this slab fixity point. As such, this tended to decrease the computed moment around the fixity point, slightly. In future research, it would be interesting to setup a tabular line load as opposed to the constant average line load that was used in this study to examine results. But, using a tabular line load is not expected to change results significantly because the controlling factor that led to the difference between survival and structural failure was the initial water-elevation.

Overall, results suggest that the reason the failures were observed in the locations they were observed at 1101 FL-30/US-98 is that the grade-level slab was improperly connected to the piles, or a space (or large enough space) was not provided between the grade-level slab and the piles as required by the Florida Building Code. Furthermore, results imply that the water level was higher than +15.6 ft NAVD at this location and that even if a space (or sufficient space) had been provided between the piles and the grade-level slab, failure still would likely have occurred – albeit closer to the mudline.
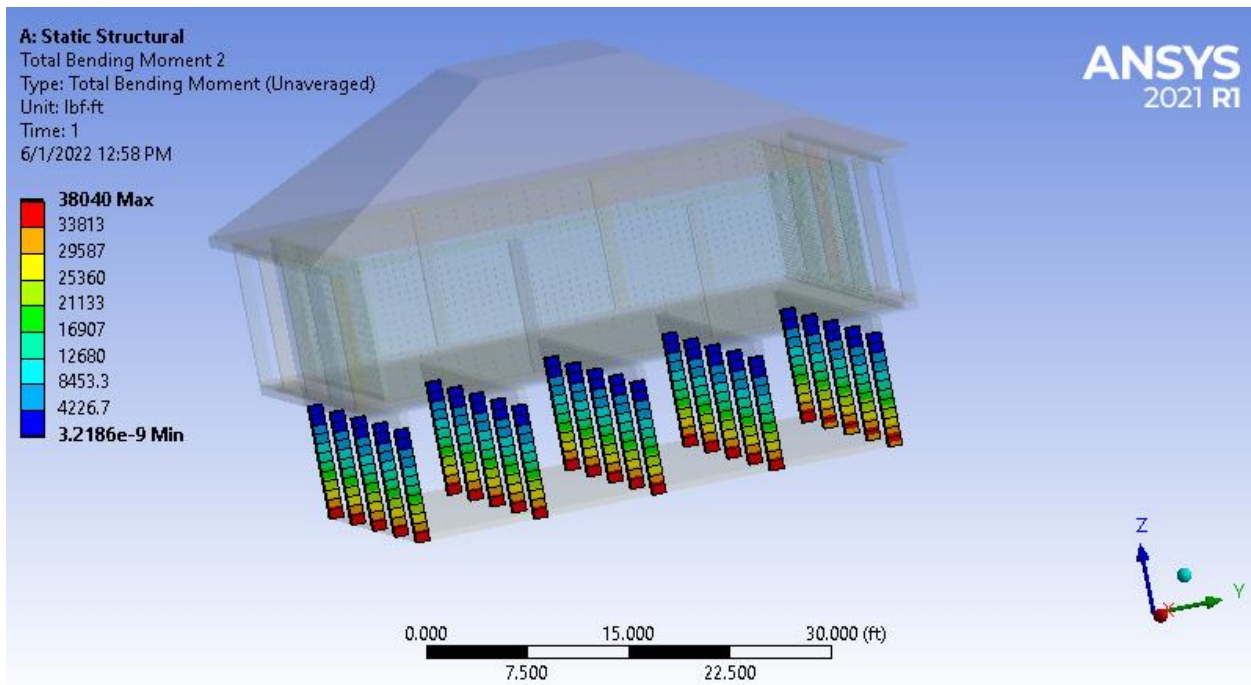
Figure 4-3. Results from model FEA1
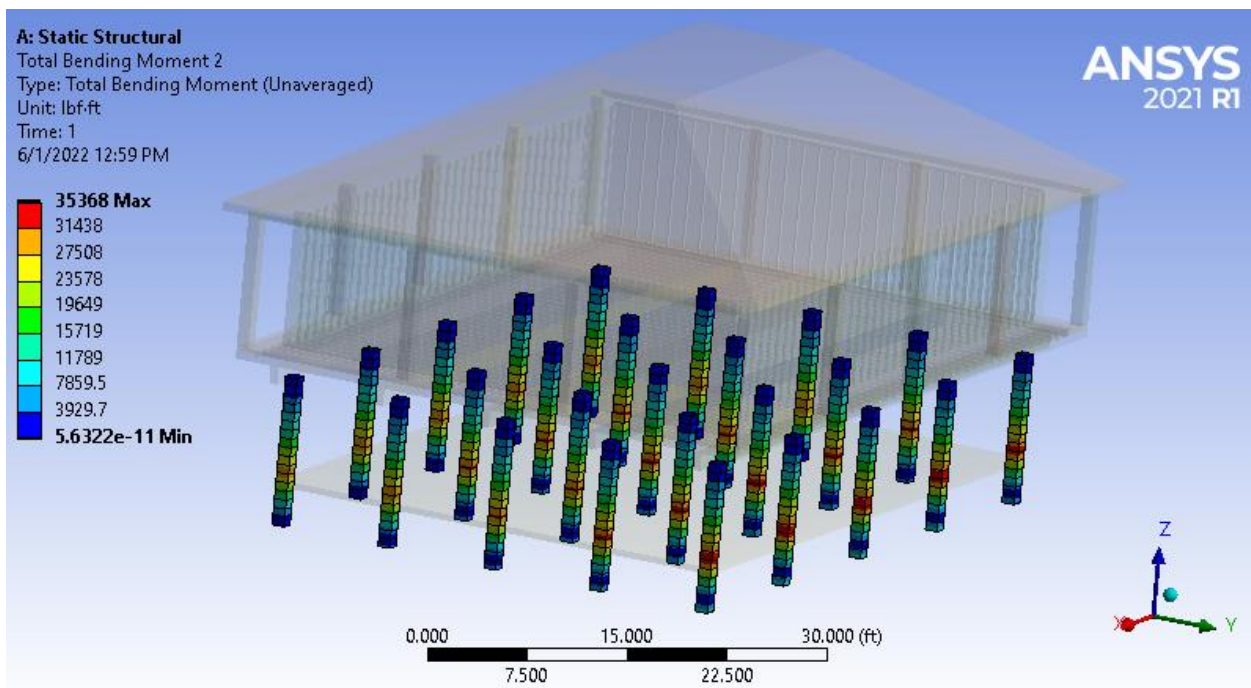
Figure 4-4. Results from model FEA2
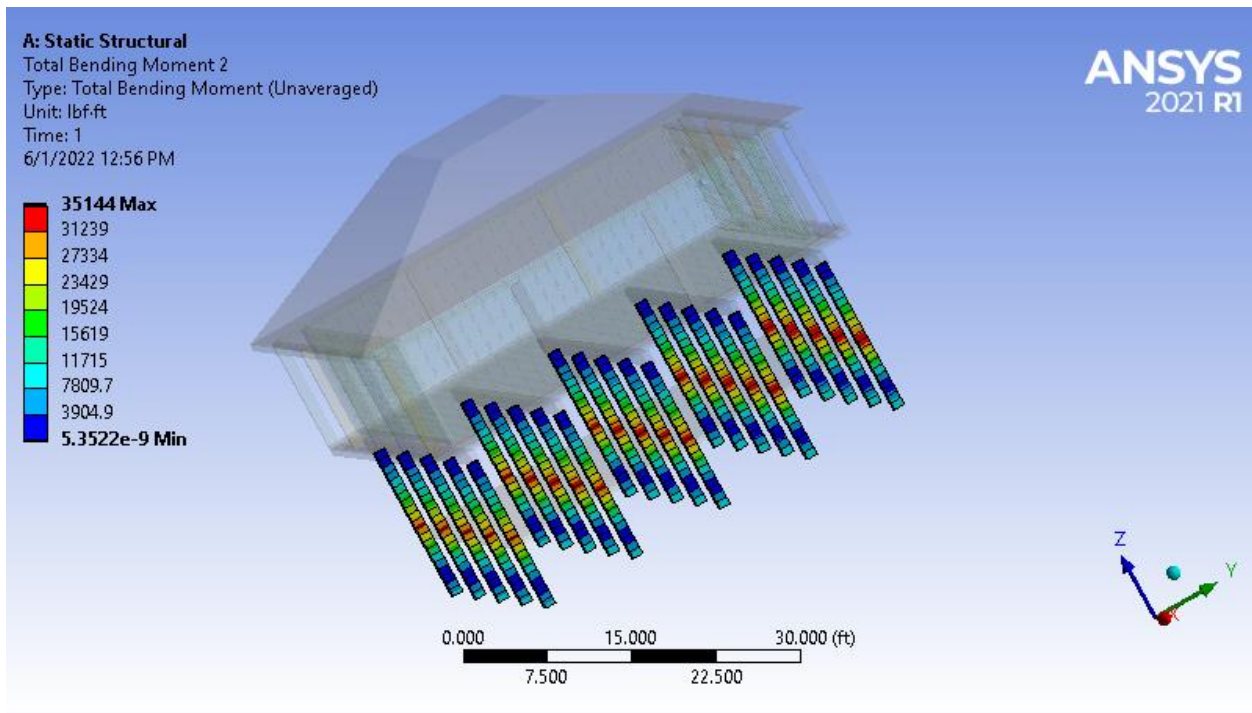
Figure 4-5. Results from model FEA3
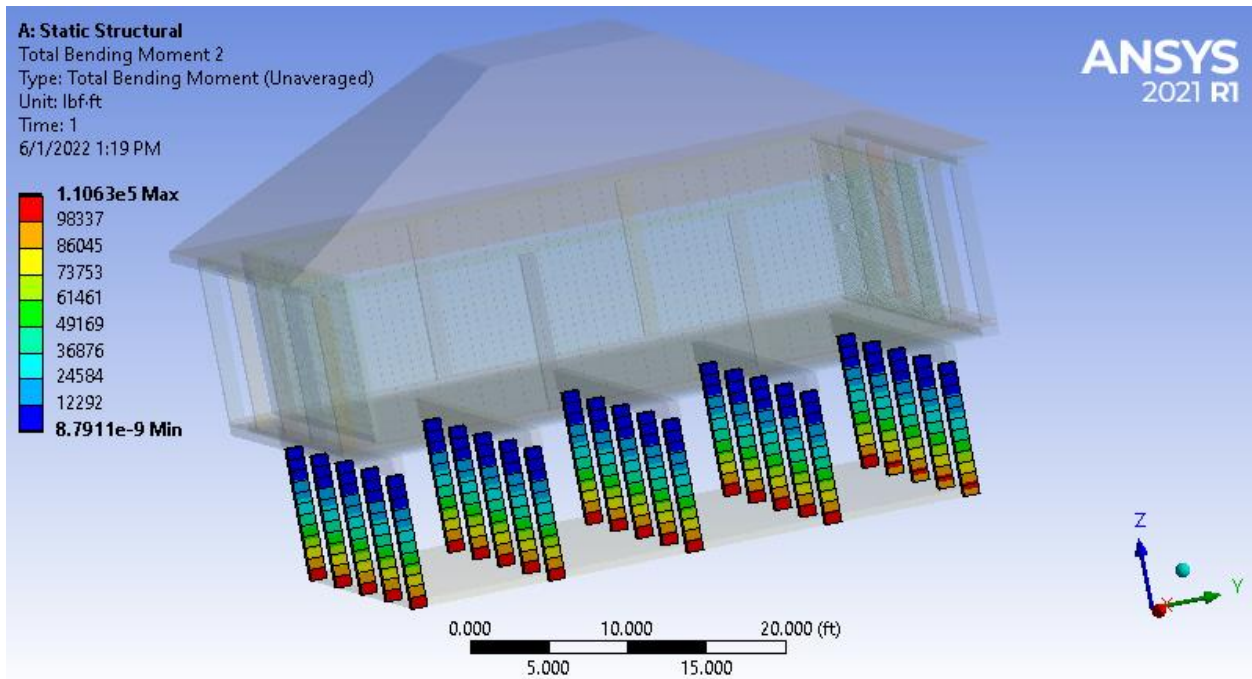
Figure 4-6. Results from model FEA101
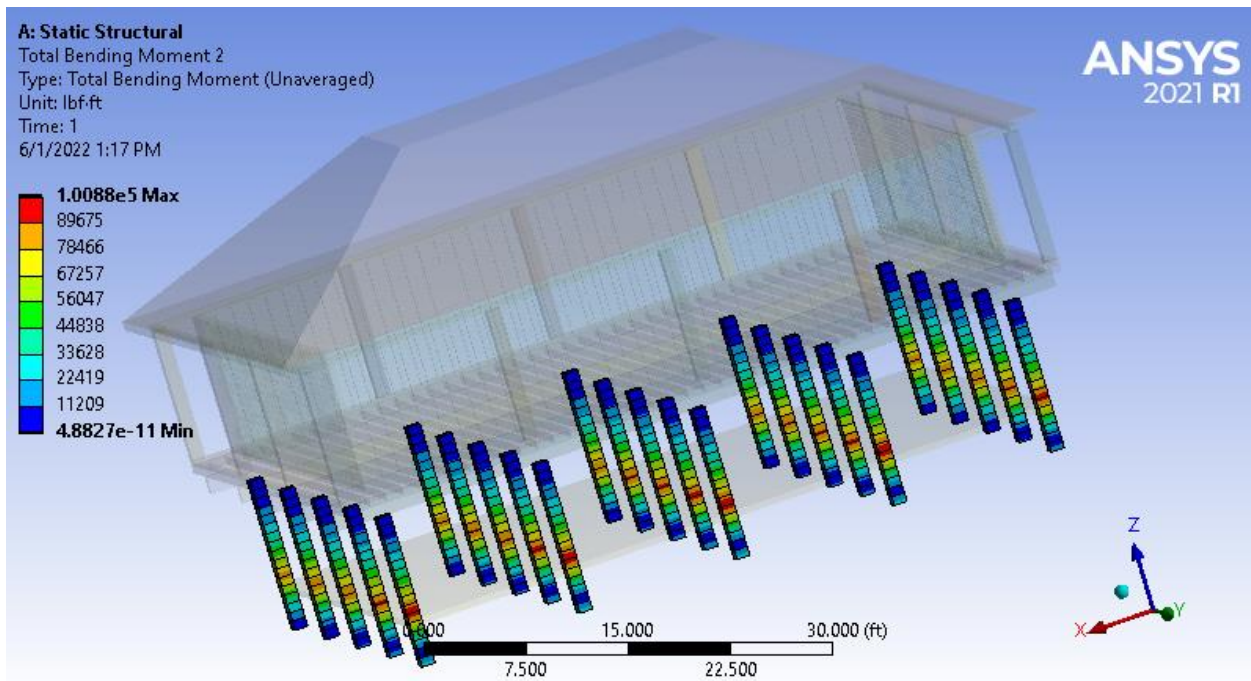
Figure 4-7. Results from model FEA102
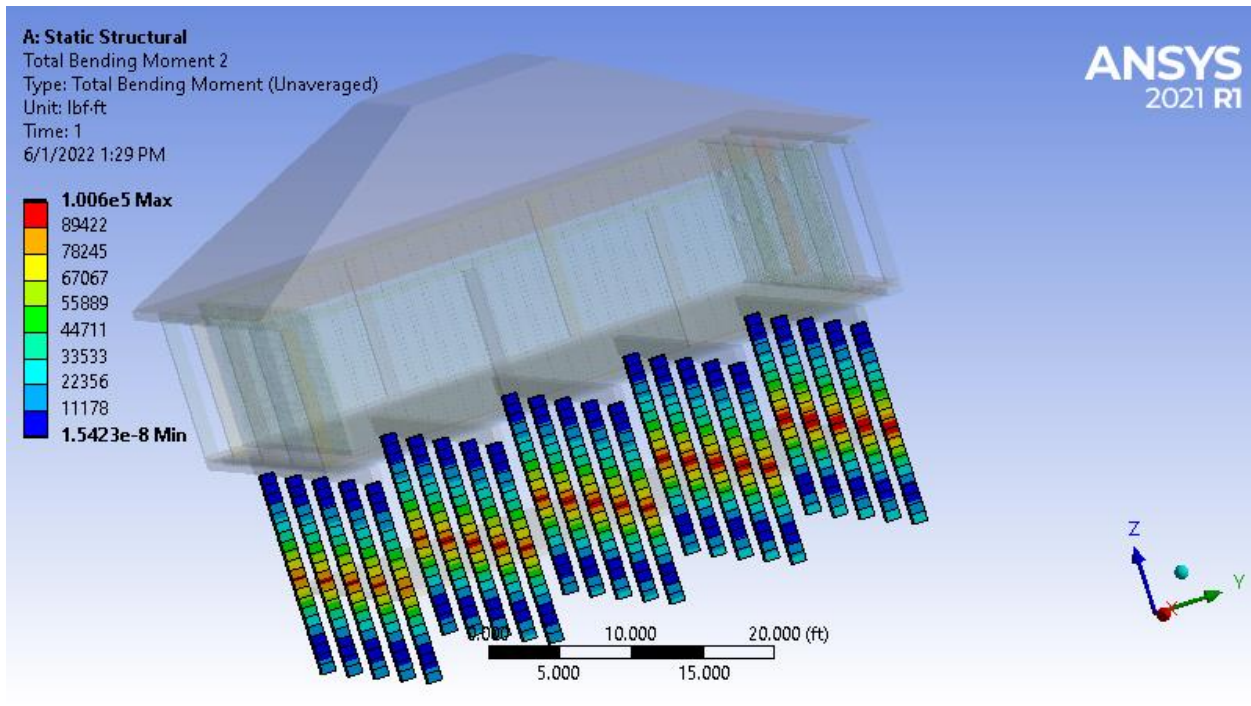
Figure 4-8. Results from model FEA103
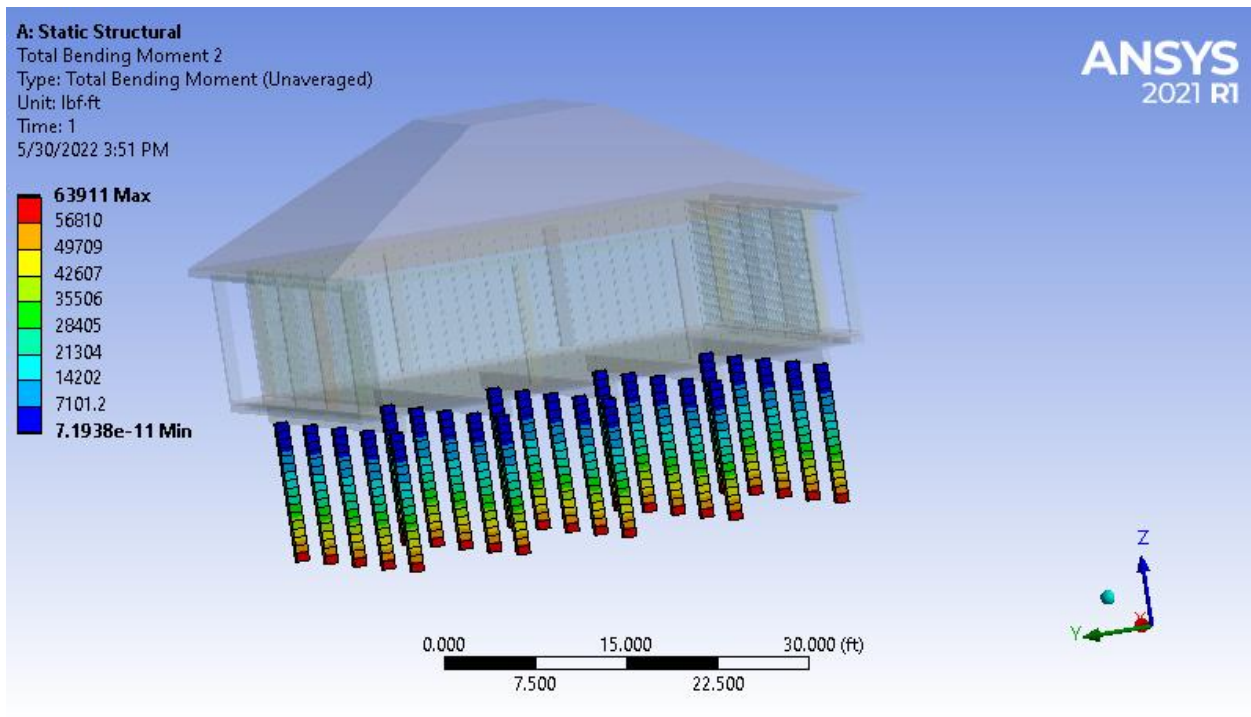
Figure 4-9. Results from model FEA202
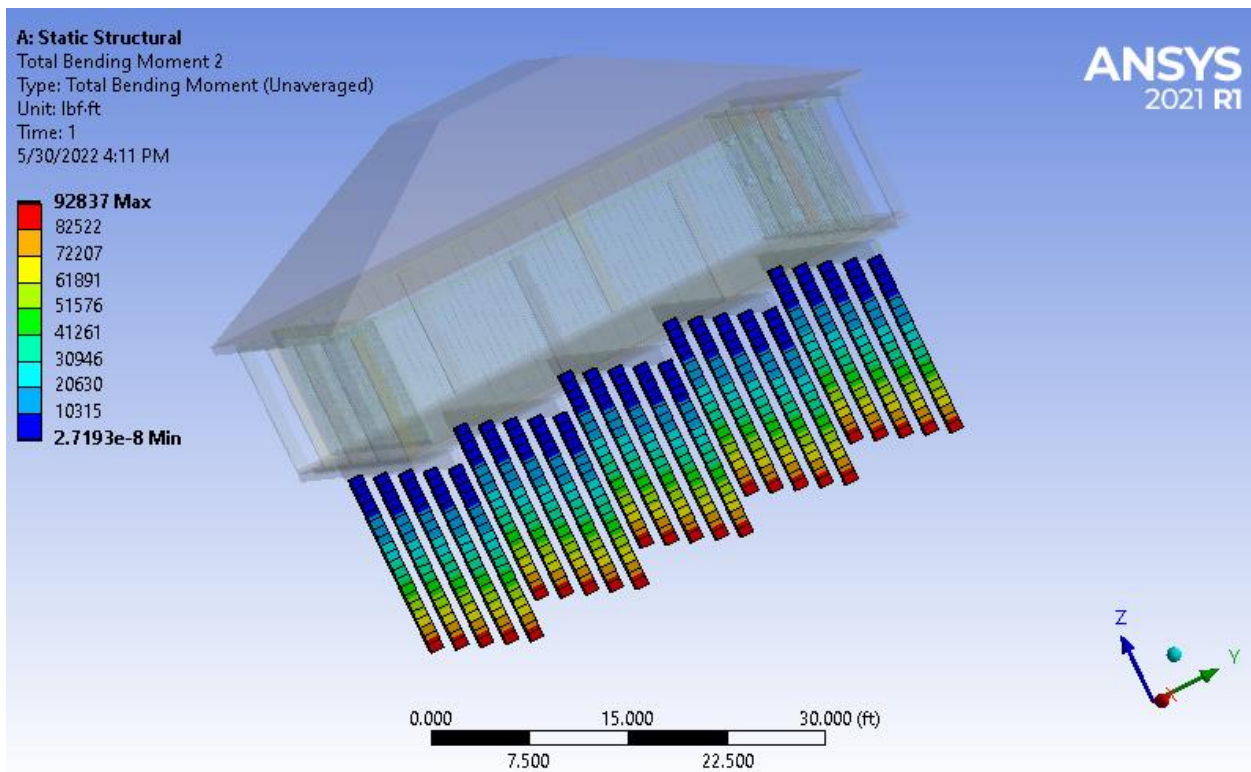
Figure 4-10. Results from model FEA203
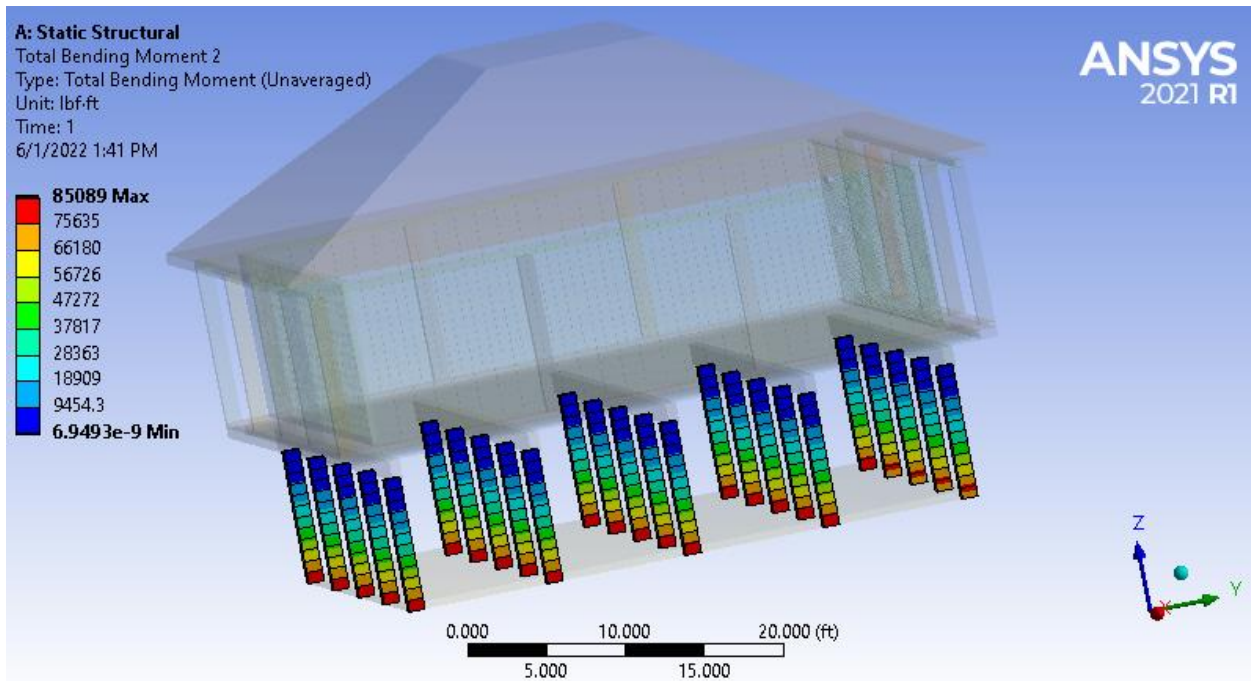
Figure 4-11. Results from model FEA301
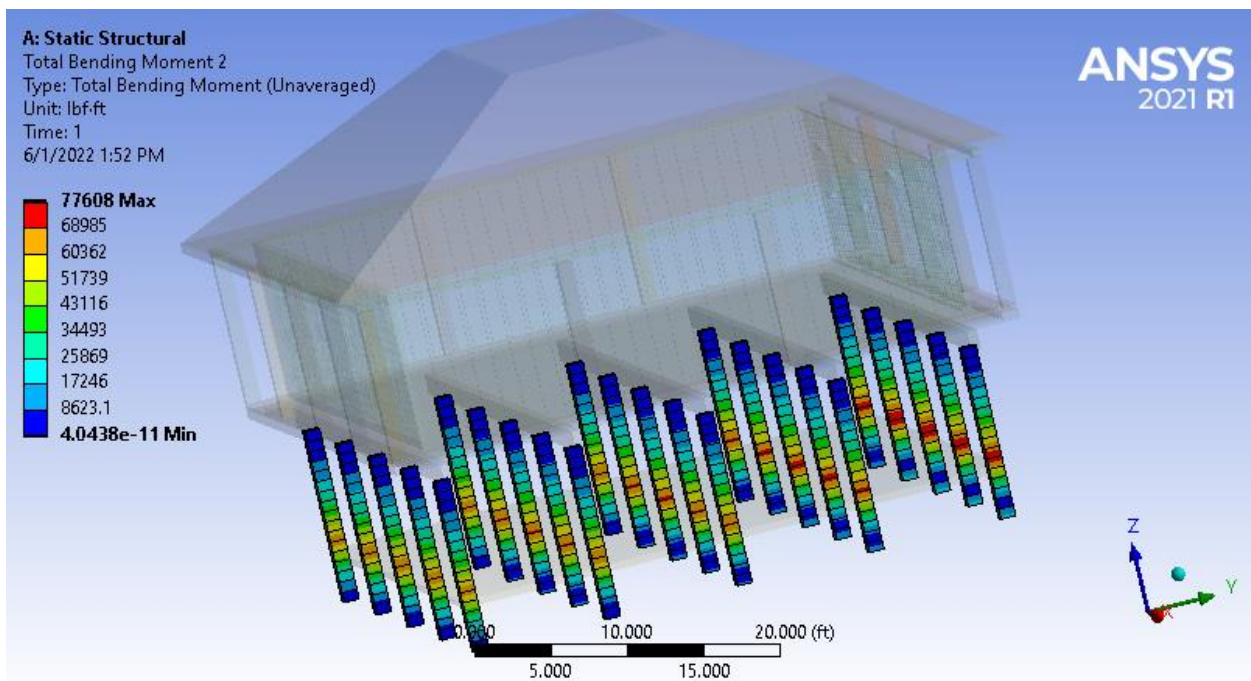
Figure 4-12. Results from model FEA302
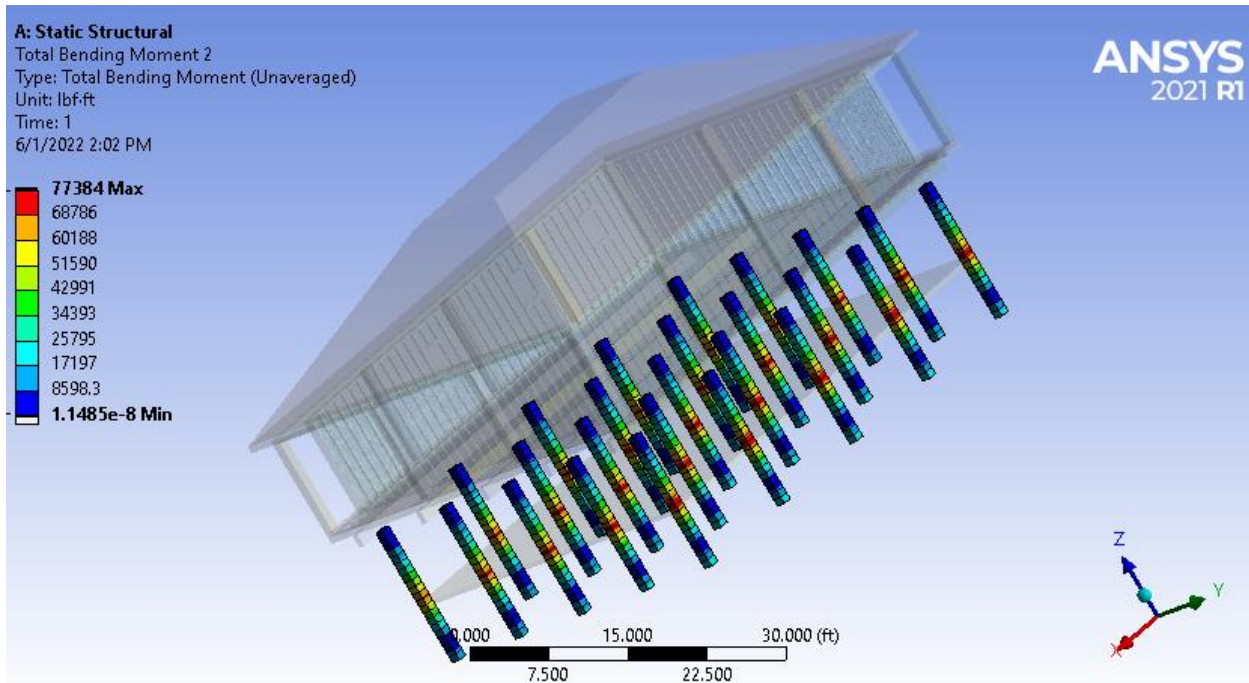
Figure 4-13. Results from model FEA303

4.4 Soil Structure Pile Analysis

Field reconnaissance and FEA results suggested that failure of the structures at Mexico beach was primarily a result of insufficient moment capacity. Nonetheless, a geotechnical analysis was performed to investigate the occurrence of lateral deformation (i.e., pile distortion or *tilting*) that could have resulted from the anticipated loading if moment capacity had been sufficient. For this analysis, a simulated pile for the structure located at 1101 FL-30/US-98 was modeled using GEO5 (2022) software. This software was utilized to determine (1) the soil response to a laterally loading pile equivalent to the storm surge loading presented earlier in this report, and (2) the estimated internal structural capacities of the pile coupled with the response of the soil.

The following steps were performed in this subtask and are presented herein: (1) an investigation of available subsurface testing data regional to Mexico beach's surficial geology; (2) establishment of typical soil profile and soil model parameters; (3) analysis of soil response using a simplified "rigid" pile with varying total length (L); (4) analysis of soil response using a modeled pre-stressed concrete pile with varying total length (L); and (5) analysis of structural response using an assume pile length and varying scour depth. When applicable, horizontal loading was also deviated within the ranges of lateral loading described in Task 2. Although this analysis is limited due to the lack of information regarding the structural characteristics of the pile (e.g., total

length, prestressing, reinforcement, etc.), the research team can at least conclude that distortion of the pile due to loading had minimal effect on the failure of the piles at this location.

4.4.1 Subsurface Investigation

1101 FL-30/US-98, along with much of the coastal regions of the panhandle of Florida, lies within the surficial geological unit of *Holocene Sediments* (Qh) (Scott 2001). This type of geology consists primarily of unconsolidated quartz sand and carbonate sands with little to no clay. Well drilling logs in the area also identified the Qh sediments consisting of angular to sub-angular sands to a depth of 100-120 ft below grade, until a shell bed was encountered (FDEP 1953).

Even with an anticipated homogenous subsurface soil condition being primarily a beach quartz deposited sand, geotechnical insitu testing is still required to estimate the strength parameters needed for the GEO5 analysis. Due to this area being primarily private residences, open-source geotechnical testing results within the city limits of Mexico were not available. However, using the Florida Department of Transportations' *online public soil boring viewer* application (2022), two nearby reports were identified in the city of Rosemary Beach. Although these project sites are approximately 40 miles to the northwest of 1101 FL-30/US-98, they fall within the same surficial geologic unit boundary proposed by Scott (2001), as shown in Fig. 4-14. Therefore, it was assumed that the anticipated geotechnical conditions at 1101 FL-30/US-98 were likely to be consistent with the subsurface conditions at encountered at the two Rosemary Beach project sites.
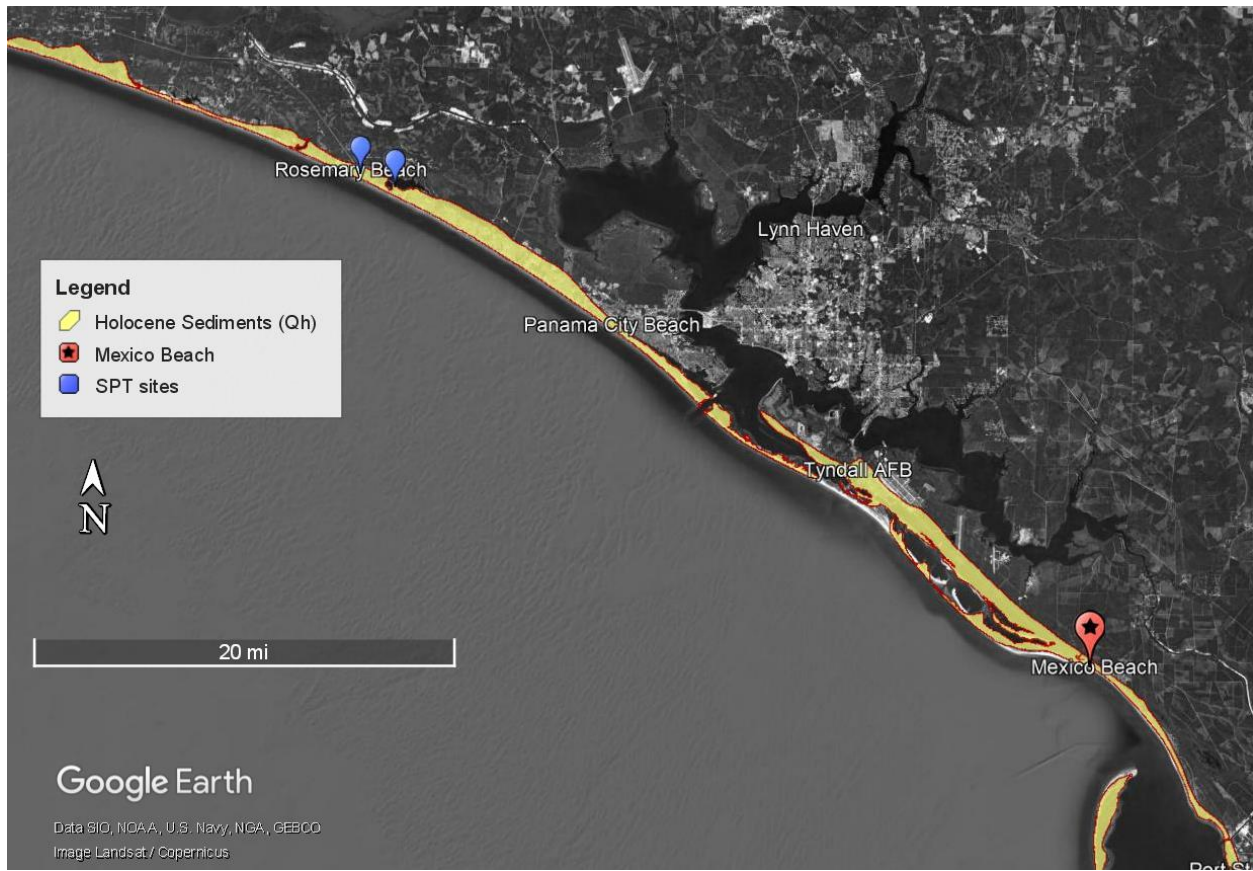
Figure 4-14. Regional map of Florida Panhandle with Surficial Geology (Scott 2001), study site, and subsurface data collection sites highlighted.

The two available geotechnical subsurface reports located in Rosemary Beach consisted of a total of six (6) standard penetration tests (SPTs). As anticipated, all 6 SPTs encountered sandy soil for the entirety of the testing depth. Further information from the SPTs include the soil resistance values, in terms of the SPT uncorrected N-value (blows/ft), as well as various lab testing from depths of 1-ft to 30-ft below ground surface. Lab testing consisted of the percent natural moisture content (%NMC) and the percent of soil particles less than 0.075mm (i.e., percent *fine* content, or %FINES). The laboratory testing verifies that the subsurface conditions are indeed a *clean and subangular* quartz-based sand, as suggested by the well drill logs in Mexico beach.

The most important soil parameter obtained from these reports is the N-value. The N-value is obtained by recording the number of "blows" it takes to progress the drill rod and sampler 1.5-ft into the soil, via a 140-lb hammer dropped 30 inches onto the drill rod (ASTM D1586). This value is then corrected based on the drilling equipment to produce the N_{60} value, or N-value assuming the system is operating at 60% efficiency. The N_{60} value can then be correlated to various

physical and strength properties, which are used as input for the analytical solutions in GEO5. The calculated N60 values for the 6 SPTs, presented as a profile with depth, is shown along with the laboratory testing results, in Fig. 4-15. Based on the subsurface testing presented, the subsurface conditions at the 1101 FL-30/US-98 site were assumed to be a medium dense clean sand with a conservative N_{60} value of 10 blows/ft for the entire testing and modeling subsurface space.
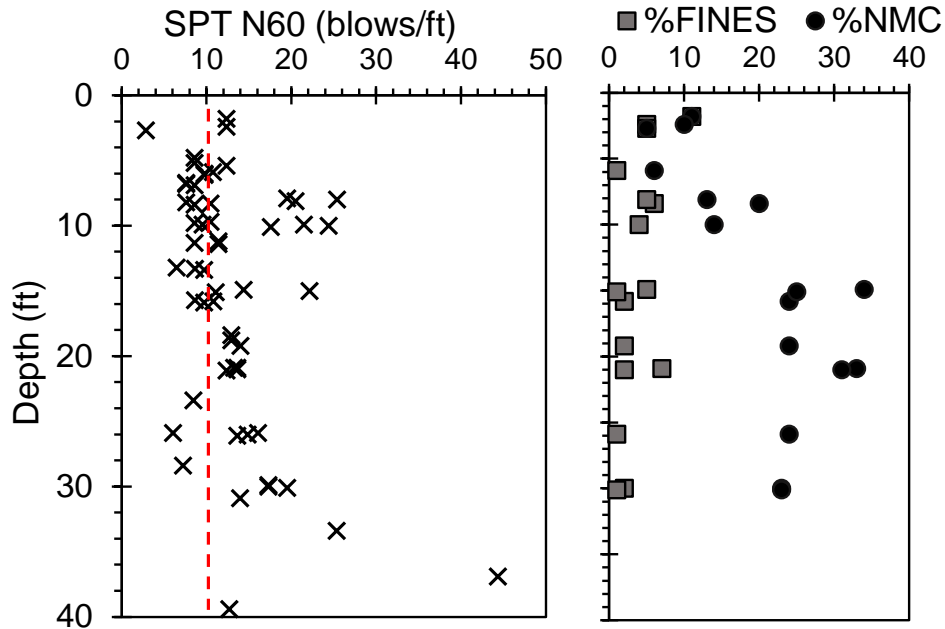
Figure 4-15. Subsurface testing data obtained from Rosemary beach site

4.4.2 Subsurface Model setup

The GEO5 software calculates the horizontal bearing capacity soil, assuming a discretized elastic subsoil with a non-linear response (p-y method). Essentially, the horizontally loaded pile is analyzed using fine element method (FEM), as a beam on an elastic Winkler foundation (GEO5 2022). As mentioned previously, the program calculates the internal stresses within the pile, as well as the subsoil reaction and displacements. The subsoil reaction and displacements were calculated using Vesic's theory (1977), where the horizontal earth modulus (k_h) is used as input for the elastic spring resistance, as shown below. The combination of these two analyses is widely used to analyze the interaction of a pile-soil system subjected to lateral loading (FHWA 2016).

$$k_h = \frac{0.65}{d} \sqrt[12]{\left(\frac{E_s}{E_p}\frac{d^4}{I_p}\frac{E_s}{1-v^2}\right)}$$ (4-12)

Where: E_P = modulus of elasticity of Pile

I_P = moment of inertia of pile

E_s = modulus of elasticity of soil

D = pile width

v = Poisson's ratio

The remaining soil input parameters required for the GEO5 model were obtained using the N60 values and several correlations widely used in the Geotechnical literature for sandy soil. Table 4-2 presents the typical soil parameters used for the GEO5 model, along with each respective reference. Whenever applicable, the lower-end value was chosen for the subsurface strength value to provide a more conservative analysis. This was chosen due to the uncertainty of the loading conditions, pile geometry, and lack of subsurface testing information locally within the project site.

Table 4-2. Typical subsurface soil conditions and strength parameters used in GEO5 model

Soil Properties for Qh1	Value	Unit	Reference(s)
Unit Weight (γ)	120	lb/ft^3	Bowles 1997
Poisson's ratio (v)	0.33	-	Bowles 1997
Saturated unit weight (γ_{sat})	125	lb/ft^3	Bowles 1997
Elastic modulus of soil (E_s)	2000	lb/in^2	Schmertmann 1978
Coefficient of lateral stress (K)	1.50	-	Mansur and Hunter 1970
Pile skin friction (δ)	24	degrees	Bowles 1997
Soil angle of internal friction (ϕ')	30	degrees	Bowles 1997

4.4.3 GEO5 model set up

4.4.3.1 Assumptions

To isolate the soil-structure response under the anticipated extreme loading in GEO5, the following was assumed of the numerical model:

- External loading from the storm event was only applied to the pile head and was assumed to only be in the horizontal direction (H_x). External vertical loading from the structure was assumed to be negligible in comparison to the maximum horizontal force.

- Since only the lateral response of the soil was analyzed, the model consisted of a single pile and no grouping effects were considered. All max loading (H_x) was assumed to be

evenly distributed across the total number of piles supporting the structure. Therefore, the horizontal force (F_x) acting on the singular pile was calculated by dividing the max force by the total number of piles (i.e., 25 total piles).

- A normal force (N_z) was applied to the pile top of the pile to simulate the prestressing forces. Since actual design specifications were not available for this structure, a conservatively low value of 270 ksi was chosen based on suggested ranges for a 12"x12" piles by PCI (2019).

- Groundwater table (GWT) was assumed to be at pile head for each model and drained strength parameter were used since soil is a clean coarse sand.

- Pile grouping efficiency was kept at 1.0 since the spacing at 1101 FL-30/US-98 was approximately 9b to 12.5b (McVay 1995).

- Any stiffness or fixity from concrete on-grade slab was not included in the model since significant scour was anticipated prior to the failure of the pile.

4.4.3.2 Geometry

The dimensions and structural components presented in earlier in Task 3, were used as input for the geometrical parameters of the GEO5 model. Fig. 4-16 provides the variables within the model user interface. It was assumed initial exposed pile length was 10-ft (pre scour) and it was also assumed that the embedded pile was identical geometry and material to the exposed pile (i.e., 12" x 12" inch prestressed concrete square). As mentioned earlier, the soil conditions (Qh) are homogenous for the entire depth of analysis. Since the total length of pile is not known for the study site, the results of the analysis will be presented as a function of pile length, L.
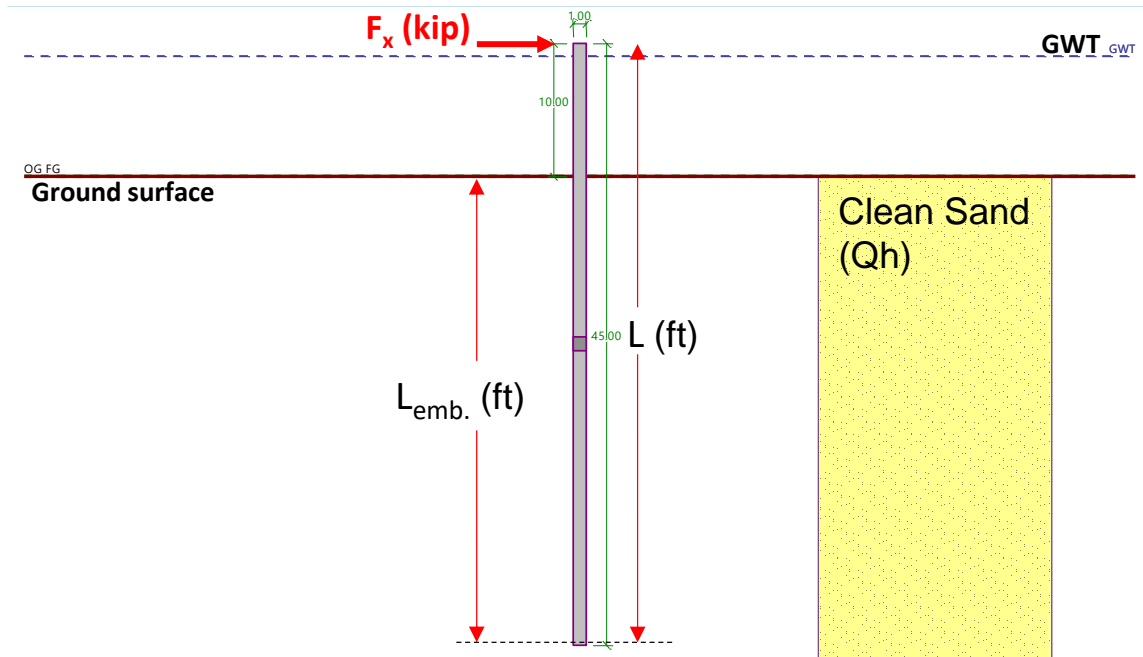
Figure 4-16. GEO5 user interface showing model parameters

4.4.3.3 Materials

Two types of analysis were performed using the GEO5 software. The first was the isolated soil response to the laterally loaded pile. To isolate the soil response (i.e., displacement from the pile pushing on the soil), the pile material needed to be 100% structurally rigid. To achieve this, the strength values for the pile material (i.e., pre-stressed concrete) were extremely overly exaggerated. The second type of analysis performed was a coupled soil-structure response, with the actual deformations in the structural pile effecting the lateral stresses applied to the soil column. Typical pre-stressed concrete strength and design values were applied following PCI (2019) for the second level analysis and the material inputs for both "pile types" are presented below in Table 4-3.

Table 4-3. Material inputs for the two "pile types"

Parameter	*RIGID*	*Pre-stressed Concrete*
Concrete comp. strength, f'_c	1×10^{11} psi	6,000 psi
Concrete Shear modulus, G	1×10^{11} psi	1,690 ksi
Prestressed steel strands yield strength, f_y	1×10^{11} psi	243,000 psi
Transverse shear reinforcement, f_y	1×10^{11} psi	60,000 psi

4.4.4 Results and Analysis

4.4.4.1 Rigid pile horizontal displacement

The initial scope of GEO5 pile analysis was to determine if any potential lateral displacement of the pile occurred during Hurricane Michael. For this analysis, the RIGID pile was first applied to directly measure the soil response. Three separate loading scenarios were applied in this step: 100 k (4 kip/pile), 300 k (12 k/pile) and 400 k (16 kip/pile), all based to cover the minimum, expected, and high values of loading due to Hurricane Michael. In all loading scenarios, a truly rigid response was observed as shown from the linear displacement profile (e.g., Fig. 4-17).

Although it was possible to make qualitative observations of the pile geometry from the field reconnaissance (i.e., pile geometry and height of exposed pile prior to storm event), the total length of piles installed at 1101 FL-30/US-98 was unknown at the time of this study. Therefore, this original analysis was performed for a range of modeled pile lengths from 20 ft to 50 ft. Maximum displacement was recorded for each pile length and loading value with the results shown in Fig. 4-18.

As anticipated, lateral displacement of the pile, when modeled as a rigid member, is a function of the total length of the construction pile. Analysis shows there is a convergence of recorded displacement for the full range of anticipated storm loading once the pile reached a total length of 35 ft. Note: displacements values are shown in inches while the total pile lengths are provided in ft. Therefore, at a pile length of 35 ft. The anticipated distortion of the pile (i.e., the displacement per length) is between 1/280 to 1/850. The minimal observed displacement with a rigid pile suggests that the soil bearing capacity was not a major contributing factor to the failure of the pile.
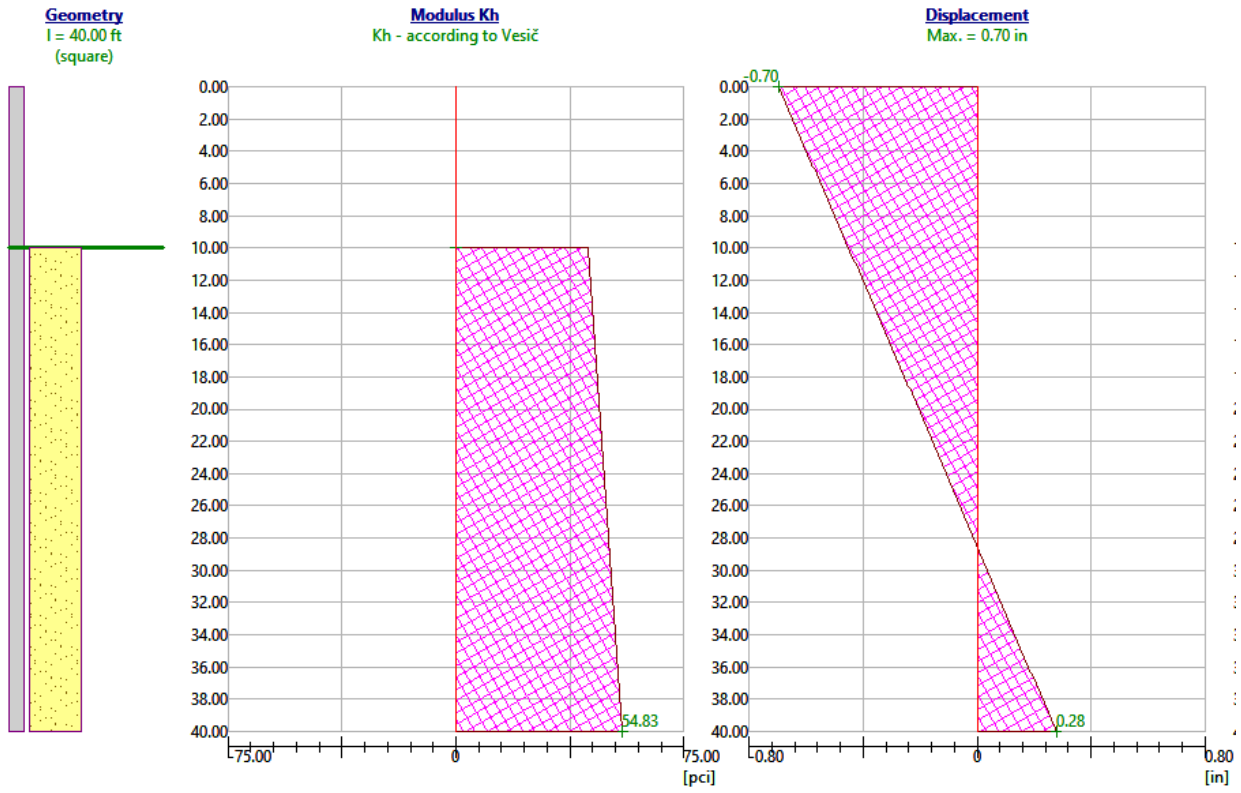
Figure 4-17. GEO5 analysis output showing max lateral displacement from RIGID pile as indicated by linear displacement profile.
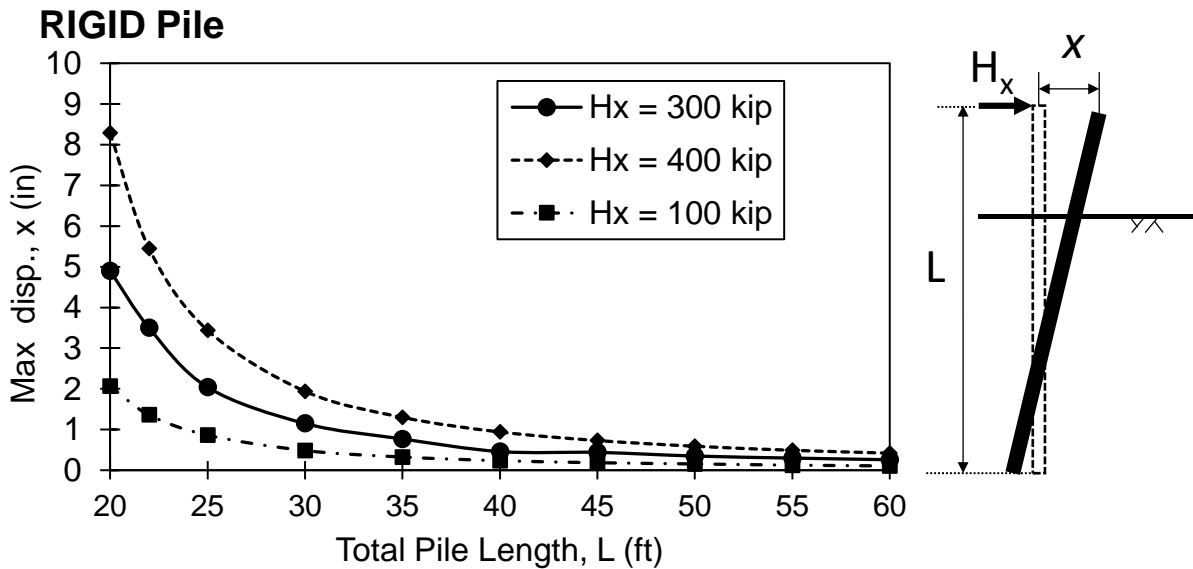
Figure 4-18. Recorded maximum horizontal pile displacement for varying horizontal loading and total pile length.

4.4.4.2 Prestressed pile horizontal displacement and forces

Although not in the original scope of this project, the GEO5 program was also utilized to calculate and compare the internal forces in the laterally loaded pile, coupled with the response of the soil conditions. For this analysis, the pile was constructed using the "prestressed concrete" parameters shown earlier in Table 4-3. As one would expect, the resulting lateral displacements were significantly higher than the values calculated from the rigid pile. However, it was observed that the displacements were only dependent on the loading applied and had no change in value as the total length of pile was deviated. The same pattern was observed for the trends of calculated maximum shear and maximum bending moment, as shown in Fig. 4-19(a). This occurrence is most likely a result of a point of fixity occurring at the grade-level, thus causing the critical forces to only develop in the exposed pile length section. This is also noticeable when viewing the profiles of displacement, shear, and moment, along the total pile depth (see Fig. 4-20).
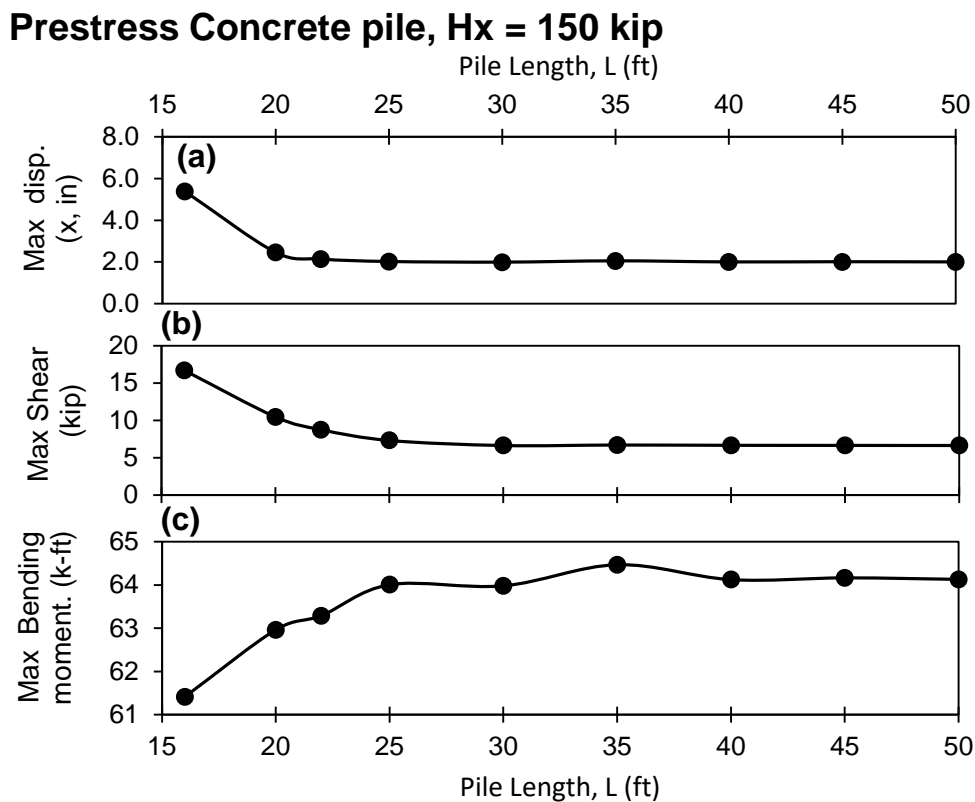
Figure 4-19. Analysis results for the prestressed concrete pile with Hx =150 kip showing (a) maximum horizontal displacement, (b) maximum internal shear, and (c) maximum bending moment within the pile, as a function of modeled pile length.
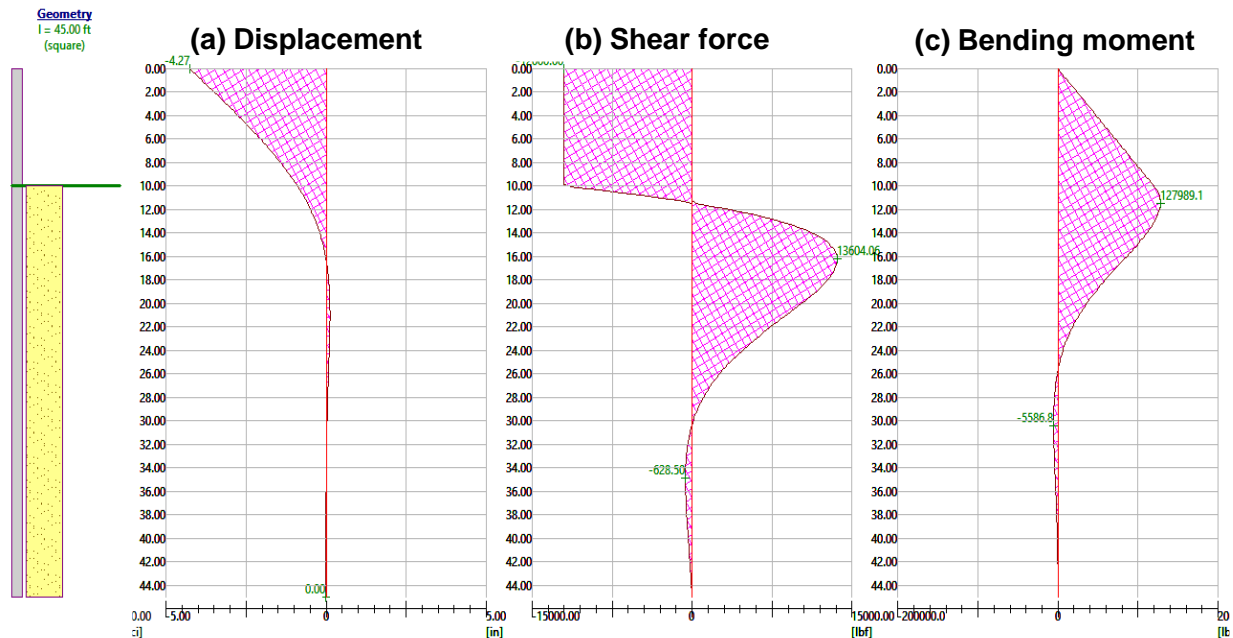
Figure 4-20. Example of results from GEO5 for prestressed pile with L=45 and Hx = 300 kip

It was observed that, regardless of the loading and the pile length, the maximum bending moment occurred at approximately 0.5 ft below the grade-level. As noted previously, the piles at the 1101 FL-30/US-98 appear to have all failed in bending at a location at or above the grade-level slab. As previously mentioned, the GEO5 pile analysis presented thus far differs from the "real-world" condition by not including any additional reaction forces (and subsequent addition to the pile stiffness) from the grade-level slab nor the superstructure. Moreover, several feet of scour were known to have occurred during the storm event. Although the contributions of the grade-level slab and the superstructure are not able to be modeled using the GEO5 software, the scour could be modeled by incrementally lowering the grade line in the model domain.

4.4.4.3 Prestressed pile (L=35ft) with variable scour

A modeled prestressed pile with L = 35 ft was investigated further to determine the effects of scour on the resulting lateral displacement and maximum bending moment. The 35-ft foot pile was chosen as an example of a probable pile length for the study site in Mexico beach since there was verification of nearby piled structure on 40-ft piles (ICF 2019). For this analysis, the pile dimensions were kept constant, and scour was simulated by lowering the finished grade line in 1.0-ft increments. This was performed for each of the three loading scenarios (Hx) and the maximum displacement and maximum bending moment was recorded for each trial. The resulting

trend of max displacements and max bending moment is plotted with the modeled scour depth in Fig. 4-21. Although approximately 2-3 ft of scour was estimated, the analysis was performed for a total of 8 ft of scour, essentially ranging the free length of pile from 8 ft to 16 ft.

Prestress Concrete pile, L = 35 ft
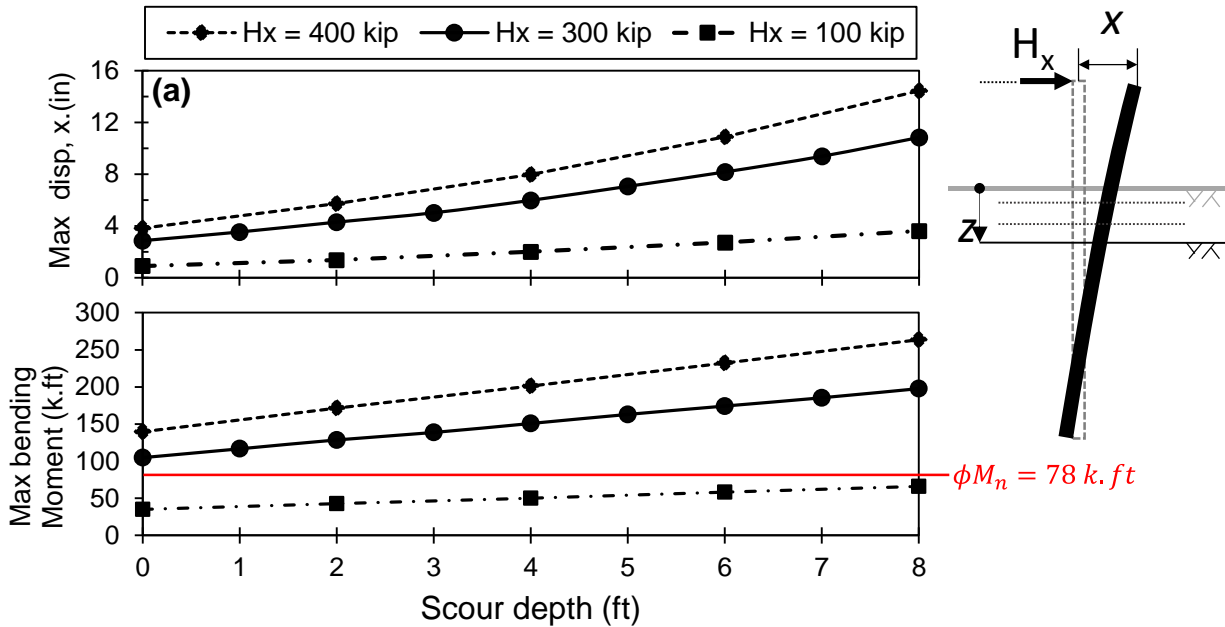
Figure 4-21. Analysis results for the prestressed concrete pile with assumed pile length of 35 ft, showing (a) maximum horizontal displacement and (b) maximum bending moment within the pile, as a function of scour depth.

As shown in Figure 4-21, both the displacement and max bending moment increases for all three loading scenarios, as scour depth increases. If the maximum bending moment trend is normalized, it is observed that 1 ft of scour will increase the maximum moment by 11%.

4.4.5 Key Findings

To summarize the key findings of the GEO5 pile investigation:

- The subsurface conditions consisted of medium to dense quartz-based sand from the Holocene. Using Vesic's modulus and the p-y analysis for lateral pile displacement, the subsoil bearing capacity produced negligible lateral movement and subsequent pile distortion, suggesting that

- Maximum bending moment was observed in the modeled GEO5 prestressed pile at a point approximately 0.5 foot below the grade and was not dependent on the pile length. The pile

was satisfactory in shear resistance but failed in bending for all three loading conditions. Although the observed failure in the piles located at 1101 FL-30/US-98 did not match the maximum bending from the GEO5 analysis, the occurrence of scour and the addition of the point of fixity from the superstructure was not analyzed in depth for this task.

- For a 35-ft pile with an initial exposed pile of 10 ft, every foot of scour will increase the calculated maximum moment bending by 11%, regardless of loading conditions. Although not necessarily accurate for the structure in this study, this type of analysis can provide an estimation of critical conditions which will produce bending moments exceeding the piles capacity.

4.5 Key Conclusions from Structural Response Analysis

Taken together, results from FEA and GEO5 pile appear to imply the following:

- The reason the structure at 1101 FL-30/US-98 failed *the way* (i.e., overturning moment failure above the grade line) it did was likely due to a combination of scour and higher water levels than +15.6 ft NAVD. While stated earlier, it is important to note that even the +15.6 ft NAVD water elevation represents a storm with a return period greater than 500 years. This sort of return period is well beyond the return period specified in the Florida Building Code.

- The reason the piles failed *where* they failed (i.e., near the location of the grade-level slab) was likely because the grade-level slab was improperly connected to the piles or that there was insufficient space left between the grade-level slab and the piles.

- However, even if the grade-level slab had been built according to requirements from the Florida Building Code (i.e., with the space), the structure likely would have failed anyway. FEA analysis suggests that the failure would have occurred close to the mudline where a fixed support had been assumed. GEO5 Pile analysis suggests that this failure would have occurred just below the subsurface at a depth of approximately 6 in.

5   MITIGATION

5.1 Environmental Loading

When this project was scoped, it was hypothesized that the loading on the structure due to wave action may have been improperly quantified in the sense that it was hypothesized that high-frequency, high-amplitude oscillatory forces may have developed during wave action on the underside of the structure due to trapped air between the water surface and the structure. It was further hypothesized that these high-frequency oscillatory wave forces would have been higher than forces computed using a relatively simple quasi-static analysis. Similar high-frequency oscillatory loading caused the failure of several high-profile bridges during several recent hurricanes (e.g., the Escambia Bay Bridge during Hurricane Ivan, among others). However, CFD results showed that the presence of high-frequency oscillatory loading due to wave action on the structure located at 1101 FL-30/US-98 was unlikely. Instead, results showed that the forces due to waves on this structure were likely mostly quasi-static and that a relatively simple quasi-static analysis produced relatively accurate results for loading on the structure.

When this project was scoped, there was little question about the accuracy of wind loads computed using ASCE7. Nonetheless, analysis presented here appears to indicate that ASCE7 performs well when compared to CFD in the context of predicting wind loads on a structure like the structure at 1101 FL-30/US-98.

If trapped air had been an issue (once again, results imply that it was not), then some form of "venting" along the underside of the structure could have been analyzed to determine its relative benefit in terms of reducing the trapped air forces on the structure. However, results showed that during wave action, the forces responsible for lateral and uplift loading on the structure mirrored the water levels associated with wave action. This indicates that water forcing, and wind alone were responsible for the loading on the structure. In the context of wave action, it would not be possible to "vent water," and thus, vents were deemed ineffective as a mitigation technique. Others (see Kerenyi et al. 2009 for example) have investigated reducing wave/surge loading on bridges by using more streamlined shapes, but streamlining a residential structure (i.e., making it more aerodynamic) would not appear to be feasible. As such, investigators concluded that from an environmental loading perspective, mitigation would be ineffective at reducing the force on coastal structures like the one used as a case study at 1101 FL-30/US-98.

Of course, these conclusions are based upon results from CFD. While these results were verified for computational convergence using a mesh study, these results were not verified against physical data. In future research, it would be beneficial to physically model a structure like the structure at 1101 FL-30/US-98 to verify further that the CFD results are truly representative of forcing on the structure.

5.2 Structural Mitigation

Results from Task 3 imply that the reason the structure at FL-30/US-98 failed was because the water elevations were too high relative to the pile elevations. As shown in Fig. 4-3 through Fig. 4-5, if the initial water elevation was +15.6 ft NAVD, the structure would not have failed even if up to 6 ft of scour developed around the structure. On the other hand, Fig. 4-11 through Fig. 4-13 show that failure was likely at an initial water elevation of +18.4 ft NAVD; and Fig. 4-6 through Fig. 4-8 show that failure was almost guaranteed with an initial water elevation of +21.2 ft NAVD. If the structural elevation had been raised another 5 ft to 6 ft, the structure would have responded more like Fig. 4-5 in the sense that the water would have mostly passed below the structure's first floor, and the structure likely would have survived assuming the 6-ft of scour was an overestimation and actual scour was closer to 3-ft. This may have been why the foundation at 112 S 31st St. survived the storm while the structure at 1101 FL-30/US-98 failed. Water level elevations from the FEMA MAT report are presented below in Fig. 4-1:
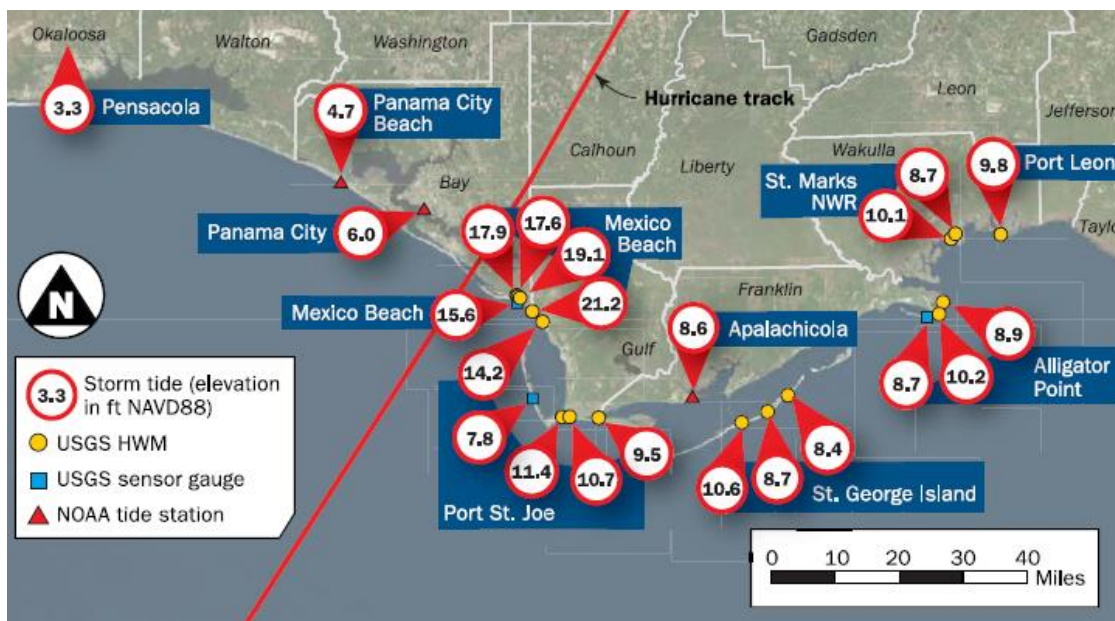

Figure 5-1. Water level elevations from FEMA MAT report

Note that in Fig. 5-1, the +21.2 ft NAVD approximate water-elevation appeared to be relatively localized. If the water elevation at 112 S 31st St. had been just slightly lower, there may have been sufficient space between the water and the structure to prevent failure – see Fig. 5-2 below, for example:
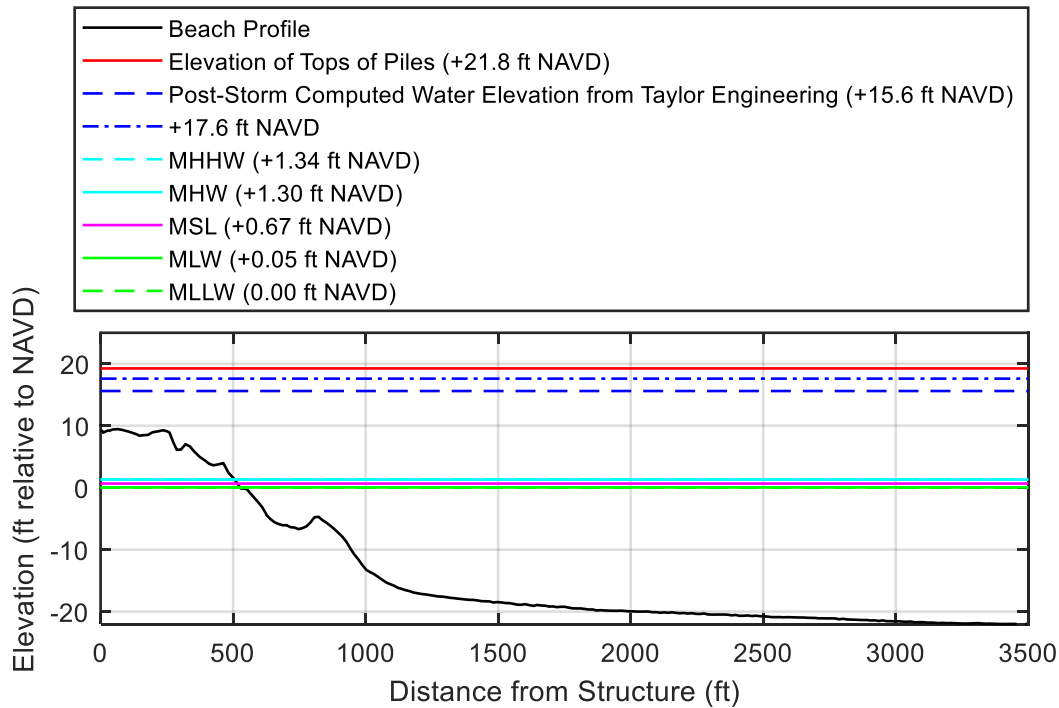
Figure 5-2. Beach profile near 112 S 31st St., Mexico Beach showing a presumed worst-case water level of +17.6-ft NAVD

When analyzing these scenarios, it is important to reiterate that even the best-case +15.6 ft NAVD initial water-elevation is still greater than a 500-year storm return period, and a 500-year return period is much greater than the 100-year return period specified by the Florida Building Code or its reference to ASCE24, Chapter 4.

Alternatively, if one did not wish to build the structure higher, one could instead use more longitudinal reinforcement in the piles. For example, if one increased the number of prestressing strands in the piles from 4 strands to 6 strands, each pile's design moment capacity would increase from 78 k-ft to 89 k-ft (i.e., increase A_{ps} in Section 3.1). This would mitigate failure under the +18.4 ft NAVD elevation scenario, although the structure may have still failed under the +21.2 ft NAVD elevation scenario.

Scour appears to have played some role in structural response, but its effect is relatively minor when compared to the effect of water impacting the first floor of the structure. Results in Chapter 3 show that if most of the water passes below the structure's first floor (i.e., Fig. 4-3 through Fig. 4-5), then the structure still withstands the storm. If on the other hand, the structure's first floor elevation is too low relative to the initial water level, then the structure will still likely fail (Fig. 4-6 through Fig. 4-8 for example). Results in Fig. 4-11 through 4-13 combined with results from Fig. 4-21 imply that there is some "sweet spot" where scour would play a critical role in the sense that for a certain water elevation, failure might not occur under a 3-ft of scour (for example) but might occur under 6-ft of scour (again, for example). Thus, mitigating scour via some form of ground improvement below the structure's grade-level slab and around the structure may have helped to mitigate failure for certain storms. But, for this storm (i.e., Hurricane Michael), results imply that even scour mitigation probably would not have prevented failure at 1101 FL-30/US-98. The relatively minor effect of scour when compared to initial water level elevation is illustrated below in Fig. 5-3 which shows results from an ANSYS model at 1101 FL-30/US-98 with 3-ft of scour, the attached grade-level slab, and an initial water elevation of +18.9 ft NAVD (i.e., only 6-inches higher than the scenario presented in Fig. 4-12.
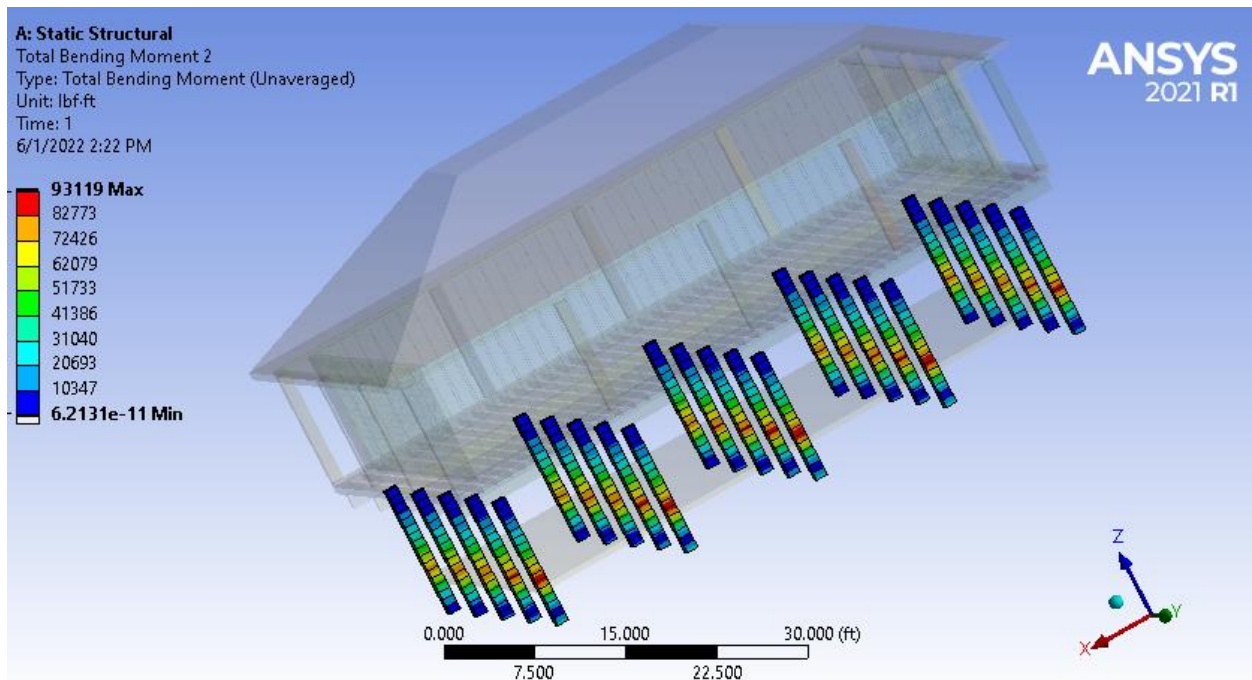

Figure 5-3. Results from ANSYS model at 1101 FL-30/US-98 with 3-ft of scour, attached grade-level slab, and initial water elevation of +18.9 ft NAVD

While results in Fig. 4-12 show that the structure was very close to failure with an initial water level of +18.4 ft NAVD, results in Fig. 5-3 show that increasing the initial water-elevation by only 6-inches is enough to cause the structure to fail. Or, conversely, reiterating the conclusions from Fig. 4-21, results show that a 1-ft increase in scour only leads to an 11% increase in overturning moment.

The third structural element – the grade-level slab – has been discussed throughout this report. Results imply that providing a space between the grade-level slab and the piles (as required by the Florida Building code) would have prevented the *type* of failure observed at 1101 FL-30/US-98, but would likely not have *prevented* failure of this structure during Hurricane Michael.

6   SUMMARY AND CONCLUSIONS

To summarize:

- Environmental loading due to wind and wave action was analyzed on the structure located at 1101 FL-30/US-98. Results from the environmental loading analysis indicated that the Florida Building Code conservatively estimates both wave and wind loading on a structure like this structure.

- The response of the structure to environmental loads located at 1101 FL-30/US-98 was analyzed. Results suggested that the reason the structure failed was that the initial water elevation associated with Hurricane Michael's storm surge was too higher relative to the structure's first floor elevation. While scour and an improper connection of a grade-level slab may have played roles in the structural failure, these effects were minor when compared to the effect of water elevation impacting the first, raised floor of the structure.

- Mitigation of the failure at 1101 FL-30/US-98 would likely require a higher structural elevation or an increase in the number of prestressing strands in the piles. However, it is unclear how this sort of measure should be specified in the Florida Building Code since doing so would presumably mean specifying that a structure needed to withstand water levels associated with storms with return periods greater than 100 years (i.e., less than 1% probability of occurrence).

LIST OF REFERENCES

ASCE (2017). ASCE 7 - Minimum Design Loads and Associated Criteria for Buildings and Other Structures, American Society of Civil Engineers, Reston, VA, ISBN 978-0784414248.

ASTM international (2022), Standard Test Method for Standard Penetration Test (SPT) and Split barrel Sampling of Soils, D1586/D1586M. West Conshohocken, PA

Bowles, J. E.:(1997) Foundations Analysis and Design. 5th edition, New York: McGraw-Hill Book Company, 1997, ISBN 0-07-118844-4, chapter 16-15.2, s. 941 (table 16-4).

Dean, R. G., and Dalrymple, R. A. (1991). Water wave mechanics for engineers and scientists, World Scientific Publishing Company.

FEMA (2020). "Hurricane Michael in Florida, Building Performance Observations, Recommendatinos, and Technical Guidance."Report No. FEMA P-2077, Federal Emergency Management Agency, Washington, DC.

Fenton, J. D. (1985). "A Fifth-Order Stokes Theory for Steady Waves." J. Wateray, Port, Coastal, and Ocean Engineering, 111, 216-234.

GEO5 (2022). Fine EU Software, Analysis of horizontal bearing capacity of a single pile [Computer Software]

Google (2022). "Google Maps." <http://www.maps.google.com>.

Florida Department of Transportation, FDOT (2022) Public Soil Boring Web Viewer, web, date accessed May 10 2022.

Florida Department of Environmental Protection, FDEP (1953) Florida geological Well Survey, W-2939 Mexico Beach, [online]

The Insulating Concrete Forms Magazine, ICF (2019), Mexico Beach Survivor, ICF Builders [web article] date accessed May 26 2022.

Kerenyi, K., Sofu, T., and Guo, J. (2009). Hydrodynamic Forces on Inundated Bridge Decks. United States Department of Transportaiton - Publications and Paper, USDOT, Washington, DC.

Mansur, C., and Hunter, A.H., (1970) Pile Tests-Arkansas River project, Journal of Soil mechanics and Foundations Div., 96,1545-1582

Mathworks. 2022. MATLAB, version R2021a (9.10.0.1602886).

Mcvay, M., Casper, R., and Shang, T-I. (1995). Lateral Response of Three-Tow Groups in Loose to Dense Sands at 3D and 5D Pile Spacing. American Society of Civil Engineers (ASCE), Journal of Geotechnical Engineering, Vol. 121, No 5, pp. 436-441.

Nicoud, F., and Ducros, F. (1999). "Subgrid-Scale Stress Modeling Based on teh Square of the Velocity Gradient Tensor." Flow, Turbulence, and Combustion, 62, 183-200.

Prestressed Concrete Institute, PCI (2019) Recommended practice for Design, Manufacture, and Installation of Prestressed concrete piling, PCI journal pg 84-116

Prevatt, D. O., and Roueche, D. B. (2019). "Survey and Investigation of Buildings Damaged by Category-III, IV, & V Hrricanes in FY 2018-2019." University of Florida, Tallahassee, FL.

Scott, TM (2001) Text to accompany the Geologic map of Florida. Florida Geologic Society Open File Report 80.

U.S. Department of Transportation, FWHA (2016), Design and Construction of Driven Pile Foundations. Report Publication No. FHWA-NHI-16-009

Vesic, A.S.: (1977) Design of Pile Foundations. National Cooperative Highway Research Program Synthesis 42, Transportation Research Board, Washington D.C., 1977.

Zillow (2022). "Zillow." <http://www.zillow.com>.